DESIGN OF SYNTHETIC SCAFFOLDS FOR TISSUE REGENERATION APPLICATIONS

By

SEOKWON POK
Bachelor of Science in Chemical Engineering
Hoseo University
Asan, South Korea
2005

Master of Science in Chemical Engineering
Oklahoma State University
Stillwater, Oklahoma
2008

Submitted to the Faculty of the
Graduate College of the
Oklahoma State University
in partial fulfillment of
the requirements for
the Degree of
DOCTOR OF PHILOSOPHY
December, 2010

DESIGN OF SYNTHETIC SCAFFOLDS

FOR TISSUE REGENERATION

APPLICATIONS

Dissertation Approved:

Dr. Sundararajan V. Madihally

Dissertation Adviser

Dr. A.J. Johannes

Dr. Josh D. Ramsey

Dr. Brenda Smith

Dr. Mark E. Payton

Dean of the Graduate College

ACKNOWLEDGMENTS

The completion of this dissertation would not have been possible without the help and support of many people.

I would like to express appreciation to my advisor, Dr. Sundararajan V. Madihally, for teaching me how to think and write in a scientific manner. I also thank him for the countless hours spent working on papers, proposals and this dissertation, and his kind consideration for my family.

I would like to express appreciation for the support and confidence that my parents constantly showed in helping me to achieve my life goals.

I would like to express appreciation to my wife most of all for her being willing to accompany me on this journey. She is everything to me.

I would like to thank my Committee: Dr. AJ Johannes (Chair), Dr. Josh D. Ramsey, and Dr. Brenda Smith for their guidance and efforts in seeing the project through to a successful completion.

Finally, I would like to thank our group members Benjamin J. Lawrence, Jong Kyu Hong, Rahul Mirani, Pooja Iyer, Kornkarn Makornkaewkeyoon, Dhananjay Dhane, and staffs in chemical engineering department; Shelley Potter, Eileen Nelson, Carolyn Sanders, and Mindy Bumgarner.

TABLE OF CONTENTS

Chapter Page

Chapter Page

LIST OF TABLES

Table Page

LIST OF FIGURES

Figure Page

Figure Page

CHAPTER I

INTRODUCTION

Transplantation techniques for damaged or defective tissues and organs have been improved significantly. However those conventional therapies are limited in the amount of human donors. Hence, tissue engineering is being more magnified as an alternative way to meet demands for replacing damaged components of humans. Furthermore, tissue engineering potentially offers not only improvements in medical care for patients, but also reduction in medical costs dramatically. Tissue engineering involves implanting cells into supporting structural material –termed a scaffold- and allowing the cells to remodel the scaffold into natural tissue, before implanting it into a patient's body (Place, George et al. 2009).

Most materials commonly in use as scaffolds are polymers such as synthetic, naturally derived, or their composite polymers. Synthetic materials include poly(ethylene glycol) (PEG), poly(ethylene oxide) (PEO), poly(lactic acid) (PLA), polycaprolactone (PCL), or poly(lactic-co-glycolic acid) (PLGA), and examples of naturally derived materials are chitosan, gelatin, or fibrin. Those types of polymers have respective advantages and disadvantages. Synthetic polymers offer better control on mechanical properties, degradation characteristics using polymer chemistry. For example, mechanical and non-enzymatic degradation (by hydrolysis) properties of PCL, the semi-

crystalline linear resorbable aliphatic polyester with low melting point (60°C), can be altered by changing molecular weight or co-polymerizing other monomers such as vinyl alcohol (Engelberg and Kohn 1991). Thus, PCL is explored in forming various medical devices (van der Giessen, Lincoff et al. 1996), templates in tissue regeneration (Htay, Teoh et al. 2004; Li, Cooper et al. 2006), and drug delivery systems (Aliabadi, Mahmud et al. 2005). However, using high MW PCL in forming structures for biomedical applications has been the strategy since structures formed with low MW PCL are unstable (Baker, Rohman et al. 2009; Guarino, Taddei et al. 2009). High MW PCL is biostable for nearly two years (Pitt, Gratzl et al. 1981) and degradation rate is a function of MW.

Typically used halogenated hydrocarbon solvents such as chloroform generate a hydrophobic surface with smooth surface characteristics. Since a hydrophobic material fails to spread water and important nutrients dissolved in water, hydrophobicity needs to be reduced or engineered to hydrophilic condition. In addition, large scale manufacturing requires the safe disposal of those environmentally unfriendly solvents. Although grafting hydrophilic fragments of synthetic or natural polymers such as acrylates, collagen, and chitosan have been explored to reduce hydrophobicity (Jones, Djokic et al. 2002; Cheng and Teoh 2004; Jones, McLaughlin et al. 2005; Chung, Wang et al. 2006; Williamson, Black et al. 2006), regulating a number of cellular activity is also critical while retaining the possibility of tailoring mechanical and degradation properties.

For tissue engineering to be successful, building scaffolds of the shape similar to the tissue to be placed is important. Current techniques utilize porous sheets and the surgeon molds into required shape (Atala, Bauer et al. 2007). However, they have

uneven thickness due to wrinkling and overlap. Further, the quality of the regenerated tissue is dependent on the surgeons' ability to mold. Thus, it is important to develop anatomical relevant scaffolds appropriate to regenerating a specific tissue.

Regeneration is a dynamic process where the porous characteristics change due to matrix deposition and tissue maturation. Assembly and maturation of extracellular matrix (ECM) elements in tissue regeneration play a significant role in determining the quality of the regenerated tissue. These changes affect the transport characteristics and nutrient distribution. Also, *in vitro* regeneration strategies are not characterized for high aspect ratio tissues which have large surface area relative to the thickness (Heydarkhan-Hagvall, Esguerra et al. 2006). *In vitro* cultivation system referred as bioreactors have been explored for the successful tissue regeneration process. The bioreactor provides an optimized environment for the cells. Many issues have to be considered in designing of bioreactors, include nutrient fluid transfer, hydrodynamic stress, configurations of reactors, and changes in permeability due to regeneration. These factors can be achieved and optimized by computational fluid dynamic (CFD) study.

The objective of this study was to investigate a novel method of generating synthetic scaffolds that has the ability to independently regulate mechanical, degradation, and biological properties. Further, mimicking anatomically relevant structure of PCL scaffolds was also explored. Our laboratory has discovered that PCL can be dissolved in glacial acetic acid (AA) which allows spontaneous aggregation of PCL upon contact with water. *The hypothesis of this study is that PCL matrices generated in aqueous environment will have the familiar biological condition in addition to retaining the ability to regulate mechanical and degradation properties. In addition, this simple technique*

can be utilized to generate anatomically relevant scaffolds. Also, a suitable bioreactor needs to be investigated for in vitro cultivation of anatomically relevant scaffolds with appropriate cell sources. To test the hypothesis, three specific aims are described below.

1.1. Aim 1. Characterization of a novel method to make scaffolds using the synthetic polymer polycaprolactone (PCL).

PCL is a synthetic polymer, and structures formed using organic solvents. Hence, it has a limitation in long term project, and tends to show a poor cellular activity. This aim mainly focused on developing a new strategy to improve biological properties of 80 kDa Mn PCL scaffold. A novel process of dissolving PCL in acetic acid (AA) was investigated which allows the self assembly of PCL in aqueous environment. PCL matrices formed from self assembly method were compared with chloroform-cast matrices to evaluate the effect of different solvents on the surface morphologies and roughness characteristics, effects of neutralization process in the alkaline solution, tensile properties, and stress relaxation properties. In addition, cytocompatibility and cytoskeletal organization of human foreskin fibroblasts were tested in serum free medium.

1.2. Aim 2. Effect of blending different molecular weight of PCL and multi-layered scaffolds on biological properties.

The resorption of PCL matrices is considerably slower than other aliphatic polyesters due to its high crystallinity. The effects of blending low molecular weight (10 kDa, 47 kDa Mn, and 80 kDa) PCL was investigated to find the effect of MW on the degradation rate. Further, natural polymers, gelatin and gelatin-chitosan composite, were hybridized to enhance the bioreactivity of the PCL surface and to modulate cell survival.

PCL matrices were incubated in gelatin solution, and compared for the effects on the surface morphology, surface characteristics, and cellular activity. In addition, incorporating the porous structure of gelatin-chitosan mixture, known to support cell colonization (Huang, Onyeri et al. 2005), was evaluated. Gelatin-chitosan composite scaffolds were formed multi-layered scaffolds with self assembled PCL matrices using lyophilization technique, and their surface characteristics and tensile properties were evaluated. Furthermore, based on self assembly method and multi-layered scaffolds, spherical and cylindrical shaped PCL matrices were investigated to mimic anatomically relevant structures of human bladder and blood vessel.

1.3. *Aim 3. Design of a bioreactor for bladder tissue regeneration using computational fluid dynamic.*

There is a significant lack of a bioreactor technology to utilize 3-D anatomically relevant structures. Hence, prior to utilization of developed 3-D scaffolds, understanding design features of the bioreactor was investigated. The bioreactor suitable for regenerating a human bladder was simulated using COMSOL 3.5a Multiphysics. The spherical shape of the bioreactor was designed for the bladder tissue regeneration. Based on the human bladder size, the volume of the reactor was set to 820 mL, and the volume of scaffold was chosen to be 755 mL with a thickness of 3 mm, similar to the human bladder. The fluid flow analysis was performed using incompressible Navier –Stokes equation on non-porous regions and the Brinkman equation on porous regions. Nutrient consumption was evaluated using Michaelis-Menten type rate law for smooth muscle cells (SMCs), with constants extracted from literature. Steady State conditions were used with no slip condition of the walls. The effects of various factors were evaluated

including i) inlet shapes and locations to minimize shear stress at the inlet area, ii) flow rate, iii) different locations of scaffolds, iv) nutrient consumption (particularly oxygen and glucose), and v) varying cell density and permeability. Further, the diffusivity changes due to altered void fraction in the porous structure was calculated using Mackie-Meares relationship, and nutrient distribution mechanism in the porous region was characterized by calculating *Peclet* numbers.

1.4. References.

Aliabadi, H. M., A. Mahmud, et al. (2005). "Micelles of methoxy poly(ethylene oxide)-b-poly(epsilon-caprolactone) as vehicles for the solubilization and controlled delivery of cyclosporine A." J Control Release **104**(2): 301-311.

Atala, A., S. B. Bauer, et al. (2007). "Tissue-engineered autologous bladders for patients needing cystoplasty." Journal of Urology **177**(4): 66-66.

Baker, S. C., G. Rohman, et al. (2009). "The relationship between the mechanical properties and cell behaviour on PLGA and PCL scaffolds for bladder tissue engineering." Biomaterials **30**(7): 1321-1328.

Cheng, Z. and S. H. Teoh (2004). "Surface modification of ultra thin poly (epsilon-caprolactone) films using acrylic acid and collagen." Biomaterials **25**(11): 1991-2001.

Chung, T. W., Y. Z. Wang, et al. (2006). "Poly (epsilon-caprolactone) grafted with nano-structured chitosan enhances growth of human dermal fibroblasts." Artif Organs **30**(1): 35-41.

Engelberg, I. and J. Kohn (1991). "Physico-mechanical properties of degradable polymers used in medical applications: a comparative study." Biomaterials **12**(3): 292-304.

Guarino, V., P. Taddei, et al. (2009). "The Influence of Hydroxyapatite Particles on in vitro Degradation Behaviour of PCL based Composite Scaffolds." Tissue Eng Part A.

Heydarkhan-Hagvall, S., M. Esguerra, et al. (2006). "Production of Extracellular Matrix Components in Tissue-Engineered Blood Vessels." Tissue Engineering **12**(4): 831-842.

Htay, A. S., S. H. Teoh, et al. (2004). "Development of perforated microthin poly(epsilon-caprolactone) films as matrices for membrane tissue engineering." J Biomater Sci Polym Ed **15**(5): 683-700.

Huang, Y., S. Onyeri, et al. (2005). "In vitro characterization of chitosan-gelatin scaffolds for tissue engineering." Biomaterials **26**(36): 7616-7627.

Jones, D. S., J. Djokic, et al. (2002). "Poly(epsilon-caprolactone) and poly(epsilon-caprolactone)-polyvinylpyrrolidone-iodine blends as ureteral biomaterials: characterisation of mechanical and surface properties, degradation and resistance to encrustation in vitro." Biomaterials **23**(23): 4449-4458.

Jones, D. S., D. W. McLaughlin, et al. (2005). "Physicochemical characterisation and biological evaluation of hydrogel-poly(epsilon-caprolactone) interpenetrating polymer networks as novel urinary biomaterials." Biomaterials **26**(14): 1761-1770.

Li, W. J., J. A. Cooper, Jr., et al. (2006). "Fabrication and characterization of six electrospun poly(alpha-hydroxy ester)-based fibrous scaffolds for tissue engineering applications." Acta Biomater **2**(4): 377-385.

Pitt, C. G., M. M. Gratzl, et al. (1981). "Aliphatic polyesters II. The degradation of poly (DL-lactide), poly (epsilon-caprolactone), and their copolymers in vivo." Biomaterials **2**(4): 215-220.

Place, E. S., J. H. George, et al. (2009). "Synthetic polymer scaffolds for tissue engineering." Chem Soc Rev **38**(4): 1139-1151.

van der Giessen, W. J., A. M. Lincoff, et al. (1996). "Marked inflammatory sequelae to implantation of biodegradable and nonbiodegradable polymers in porcine coronary arteries." Circulation **94**(7): 1690-1697.

Williamson, M. R., R. Black, et al. (2006). "PCL-PU composite vascular scaffold production for vascular tissue engineering: attachment, proliferation and bioactivity of human vascular endothelial cells." Biomaterials **27**(19): 3608-3616.

CHAPTER II

BACKGROUND

2.1. Tissue engineering.

In the United States, more than 84,000 men, women and children are waiting for organ transplants (http://www.organtransplants.org). The demands for repair and renewal of injured tissues and organs continue to increase. However, it is apparent that this demand cannot be met from human donors alone. Tissue engineering is one of the alternative ways to solve this problem.

Tissue engineering is defined as an interdisciplinary field that applies the principles of engineering and life sciences toward the development of biological substitutes that restore, maintain, or improve tissue functions (Sterodimas, De Faria et al. 2009). Tissue engineering uses biodegradable templates referred as scaffolds made of naturally derived or synthetic polymers to replace damaged or defective tissues, such as bone, skin, and even organs. Tissue engineering offers improvements in medical care for many patients, and it could reduce the medical costs dramatically.

The basic concept of tissue regeneration is shown in the **Figure 2.1**. There are three essential elements for tissue engineering, which include (a) cell sources, (b) supporting materials, and (c) regulations of cell-material interactions. Cells are harvested

from donors or patients and populated in vitro. Then expanded cells are seeded into supporting biodegradable devices referred as scaffolds, and they are regenerated to remodel the scaffold into the natural tissue before implanting into patients' bodies. In some cases, the scaffolds are placed directly into the recipient, utilizing a compartment of the host's own body as a regenerative device (Place, George et al. 2009). However, the most common approach is that cell seeded scaffolds are regenerated using *in vitro* cultivation system referred as a bioreactor. For tissue engineering to be successful, scaffolds have to promote cell colonization while providing necessary mechanical support and need to degrade as the tissue regenerates. Hence, scaffold design is pivotal to the success of tissue engineering and this research will mainly focus on the design of scaffolds with a novel method for bladder tissue regeneration application.

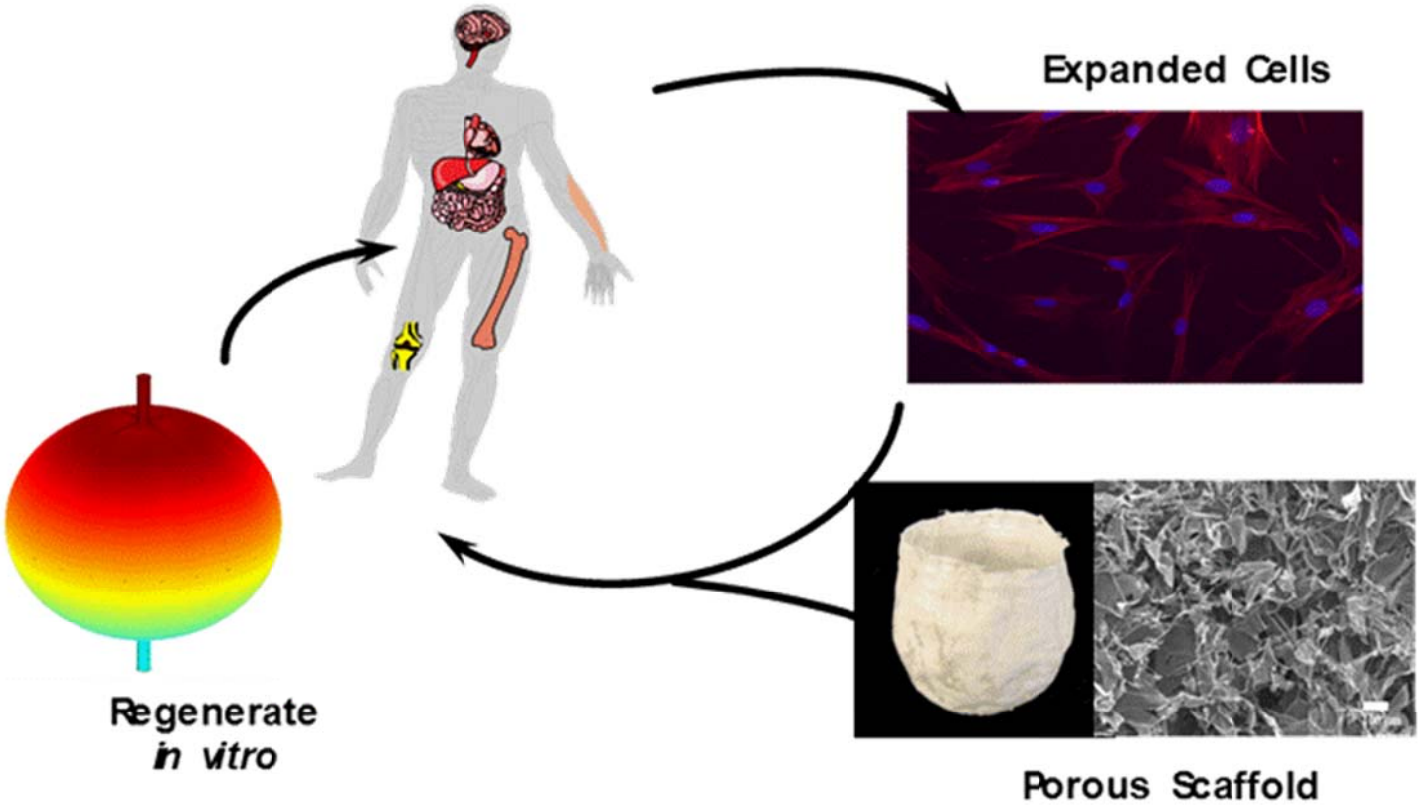

Figure 2.1. Concept of Tissue Regeneration.

2.2. Scaffolds.

Biomaterials referred as scaffolds play a critical role in the engineering of new functional tissues for the replacement of lost or malfunctioning tissues(Kim, Baez et al. 2000). In other words, scaffolds should have the structural integrity to support cells, supply nutrients for cells, and control cells. Hence, the scaffold needs to be biocompatible, biodegradable, bioresorbable, mechanically strong, and capable of being formed into desired shapes. Since the scaffold degradation influences not only the mechanical and structural integrity but also the cell viability and host response over the time, degradation rate should be predictable and controllable while the tissue is remodeled and matured (Schantz, Hutmacher et al. 2002). Degradation characteristics of the most common biomaterials are shown in the **Table 2.1**. Polymers are commonly used as a material for the scaffold as their mechanical properties can be tailored to tissue. In addition to biological properties, ease of processing, and fundamentals are well developed. Polymers as biomaterials used in tissue engineering can be classified into two categories synthetic or naturally derived polymers, with a middle ground of semi-synthetic materials rapidly emerging. Synthetic and naturally derived polymers have their respective advantages and disadvantages described below.

Table 2.1. Degradation characteristics of scaffolds.

Materials	Molecular weight	Degradation Time	Degradation Mechanism
Gelatin	50,000 Mw	95 % weight loss after 18 days (Wu, Liu et al. 2010)	Enzymatic
Chitosan	83,600 Mw Degree of deacetylation (DD); 53% and 72%	50 % weight loss after 10 days for DD of 53% and 84 days for DD of 72% (Ren, Yi et al. 2005)	Enzymatic
Poly(glycolic acid) (PGA)	200,000 Mn	6 to 12 months (Middleton and Tipton 2000)	Hydrolytic
Poly(lactic-co-glycolic acid) (PLGA)	70:30 (lactide: glycolide)	7 weeks (Li, Feng et al. 2010)	Hydrolytic
Poly-caprolactone (PCL)	80,000 Mn	4% weight loss after 6 months (Schantz, Hutmacher et al. 2002)	Hydrolytic

2.2.1. Naturally Derived Polymer.

Naturally derived polymers such as gelatin, chitosan, etc. are obtained from polymers found in nature. They are derived from a variety of sources such as fish scales, pig skins, animal bones, and crab shells. The human body also contains many natural polymers such as proteins and nucleic acids. Cellulose, another natural polymer, is the main structural component of plants. Many methods have been explored to form porous three dimensional scaffolds such as gas-forming (Mooney, Baldwin et al. 1996), electro spinning (Dhandayuthapani, Krishnan et al. 2010), three dimensional printing (Sherwood, Riley et al. 2002), and freeze-drying (Madihally and Matthew 1999). However, lyophilization , or freeze-drying, technique is a most common method to fabricate naturally derived polymers, because it is beneficial for those dissolved in aqueous media (Wu, Liu et al. 2010).

Most natural polymers are condensation polymers, and water is a by-product in their formation from monomers (Joesten 1996). Major advantages of natural polymers are that their chemical compositions are similar to the materials present in the body and promote cellular activity. However, many naturally derived polymers might not meet all the requirements as an adequate scaffold because of the lack of mechanical strength and assurance of pathogen removal.

One example of the naturally derived polymer is gelatin (**Figure 2.2**) denatured form of collagen which is a completely bioresorbable material. Collagen is the major component of the extracellular matrix (ECM) in the skin, bone, and connective tissue. Gelatin is produced by boiling the connective tissues, bones, and skins of animals,

usually cows and pigs. Since gelatin has excellent biodegradability and biocompatibility, it is regarded as an ideal biomaterial for applications in tissue engineering and cell transplantation (Hu, Kurisawa et al. 2009). Similar to collagen, gelatin is composed of a unique sequence of amino acids (Mao, Zhao et al. 2003). Structurally, gelatin molecules contain repeating sequences of glycine-X-Y triplets, where X and Y frequently are proline and hydroxyproline (Pangburn, Trescony et al. 1982).

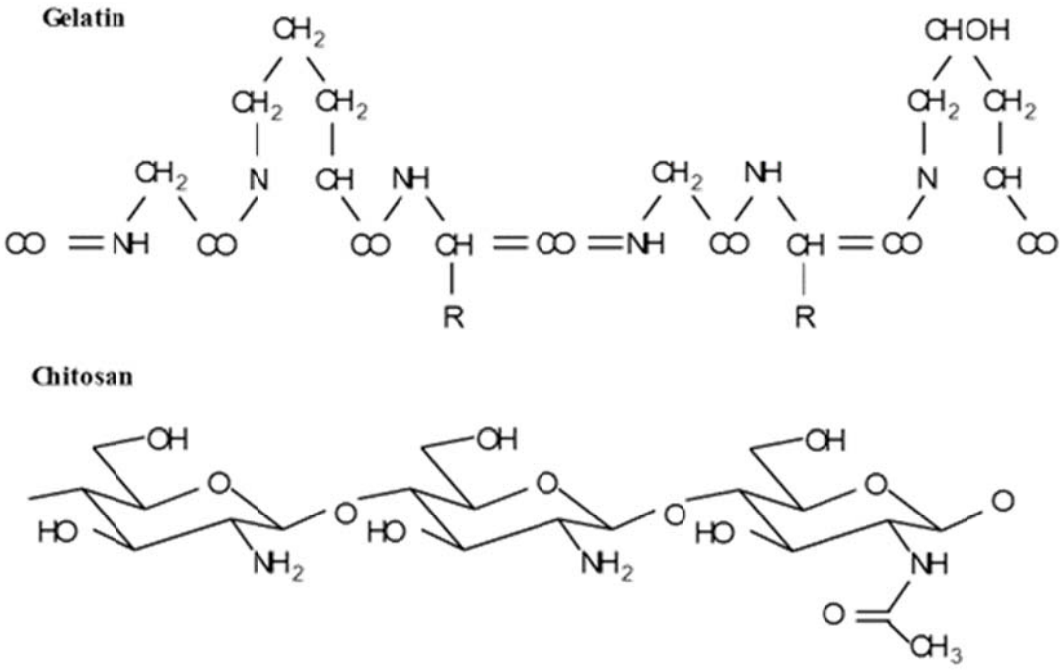

Figure 2.2. Chemical structures of gelatin and chitosan.

Chitosan is the N-deacetylated derivative of chitin which forms the exoskeleton of crustacean shells, and its structure is similar to glycosaminoglycan. Since, chitosan demonstrates excellent biocompatibility (VandeVord, Matthew et al. 2002), antimicrobial and antifungal activities (Choi, Kim et al. 2001), and controllable degradation rate dependent on its degree of deacetylation, chitosan is widely investigated in wound

dressing (Risbud, Hardikar et al. 2000) and drug delivery systems (Ishihara, Obara et al. 2006). Further, chitosan can be easily fabricated into porous structures with orientated direction. Chitosan is insoluble in water or organic solvents but soluble in aqueous acids (pH< 6.3), which provides convenience for processing chitosan into different shapes. Due to the protonation of the free amine groups on the chain backbone (**Figure 2.2**), chitosan exhibits a high charge density in solution (Madihally and Matthew 1999). Chitosan is also blended with collagen, alginate, GAGs and synthetic polymers (i.e. PLGA, PCL) to fabricate suitable scaffolds (Mei, Chen et al. 2005).

2.2.2. Synthetic Polymer.

The most widely used synthetic biodegradable polymers are poly(α-hydroxy acids), poly(lactic acid) (PLA), poly(lactic-co-glycolic acid) (PLGA), poly(glycolic acid) (PGA), polycaprolactone (PCL) and their copolymers (**Figure 2.3**). These polyesters degrade by hydrolysis, eventually releasing oligomers or monomers that feed into natural metabolic pathways (Place, George et al. 2009). Further, these synthetic polymers can be easily mass produced and sterilized. The advantages of synthetic polymers are that they are easy to regulate the microstructure and degradation rate. Synthetic polymers have strong and controllable mechanical properties. However, most synthetic scaffolds have poor cell adhesions, thus they do not interact with a tissue in an active manner.

PGA is formed from ring opening polymerization of glycolide. When subjected to a catalytic polymerization process, alpha glycosides polymerize to form high molecular weight of PGA (Hutmacher, Goh et al. 2001). Since PGA is a rigid thermoplastic material with high crystallinity, it has a high meting point of 225 °C, and

low solubility in most organic solvents except highly fluorinated organic solvents such as hexafluoro or propanol (Gunatillake and Adhikari 2003). However, fabricated PGA into the porous scaffolds has strong mechanical properties initially with biocompatibility. Although PGA has a high crystallinity, its degradation product glycolic acid is a natural metabolite. A major application of PGA is synthetic bioresorbable sutures (Dexon, American Cyanamide Co). However, PGA scaffolds have a significant decrease in mechanical strength due to the bulk of mass loss. To increase its utility and control the degradation time, PGA is often used as a co-polymer with poly (L-lactic acid) or PLA (Falco, Patel et al. 2008).

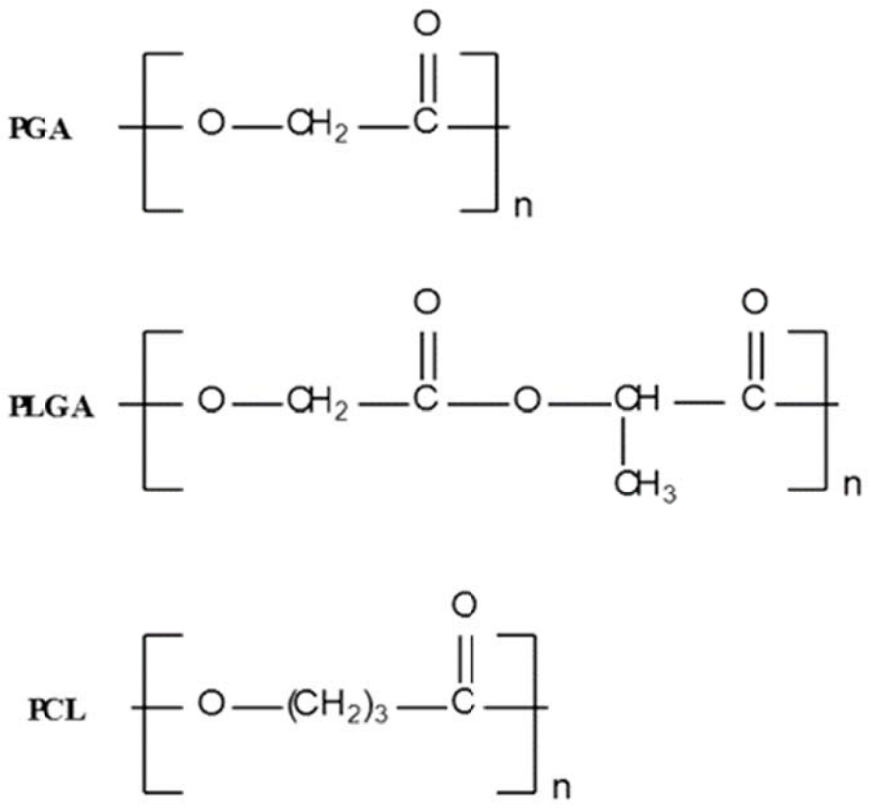

Figure 2.3.Chemical structures of synthetic polymers.

PLGA is a semi-crystalline synthetic polymer and formed by copolymerization of glycolic acid and lactic acid. Since degradation rate is a function of its lactide-to-glycolide acid ratio and more percentages of glycolic acid increase degradation rate, different ratios of PLA and PGA have been explored to regulate biological properties for different purposes in biomedical applications. PLGA scaffolds are widely used for delivery systems of long-term applications such as vaccines, drugs, genetic materials, and its biocompatibility makes it one of the main choices (Sousa, Luzardo-Alvarez et al. 2010). Amorphous 50:50 PLGA (50% lactic acid, 50% glycolic acid) is preferred for various tissue engineering applications because it degrades faster than other co-polymer ratios (Lawrence, Maase et al. 2009).

PCL is a semi-crystalline linear resorbable aliphatic polyester and relatively inexpensive relative to biomedical grade PLGA. PCL membranes formed after dissolving in chloroform show elongation up to 1000% before breaking. PCL is subjected to biodegradation because of the susceptibility of its aliphatic ester linkage to hydrolysis. PCL is explored in forming various medical devices (van der Giessen, Lincoff et al. 1996), templates in tissue regeneration (Htay, Teoh et al. 2004; Li, Cooper et al. 2006), and drug delivery systems (Aliabadi, Mahmud et al. 2005). PCL scaffolds can be restricted because its degradation and resorption rates are considerably slower than other aliphatic polyesters due to its hydrophobic character and high crystallinity. However, degradation properties and mechanical properties can be altered by blending low MW with high MW PCL as low MW has faster degradation rate(Pitt, Gratzl et al. 1981). Nevertheless, similar to all synthetic polymers, PCL might not be useful for the scaffold

independently because of their poor wettability and the lack of support for cellular activity.

2.2.3. Hybrid Polymers.

There are limitations of current synthetic and natural material for the tissue regeneration applications. Although natural polymers have the advantages of promoting cell adhesion and repopulation by providing critical signals, their mechanical properties may not be suitable for all tissue regeneration applications. In contrast synthetic materials have strong mechanical properties, and easiness of controlling microstructure and degradation rate, they lack the attachment domains and cellular signals that direct cell growth, proliferation, and differentiation (Xue and Greisler 2003). For instance, although bladder cells may show biocompatibility with synthetic materials *in vitro* (Elbahnasy, Shalhav et al. 1998; Pattison, Wurster et al. 2005), historically, the incorporation of synthetic materials into the bladder has met with failure due to biomechanical failure or biological incompatibility (Elbahnasy, Shalhav et al. 1998). Therefore, hybridization of natural and synthetic polymers can combine their respective advantages in order to exploit the benefits of each polymer while minimizing the weaknesses. Several types of hybridization methods are involved. Examples of these methods are shown in the **table 2.2**: (i) *blending*; polymers are blended physically without forming chemical bonds using solvents (e.g. chloroform, benzene, and methylene chloride), and matrices are formed by freezing and lyophilization method. (Moshfeghian, Tillman et al. 2006; Sarasam, Samli et al. 2007), (ii) *coating* with other materials; natural matrices are coated on the surface of synthetic scaffolds by submerging or spraying methods (Pankajakshan, Philipose et al. 2008; Sahoo, Toh et al. 2010), (iii) *copolymerizing* by modifying the surface of a polymer

structure or forming multiple block monomers and then polymerizing the whole matrix (Kubinova, Horak et al. 2009), and (ix) *multi-layering;* different types of scaffolds are sandwiched and tightened through the holes or perforations (Lawrence, Maase et al. 2009; Francis, Meng et al. 2010).

Table 2.2. Examples of hybridization methods.

Method	Material	Cell Sources	Characteristics
Blending	Chitosan - PLGA	Smooth muscle cells (SMCs)	• Controlled pore morphology • Altered degradation kinetic
Surface coating	Fibrin – Poly (ε-caprolactone)	Human umbilical vein endothelial cells (HUVEC)	• Developed porous structure • Improved mechanical property and cellular activity
Copoly-merizing	Cholesterol-Poly(2-hydroxyethyl methacrylate)	Mesenchmal stem cells (MSCs)	• Improved cell adhesion and proliferation
Multi-layering	Chitosan – PLGA	Mouse embryonic fibroblasts (MEFs)	• Mimicked SIS • Improved cellular activity • Substantially degraded after 8 weeks

2.2.4. Scaffolds Fabrications.

A number of fabrication techniques have been investigated to process porous scaffolds (**Figure 2.4**), including textile technologies, solvent casting/particulate leaching, freeze-drying (or lyophilization), solid free form and electrospining. PGA fibrous scaffolds have been formed using textile processing techniques, which involves sufficient structural integrity to maintain dimensions when seeded with isolated cartilage cells (Freed, Vunjak-Novakovic et al. 1994). Another method to fabricate porous scaffolds is to introduce porogen such as salt (NaCl) into the particulate leaching process. The leaching of salt from PLLA polymer allows to form pores within scaffolds, the pore sizes are dependent on the size and amount of salt crystals and are difficult to control(Lee, Kim et al. 2004). Natural polymers such as gelatin, chitosan, or blends can be fabricated simply using lyophilization process (Shapiro and Cohen 1997; Madihally and Matthew 1999; Ma, Wang et al. 2001).

Another technique to form porous scaffolds is using solid free form fabrication (SFF), also known as rapid prototyping (RP). RP is the process of creating a three-dimensional object through repetitive deposition and processing of material layers using computer-aided-design (CAD) model of the object. There are several RP systems developed such as stereolitography, selective laser sintering (SLS), laminated object manufacturing (LOM), three-dimensional printing (3-DP), and fused deposition modeling (FDM). SFF allows exact control of the internal microstructure and tissue shape; however, problems such as residue removal and poor mechanical strength arise. The intertwining of SFF with other methods has promising potential to create optimized scaffolds (Hutmacher 2001).

Electrospining has also been explored recently for tissue engineering applications. Micro or nano scale fibers are formed using an electrical charge from a liquid. This technique provides easily applicable nano-sized structures with the high surface area of the fibers (Jin, Fridrikh et al. 2002). However, the general electrospining has been limited to the fabrication of a variety of anisotropic mechanical properties, which are important factors for designing a muscular or skeletal system (Kim 2008). The mechanical properties are poor due to an increased pore size and porosity.

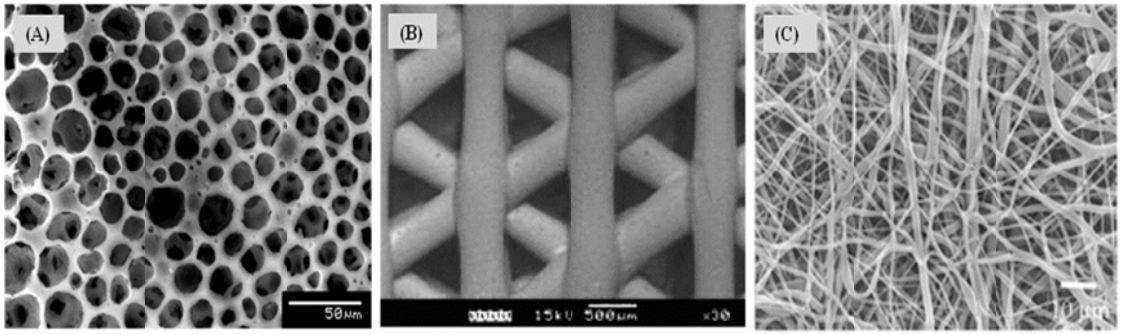

Figure 2.4. PCL matrices with different fabrication method formed by (A)solvent casting, (B) rapidprototyping (Hoque, Hutmacher et al. 2005), and (C) electrospining (Hiep and Lee 2010).

2.2.4. Scaffolds Properties.

Scaffolds used for tissue regeneration applications need to serve as biomaterials to promote cell colonization and cell growth. There are some studies where cells were implanted directly into desired locations to be regenerated. One of the examples is that healthy chondrocytes cells from cartilage obtained from an uninvolved area of the injured knee were isolated and cultured in the laboratory for 14 to 21 days, and the cultured chondrocytes were then injected into the area of the defect (Brittberg, Lindahl et al. 1994).

However, for the most cases of direct injections, implanted cells cannot be controlled by their desirable locations. Further, the majority of mammalian cell types are anchorage-dependent and will die, if cell substrates are not provided (Kim, Baez et al. 2000). In this reason, scaffolds (**Figure 2.5**) should be biocompatible and biodegradable with the possessions of appropriate mechanical properties and specific configurations, those allow the initial cell attachment and colonization and provide all the signals that are needed for cell growth, differentiation, and cell interaction (Li, Laurencin et al. 2002).

Scaffolds have to provide appropriate mechanical properties to resist *in vivo* forces temporarily, and maintain mechanical support until tissues are structurally stabilized by themselves during regeneration process. This could potentially be achieved by an appropriate choice of mechanical and degradable properties of the biomaterials (Kim and Mooney 1998). Since, most of naturally derived polymers lack the mechanical strength as used in tissue and organ applications, they are often blended or multi-layered with synthetic materials, e.g. chitin/PLGA blend scaffold (Mi, Lin et al. 2002) and Chitosan/PLGA multi composite scaffold (Lawrence, Maase et al. 2009).

Another important consideration of tissue engineered scaffolds to regulate cell behavior is their structural configurations such as pore size, porosity, topography, and scaffold stiffness, because these factors promote tissue in-growth from the surrounding host tissue. For instance, a large surface-area-to-volume ratio is often desirable, as it allows the delivery of a high density of cells (Kim, Baez et al. 2000). Several techniques have been explored to control porosity, pore size, and porous structure.

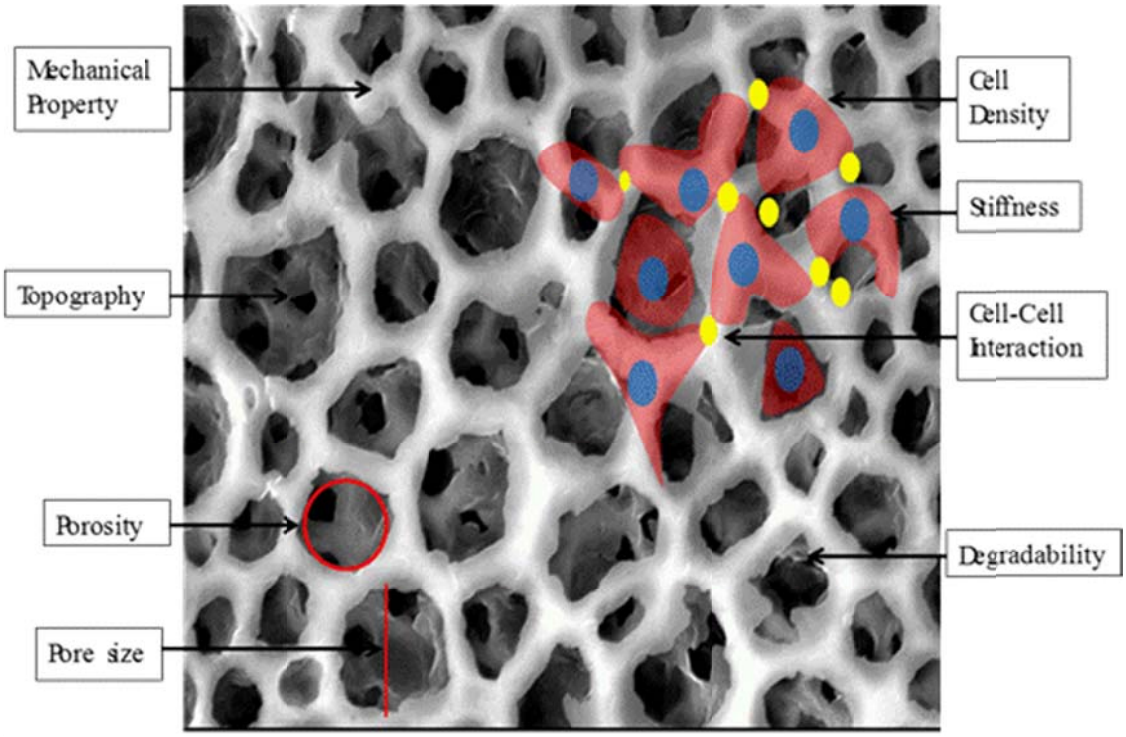

Figure 2.5. Requirements for adequate scaffolds, modified from (Owen and Shoichet 2010).

Pore size is a spatial element to support cell in-growth, migration, and morphology. Uniform distribution of cells and improvement of seeded cell density can be achieved by employing the porous scaffold with the adequate pore size. Inappropriate pore size ranges lead to failure in the initial network formation or cell spreading. Thus, scaffold pore sizes can be exclusive and highly depend on the cell types (Leong, Chua et al. 2008).For example, 3T3 fibroblast cells (ATCC) with cell size of 20 to 50 μm can bridge greater pores than endothelial cells (ECACC) with cell size of 60 to 200 μm. Fibroblasts can span void spaces up to 200 μm, while endothelial cells can only bridge pores with 30 to 80 μm (Salem, Stevens et al. 2002). Determination method of the pore size is still an essential tool. Scanning electron microscopy (SEM) is widely used for

taking surface images of porous structures. However, SEM images cannot prove three dimensional architectures and connectivity inside of scaffolds. Historically, the pore size distributions of materials have been measured by mercury intrusion porosimetry(MIP), which applies the Washburn equation to changes in capacitance as it is forced into the scaffolds as a function of pressure (Jones, Atwood et al. 2009).

Porosity also is an important factor that regulates cell and matrix interactions, and this is the commonest parameter to describe the scaffold network. The porosity is a measure of the average void volume fraction in a specific region of porous medium (Truskey, Yuan et al. 2004). Scaffolds with high porosity (around 90%) provides a high surface area for cell-matrix interactions, sufficient space for ECM regeneration uniform cell seeding, and better cell colonization (Agrawal and Ray 2001; Zeltinger, Sherwood et al. 2001). Pore interconnectivity increases the overall surface area for cell attachment and facilitates cell in-growth in the scaffolds. Increased interconnectivity and porosity also affect the deposition of ECM elements (Miot, Woodfield et al. 2005).In addition, by controlling the scaffold porosity and pore-interconnection, suitable flow channels for the scaffold can be designed as to result in the appropriate transport of nutrients and wastes and cellular signals for proper tissue regeneration (Sun, Darling et al. 2004).

Topography also has been found to influence cell morphology and phenotypic expression due to the difference in cell size and cell-matrix adhesion mechanism (Nehrer, Breinan et al. 1997; Salem, Stevens et al. 2002). Especially, surface roughness characteristics and hydrophilicity have an important role in the regulations of cell attachment, cell spreading, and ECM deposition. Further, different cell types respond differently to the same surface property (Singhvi, Stephanopoulos et al. 1994). For

example, human gingival fibroblasts (HGF) were seeded on ceramic discs with varied roughness factor by polishing. Significantly more cells were attached on the rougher surface (around 90nm of roughness factor) rather than polished surface (around 3nm of roughness factor) (Mustafa, Oden et al. 2005). However, the optimal mechanisms for the interaction between surface roughness and cell behavior have not completely determined yet.

Stiffness of the scaffold has a significant effect on cellular activity besides porous characteristics. Young's modulus (*E*) can be used to measure the stiffness by calculations from the slope of the linear portion of the stress-strain curve in the specific range of stress. The bulk stiffness controls the overall deformation of the scaffold while each individual cell with encounter the stiffness of the individual fibers during cell colonization (Lawrence and Madihally 2008). Maximum contractile force generated by cross-bridging interactions of actin and myosin filaments could be as much as 10-15% of substrate modulus (Lo, Wang et al. 2000; Discher, Janmey et al. 2005). Effect of the different scaffold stiffness (0.001 to 1000 MPa) on cell differentiations of three cell types (Fibroblasts, chondrocytes, osteoblasts) has been characterized (Khayyeri, Checa et al. 2010). This result shows that percentages of cell differentiation of chondrocytes and osteoblasts were increased by increasing scaffold stiffness whereas fibroblasts differentiation was decreased significantly. Hence, it is apparent that determining the adequate scaffold stiffness is also crucial factor to understand better cellular activity.

2.3. Cellular Activity.

Cells are the functional elements of repair and regeneration. Successful tissue regeneration depends on the ability of cells to populate the porous structure and synthesize appropriate extracellular matrix elements. Colonized cells proliferate and differentiate to an appropriate phenotype or function (Nancy 2003). For that reason, the ability to control cell proliferation and differentiation is one of the important aspects of cellular tissue engineering. The scaffold can be considered as the part of structural support for cells, nutrient supply for cells, and functional control of cells. Many potential scaffolds have been tried, but the ability to define critical biomaterial properties on the basis of specific tissue engineering applications and on a mechanistic understanding of how cells interact with scaffolds is still in its infancy (Wood and Southgate 2008). To select appropriate scaffolds for tissue engineering, the influence of the materials on cellular viability, growth and function should be understood. For this purpose, cells from appropriate region are seeded and tested in the generated scaffolds for utility in tissue engineering.

2.4. Bladder Tissue Regeneration.

Regeneration of the bladder is utilized as a paradigm in this study. Functions of the urinary bladder are to store urine at low pressure and to empty urine while maintaining chemical gradients between urine and blood. Both these functions are inherently mechanical and, in essence, the bladder is a pressure vessel subjected to significant stresses during filling and voiding (Korossis, Bolland et al. 2006). Cellular and extracellular components come up with those functions. The cross-sectional view of

the bladder structure is shown in the **Figure 2.6**. In terms of cellular components, urothelial cells form a multi-layered, specialized epithelium that serves as an effective blood-urine permeability barrier. The smooth muscle cells are responsible for accommodating bladder filling at low pressure and contract during emptying. Extracellular components consist of collagens, proteoglycans, and glycosaminoglycans; this matrix serves as a reservoir for growth factors and profoundly influences cell growth, differentiation, development, and metabolic responses (Wallis, Yeger et al. 2008).

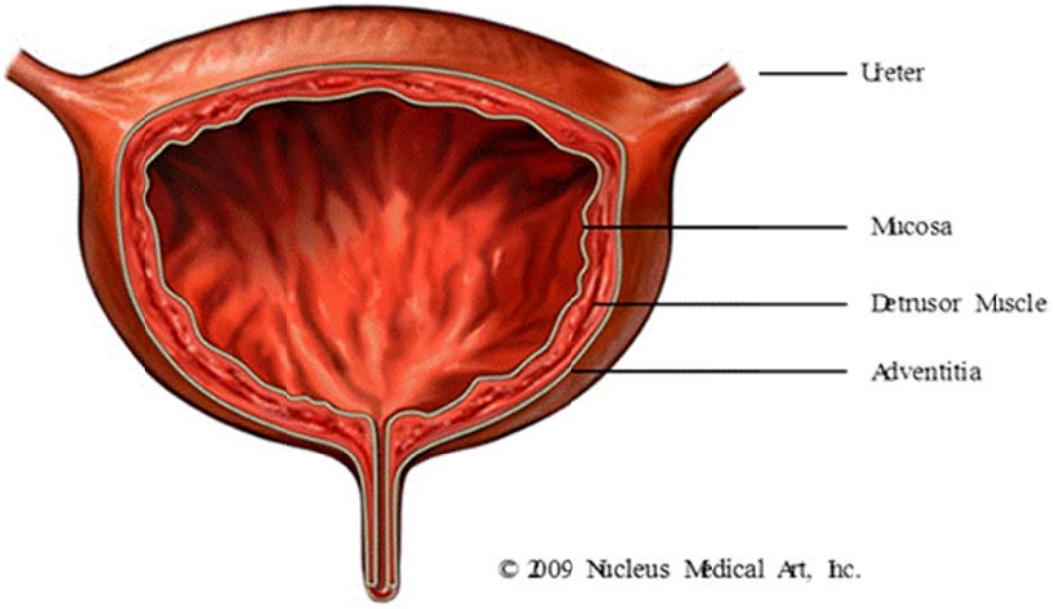

Figure 2.6.The cross-sectional view of the urinary bladder.

The development of organ replacement therapy through cell culture, tissue construction and implantation has attracted considerable attention from life and materials scientists, clinicians and engineers (Dan Wood 2008). Naturally occurring materials have often been used to repair the bladder when it has been disrupted due to such resection, trauma, infection, inflammation, or any number of other conditions, such as bladder allografts, dura, placenta, and pericardium (Tsuji, Ishida et al. 1961; Kelami, Ludtke-Handjery et al. 1970; Fishman IJ 1987; Kambic, Kay et al. 1992; Falke, Caffaratti et al. 2000). However, these materials have met failure mainly due to mechanical failure and poor biocompatibility properties. Hence, recent studies have focused on synthetic materials for bladder reconstruction. Synthetic materials which are widely used in experimental and clinical settings include poly(lactide-co-glycolide) (PLGA), polyvinyl sponges, polytetraflouroethylene (Teflon), gelatin sponge, collagen matrices, silicone, resin-spayed paper, and polyglactin 910 (Vicryl) matrices (Kudish 1957; Bono and De Gresti 1966; Fujita 1979; Monsour, Mohammed et al. 1987; R. Gonzalez 1995; Rohrmann, Albrecht et al. 1996). Using pure natural or synthetic materials does not fulfill necessary requirements (as described above) and hence, combining two polymeric systems would be an ideal solution.

A biodegradable composite scaffold made of collagen and PGA (a material used as a mesh for hernia repair; Sherwood Medical, St Louis, MO, USA) was shaped like a bladder (**Figure 2.7.**) with polyglycolic sutures (Atala, Bauer et al. 2007). However, they have uneven thickness due to wrinkling and overlap. Further, the quality of the regenerated tissue is dependent on the surgeons' ability to mold. Thus, it is important to develop anatomical relevant scaffolds appropriate to regenerating a specific tissue.

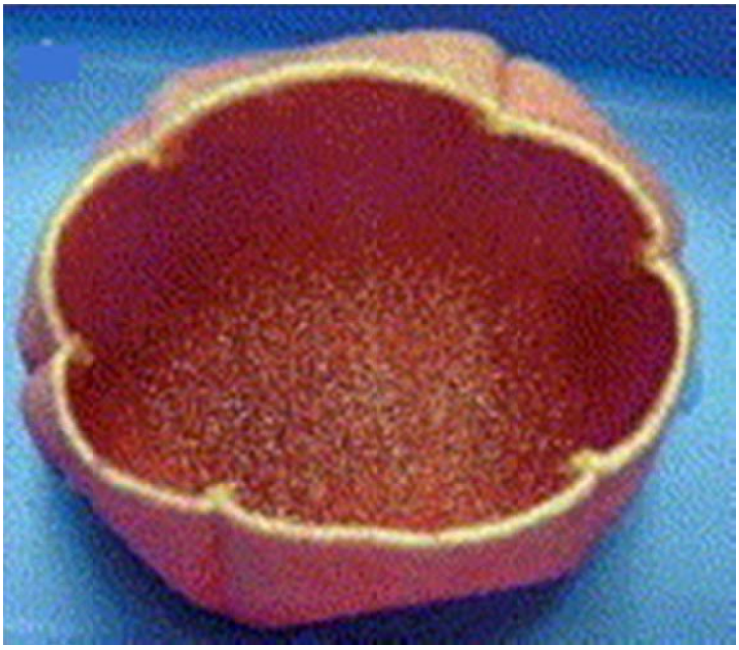

Figure 2.7. Bladder shape of collagen-PGA composite scaffolds (Atala, Bauer et al. 2007).

2.5. Bioreactor.

Bioreactors play a critical role in tissue engineering, not only because they reproduce and control changes in specific environmental factors (e.g. pH, temperature, oxygen, nutrient transfer and waste elimination) for the growth of tissue substitutes, but also because they enable systematic studies of the responses of living tissues to various mechanical and biochemical cues(Chen and Hu 2006). Bioreactors are utilized for a variety of diverse applications, such as: (i) cell expansion on both a small scale for individual patient and a large scale for multi-patient scale, (ii) production of three dimensional tissues from dissociated isolated cells in vitro, and (iii) directly as organ support devices (Shachar and Cohen 2003). However, many bioreactors were designed for two dimensional structures with small scales and disc shapes. Bioreactors with

reasonably sized scale and mimicked anatomic porous scaffolds or direct organ cultivation have not been completely understood yet. For tissue engineering to be an active manner in vitro cultivation of the engineered tissues, bioreactors should be developed in many applications to convince their requirements presented by the wide variety of desired tissue types (Martin and Vermette 2005).

Bioreactors of different configurations, which are important during in vitro maturation of cell seeded scaffolds, have been explored for in vitro tissue regeneration. Among different reactor configurations, the flow through reactor is better suited for regenerating high aspect ratio tissues due to following advantages(Lawrence, Devarapalli et al. 2009): (a) supports uniformly which prevents deformation of the scaffold, (b) continuous flow replenishes the nutrients while providing better control on hydrodynamic shear stress induced by the fluid flow, and (c) easy scaled-up to clinical requirement. The suitable bioreactor for large scale cultivation should be chosen carefully by considering bioreactor configurations with operating conditions and designs, since cell morphology influences the effect of different bioreactor configurations on cell growth and maturation (Ingram and Mavituna 2000).

One of the critical requirements for bioreactors is a mass transfer involvement such as nutrient supply and waste elimination. The most popular approach is the use of tissue culture plastic with cell seeded scaffolds along the growth medium. However, this traditional system has a limitation as they do not have their own blood system and the cells are only supplied by diffusion. Even though oxygen supply by only diffusion is sufficient for cell layers of 100-200 μm, in a reactor environment, as tissues gain on size, mass transfer has to be increased (Portner, Nagel-Heyer et al. 2005). For example, in

vitro grown chondrocyte-poly(glycolic acid) (PGA) constructs were reported to lose their diffusional permeability to up to 97% of its initial value after 4 weeks, proportionally to the quantity of extracellular matrix (ECM) deposited on the construct (Bursac, Freed et al. 1996). Further, solubility of oxygen in the culture medium is poor and limited to maximum solubility of 0.2 mol O_2/m^3. Hence mass transfer should be continually provided and recirculated through the inner and outer area of porous scaffolds using bioreactors. Nutrient transfer can be explained with diffusion and convective flow and their dominants can be changed by the location of scaffold and channel size in the reactor. Diffusion or convection dominants can be assessed by determining *Peclet number*.

$$Pe = \frac{Vr}{D_{O_2}} \tag{1}$$

where V is the velocity, r is a radius of the scaffold, and D_{O2} is the diffusion coefficient of oxygen. A Pe number between 0 and 1 indicates that the specific bioreactor configuration has a diffusion dominant mass transfer, otherwise, convection dominant.

Since the nutrient consumption is governed by diffusion rather than convection, it is important to accommodate the diffusive characteristics of nutrients through the porous structure. The change in effective diffusivity (D_{eff} in m^2/s) due to altered void fraction in the porous structure can be calculated using Mackie-Meares relationship (Mackie and Meares 1955; Mackie and Meares 1955; Sengers, van Donkelaar et al. 2005).

$$D_{effe} = D_{\infty}\left[\frac{\phi}{2-\phi}\right]^2 \tag{2}$$

where D_{∞} is the diffusion coefficient from Stokes-Einstein equation, and Φ is the porosity of the scaffold. Mackie-Meares model is based on the lattice model for liquids and

assumes that the polymer fibers are of the same size as the solutes and the polymer network only blocks the pathway of solutes without affecting their mobility.

Most cell types used in mammalian tissue engineering respond to hydrodynamic stress referred as shear stress. Since, hydrodynamic shear force influences cellular alignment (Huang, Onyeri et al. 2005; Waters, Cummings et al. 2006) in the flow direction (Gray, Pizzanelli et al. 1988; Takahashi and Berk 1996; Huang, Onyeri et al. 2005), fluid path helps align the cell in the required direction. Each different type of cells has their own maximal sustainable shear stresses. For example, heart valve leaflets have to sustain temporary shear stress in the range of 0.9 to 2.2 Pa (Weston, LaBorde et al. 1999), for the mammalian cell line, low shear stress of 1.0 Pa were found to be just as damaging as high shear stress of 100 Pa, and maximal sustainable shear stress was around 10 Pa (Mardikar and Niranjan 2000). Maximal sustainable shear stress of smooth muscle cells was around 2.5 Pa, and cell growth was significantly slower at the higher stress values (Papadaki, McIntire et al. 1996). Although these results have benefits to understand the effects of the shear stress on cell growth, however, the results were examined using small scale tissues. Since the requirements for large scale tissues or 3D culture of cells are different with a small size, a monolayer, or a 2D culture (Cukierman, Pankov et al. 2001), more studies should be conducted to understand effects of hydrodynamic stimuli.

More detailed description of bioreactor designs, complete fluid flow through reactors and porous media, and hydrodynamic forces can be characterized by using computational fluid dynamics (CFD). Further, CFD is possible to keep track the variable parameters, which need to be adjusted followed by matrix deposition, cell differentiation,

and proliferation, also can be predicted for the optimized environments. Computational simulations have simplified mathematical models and reduced scaffold size due to increased computational demand in simulating reactors suitable for clinical transplantation. Also, the kinetic models are over-simplified by ignoring the mass and structural complexities. Therefore, CFD is an invaluable tool that enables a better understanding of the implications of fluid flow and transport on cell function and provides important insights into the design and optimization of three dimensional scaffolds (Hutmacher and Singh 2008).

Previously, our group members have simulated circular shapes of bioreactors, and characterized the non-ideal fluid distribution using the residence time distribution (RTD) (Lawrence, Devarapalli et al. 2009), optimized nutrient distribution environments for several types of cells (Devarapalli, Lawrence et al. 2009). Also, several types of bioreactor designs for artificial blood vessels or cardiovascular tissues have been introduced, include a bioreactor for heart valve leaflets (Mol, Driessen et al. 2005), artery (Iwasaki, Kojima et al. 2008), and vascular tissue (Sodian, Lemke et al. 2002). These studies benefit for the tissue regeneration process, since there are significant amounts of fundamental studies of in vivo and in vitro conditions for these applications. However, cultivation systems for complex structure such as organs have not been understood. Hence CFD analyses for the bioreactor design with mimicking anatomic structures or real organs can enhance a suitability of real bioreactors for tissue regeneration. In this study, main consideration is to mimic a real bladder structure of synthetic scaffold and construct cell cultivation system.

2.6. References.

Agrawal, C. M. and R. B. Ray (2001). "Biodegradable polymeric scaffolds for musculoskeletal tissue engineering." J Biomed Mater Res **55**(2): 141-150.

Aliabadi, H. M., A. Mahmud, et al. (2005). "Micelles of methoxy poly(ethylene oxide)-b-poly(epsilon-caprolactone) as vehicles for the solubilization and controlled delivery of cyclosporine A." J Control Release **104**(2): 301-311.

Bono, A. V. and A. De Gresti (1966). "[Partial substitution of the bladder wall with teflon tissue. (Preliminary and experimental note on the impermeability and tolerance of the prosthesis)]." Minerva Urol **18**(2): 43-47.

Brittberg, M., A. Lindahl, et al. (1994). "Treatment of deep cartilage defects in the knee with autologous chondrocyte transplantation." N Engl J Med **331**(14): 889-895.

Bursac, P. M., L. E. Freed, et al. (1996). "Mass transfer studies of tissue engineered cartilage." Tissue Eng **2**(2): 141-150.

Chen, H.-C. and Y.-C. Hu (2006). "Bioreactors for tissue engineering." biotechnol Lett **28**(18): 1415-1423.

Choi, B. K., K. Y. Kim, et al. (2001). "In vitro antimicrobial activity of a chitooligosaccharide mixture against Actinobacillus actinomycetemcomitans and Streptococcus mutans." Int J Antimicrob Agents **18**(6): 553-557.

Cukierman, E., R. Pankov, et al. (2001). "Taking cell-matrix adhesions to the third dimension." Science **294**(5547): 1708-1712.

Dan Wood, J. S. (2008). "Current status of tissue engineering in urology." Current Opinion in Urology **18**: 564-569.

Devarapalli, M., B. J. Lawrence, et al. (2009). "Modeling Nutrient Consumptions in Large Flow-Through Bioreactors for Tissue Engineering." Biotechnology and Bioengineering **103**(5): 1003-1015.

Dhandayuthapani, B., U. M. Krishnan, et al. (2010). "Fabrication and characterization of chitosan-gelatin blend nanofibers for skin tissue engineering." J Biomed Mater Res B Appl Biomater **94**(1): 264-272.

Discher, D. E., P. Janmey, et al. (2005). "Tissue cells feel and respond to the stiffness of their substrate." Science **310**(5751): 1139-1143.

Elbahnasy, A. M., A. Shalhav, et al. (1998). "Bladder wall substitution with synthetic and non-intestinal organic materials." The Journal Of Urology **159**(3): 628-637.

Falco, E. E., M. Patel, et al. (2008). "Recent developments in cyclic acetal biomaterials for tissue engineering applications." Pharmaceutical Research **25**(10): 2348-2356.

Falke, G., J. Caffaratti, et al. (2000). "Tissue engineering of the bladder." World J Urol **18**(1): 36-43.

Fishman IJ, F. F., Scott B, Apjut HJ, Morrow B (1987). "Use of fresh placental membranes for bladder reconstruction." J Urol **138**: 1291.

Francis, L., D. Meng, et al. (2010). "Multi-functional P(3HB) microsphere/45S5 Bioglass-based composite scaffolds for bone tissue engineering." Acta Biomater **6**(7): 2773-2786.

Freed, L. E., G. Vunjak-Novakovic, et al. (1994). "Biodegradable polymer scaffolds for tissue engineering." Biotechnology (N Y) **12**(7): 689-693.

Fujita, K. (1979). "The use of resin-aprayed thin paper for urinary bladder regeneration." Investig Urol (Berl) **15**: 355.

Gray, M. L., A. M. Pizzanelli, et al. (1988). "Mechanical and Physicochemical determinants of the chondrocyte biosynthetic response." Journal of Orthopaedic Research **6**(6): 777-792.

Gunatillake, P. A. and R. Adhikari (2003). "Biodegradable synthetic polymers for tissue engineering." Eur Cell Mater **5**: 1-16; discussion 16.

Hiep, N. T. and B.-T. Lee (2010). "Electro-spinning of PLGA/PCL blends for tissue engineering and their biocompatibility." J Mater Sci Mater Med **21**(6): 1969-1978.

Hoque, M. E., D. W. Hutmacher, et al. (2005). "Fabrication using a rapid prototyping system and in vitro characterization of PEG-PCL-PLA scaffolds for tissue engineering." J Biomater Sci Polym Ed **16**(12): 1595-1610.

Htay, A. S., S. H. Teoh, et al. (2004). "Development of perforated microthin poly(epsilon-caprolactone) films as matrices for membrane tissue engineering." J Biomater Sci Polym Ed **15**(5): 683-700.

Hu, M., M. Kurisawa, et al. (2009). "Cell immobilization in gelatin-hydroxyphenylpropionic acid hydrogel fibers." Biomaterials **30**(21): 3523-3531.

Huang, Y., S. Onyeri, et al. (2005). "In vitro characterization of chitosan-gelatin scaffolds for tissue engineering." Biomaterials **26**(36): 7616-7627.

Hutmacher, D. W. (2001). "Scaffold design and fabrication technologies for engineering tissues--state of the art and future perspectives." J Biomater Sci Polym Ed **12**(1): 107-124.

Hutmacher, D. W., J. C. Goh, et al. (2001). "An introduction to biodegradable materials for tissue engineering applications." Annals Of The Academy Of Medicine, Singapore **30**(2): 183-191.

Hutmacher, D. W. and H. Singh (2008). "Computational fluid dynamics for improved bioreactor design and 3D culture." Trends Biotechnol **26**(4): 166-172.

Ingram, B. and F. Mavituna (2000). "Effect of bioreactor configuration on the growth and maturation of Picea sitchensis somatic embryo cultures." Plant Cell, Tissue and Organ Culture **61**(2): 87-96.

Ishihara, M., K. Obara, et al. (2006). "Chitosan hydrogel as a drug delivery carrier to control angiogenesis." J Artif Organs **9**(1): 8-16.

Iwasaki, K., K. Kojima, et al. (2008). "Bioengineered three-layered robust and elastic artery using hemodynamically-equivalent pulsatile bioreactor." Circulation **118**(14): S52-S57.

Jin, H.-J., S. V. Fridrikh, et al. (2002). "Electrospinning Bombyx mori silk with poly(ethylene oxide)." Biomacromolecules **3**(6): 1233-1239.

Joesten, M. D., and Wood, J. L. (1996). The world of chemistry. Fort Worth, TX.

Jones, J. R., R. C. Atwood, et al. (2009). "Quantifying the 3D macrostructure of tissue scaffolds." J Mater Sci Mater Med **20**(2): 463-471.

Kambic, H., R. Kay, et al. (1992). "Biodegradable pericardial implants for bladder augmentation: a 2.5-year study in dogs." J Urol **148**(2 Pt 2): 539-543.

Kelami, A., A. Ludtke-Handjery, et al. (1970). "Alloplastic replacement of the urinary bladder wall with lyophilized human dura." Eur Surg Res **2**(3): 195-202.

Khayyeri, H., S. Checa, et al. (2010). "Tissue differentiation in an in vivo bioreactor: in silico investigations of scaffold stiffness." J Mater Sci Mater Med **21**(8): 2331-2336.

Kim, B. S., C. E. Baez, et al. (2000). "Biomaterials for tissue engineering." World J Urol **18**(1): 2-9.

Kim, B. S. and D. J. Mooney (1998). "Development of biocompatible synthetic extracellular matrices for tissue engineering." Trends Biotechnol **16**(5): 224-230.

Kim, G. H. (2008). "Electrospun PCL nanofibers with anisotropic mechanical properties as a biomedical scaffold." Biomed Mater **3**(2): 025010.

Korossis, S., F. Bolland, et al. (2006). "Tissue Engineering of the Urinary Bladder: Considering Structure-Function Relationships and the Role of Mechanotransduction." Tissue Eng **12**(4): 635-644.

Kubinova, S., D. Horak, et al. (2009). "Cholesterol-modified superporous poly(2-hydroxyethyl methacrylate) scaffolds for tissue engineering." Biomaterials **30**(27): 4601-4609.

Kudish, H. G. (1957). "The use of polyvinyl sponge for experimental cytoplasty." J Urol **78**: 232-235.

Lai, C. Z., S. S. Koseoglu, et al. (2009). "Fluorous polymeric membranes for ionophore-based ion-selective potentiometry: how inert is Teflon AF?" J Am Chem Soc **131**(4): 1598-1606.

Lawrence, B. J., M. Devarapalli, et al. (2009). "Flow dynamics in bioreactors containing tissue engineering scaffolds." Biotechnology and Bioengineering **102**(3): 935-947.

Lawrence, B. J., E. L. Maase, et al. (2009). "Multilayer composite scaffolds with mechanical properties similar to small intestinal submucosa." Journal Of Biomedical Materials Research. Part A **88**(3): 634-643.

Lawrence, B. J. and S. V. Madihally (2008). "Cell Colonization in Degradable 3D Porous Matrices." Cell Adhesion and Migration **2**(1): 1-8.

Lee, S.-H., B.-S. Kim, et al. (2004). "Thermally produced biodegradable scaffolds for cartilage tissue engineering." Macromol Biosci **4**(8): 802-810.

Leong, K. F., C. K. Chua, et al. (2008). "Engineering functionally graded tissue engineering scaffolds." J Mech Behav Biomed Mater **1**(2): 140-152.

Li, P., X. Feng, et al. (2010). "Influences of tensile load on in vitro degradation of an electrospun poly(L-lactide-co-glycolide) scaffold." Acta Biomater **6**(8): 2991-2996.

Li, W.-J., C. T. Laurencin, et al. (2002). "Electrospun nanofibrous structure: a novel scaffold for tissue engineering." J Biomed Mater Res **60**(4): 613-621.

Li, W. J., J. A. Cooper, Jr., et al. (2006). "Fabrication and characterization of six electrospun poly(alpha-hydroxy ester)-based fibrous scaffolds for tissue engineering applications." Acta Biomater **2**(4): 377-385.

Lo, C. M., H. B. Wang, et al. (2000). "Cell movement is guided by the rigidity of the substrate." Biophys J **79**(1): 144-152.

Mackie, J. S. and P. Meares (1955). "Diffusion in a cation exchanger resin I." Proc. R. Soc **232**(A): 448-495.

Mackie, J. S. and P. Meares (1955). "Diffusion in a cation exchanger resin II." Proc. R. Soc **232**(A): 495-505.

Madihally, S. V. and H. W. Matthew (1999). "Porous chitosan scaffolds for tissue engineering." Biomaterials **20**(12): 1133-1142.

Mao, J., L. Zhao, et al. (2003). "Study of novel chitosan-gelatin artificial skin in vitro." J Biomed Mater Res **64A**(2): 301-308.

Mardikar, S. H. and K. Niranjan (2000). "Observations on the shear damage to different animal cells in a concentric cylinder viscometer." Biotechnol Bioeng **68**(6): 697-704.

Martin, Y. and P. Vermette (2005). "Bioreactors for tissue mass culture: Design, characterization, and recent advances." Biomaterials **26**(35): 7481-7503.

Mei, N., G. Chen, et al. (2005). "Biocompatibility of Poly(epsilon-caprolactone) scaffold modified by chitosan--the fibroblasts proliferation in vitro." J Biomater Appl **19**(4): 323-339.

Mi, F. L., Y. M. Lin, et al. (2002). "Chitin/PLGA blend microspheres as a biodegradable drug-delivery system: phase-separation, degradation and release behavior." Biomaterials **23**(15): 3257-3267.

Middleton, J. C. and A. J. Tipton (2000). "Synthetic biodegradable polymers as orthopedic devices." Biomaterials **21**(23): 2335-2346.

Mol, A., N. J. B. Driessen, et al. (2005). "Tissue engineering of human heart valve leaflets: A novel bioreactor for a strain-based conditioning approach." Annals of Biomedical Engineering **33**(12): 1778-1788.

Monsour, M. J., R. Mohammed, et al. (1987). "An assessment of a collagen/vicryl composite membrane to repair defects of the urinary bladder in rabbits." Urol Res **15**(4): 235-238.

Mooney, D. J., D. F. Baldwin, et al. (1996). "Novel approach to fabricate porous sponges of poly(D,L-lactic-co-glycolic acid) without the use of organic solvents." Biomaterials **17**(14): 1417-1422.

Moshfeghian, A., J. Tillman, et al. (2006). "Characterization of emulsified chitosan-PLGA matrices formed using controlled-rate freezing and lyophilization technique." J Biomed Mater Res A **79**(2): 418-430.

Mustafa, K., A. Oden, et al. (2005). "The influence of surface topography of ceramic abutments on the attachment and proliferation of human oral fibroblasts." Biomaterials **26**(4): 373-381.

Nancy, L. P. (2003). Cells. Tissue Engineering Research. L. V. M.**:** 23.

Nehrer, S., H. A. Breinan, et al. (1997). "Matrix collagen type and pore size influence behaviour of seeded canine chondrocytes." Biomaterials **18**(11): 769-776.

Owen, S. C. and M. S. Shoichet (2010). "Design of three-dimensional biomimetic scaffolds." Journal of Biomedical Materials Research Part A **94A**(4): 1321-1331.

Pangburn, S. H., P. V. Trescony, et al. (1982). "Lysozyme degradation of partially deacetylated chitin, its films and hydrogels." Biomaterials **3**(2): 105-108.

Pankajakshan, D., L. P. Philipose, et al. (2008). "Development of a fibrin composite-coated poly(epsilon-caprolactone) scaffold for potential vascular tissue engineering applications." J Biomed Mater Res B Appl Biomater **87**(2): 570-579.

Papadaki, M., L. V. McIntire, et al. (1996). "Effects of shear stress on the growth kinetics of human aortic smooth muscle cells in vitro." Biotechnol Bioeng **50**(5): 555-561.

Pattison, M. A., S. Wurster, et al. (2005). "Three-dimensional, nano-structured PLGA scaffolds for bladder tissue replacement applications." Biomaterials **26**(15): 2491-2500.

Pitt, C. G., M. M. Gratzl, et al. (1981). "Aliphatic polyesters II. The degradation of poly (DL-lactide), poly (epsilon-caprolactone), and their copolymers in vivo." Biomaterials **2**(4): 215-220.

Place, E. S., J. H. George, et al. (2009). "Synthetic polymer scaffolds for tissue engineering." Chem Soc Rev **38**(4): 1139-1151.

Portner, R., S. Nagel-Heyer, et al. (2005). "Bioreactor design for tissue engineering." J Biosci Bioeng **100**(3): 235-245.

R. Gonzalez, H. B., C. Reid, Y. Reinberg (1995). "Seromuscular colocystoplasty lined with urothelium (SCLU)." Urology **45**: 124.

Ren, D., H. Yi, et al. (2005). "The enzymatic degradation and swelling properties of chitosan matrices with different degrees of N-acetylation." Carbohydr Res **340**(15): 2403-2410.

Risbud, M. V., A. A. Hardikar, et al. (2000). "pH-sensitive freeze-dried chitosan-polyvinyl pyrrolidone hydrogels as controlled release system for antibiotic delivery." J Control Release **68**(1): 23-30.

Rohrmann, D., D. Albrecht, et al. (1996). "Alloplastic replacement of the urinary bladder." J Urol **156**(6): 2094-2097.

Sahoo, S., S. L. Toh, et al. (2010). "PLGA nanofiber-coated silk microfibrous scaffold for connective tissue engineering." J Biomed Mater Res B Appl Biomater **95**(1): 19-28.

Salem, A. K., R. Stevens, et al. (2002). "Interactions of 3T3 fibroblasts and endothelial cells with defined pore features." J Biomed Mater Res **61**(2): 212-217.

Sarasam, A. R., A. I. Samli, et al. (2007). "Blending chitosan with polycaprolactone: porous scaffolds and toxicity." Macromol Biosci **7**(9-10): 1160-1167.

Schantz, J.-T., D. W. Hutmacher, et al. (2002). "Evaluation of a tissue-engineered membrane-cell construct for guided bone regeneration." Int J Oral Maxillofac Implants **17**(2): 161-174.

Sengers, B. G., C. C. van Donkelaar, et al. (2005). "Computational study of culture conditions and nutrient supply in cartilage tissue engineering." Biotechnol Prog **21**(4): 1252-1261.

Shachar, M. and S. Cohen (2003). "Cardiac tissue engineering, ex-vivo: design principles in biomaterials and bioreactors." Heart Fail Rev **8**(3): 271-276.

Sherwood, J. K., S. L. Riley, et al. (2002). "A three-dimensional osteochondral composite scaffold for articular cartilage repair." Biomaterials **23**(24): 4739-4751.

Singhvi, R., G. Stephanopoulos, et al. (1994). "Effects of substratum morphology on cell physiology." Biotechnol Bioeng **43**(8): 764-771.

Sodian, R., T. Lemke, et al. (2002). "Tissue-engineering bioreactors: A new combined cell-seeding and perfusion system for vascular tissue engineering." Tissue Engineering **8**(5): 863-870.

Sousa, F. F. O., A. Luzardo-Alvarez, et al. (2010). "Development of a novel AMX-loaded PLGA/zein microsphere for root canal disinfection." Biomed Mater **5**(5): 055008.

Sterodimas, A., J. De Faria, et al. (2009). "Tissue engineering in plastic surgery: an up-to-date review of the current literature." Annals Of Plastic Surgery **62**(1): 97-103.

Sun, W., A. Darling, et al. (2004). "Computer-aided tissue engineering: overview, scope and challenges." Biotechnol Appl Biochem **39**(Pt 1): 29-47.

Takahashi, M. and B. C. Berk (1996). "Mitogen-activated protein kinase (ERK1/2) activation by shear stress and adhesion in endothelial cells. Essential role for a herbimycin-sensitive kinase." J Clin Invest **98**(11): 2623-2631.

Truskey, G. A., F. Yuan, et al. (2004). Transport Phenomena in Biological Systems. Upper Saddle River, NJ, Pearson Prentice Hall**:** 317-321.

Tsuji, I., H. Ishida, et al. (1961). "Experimental cystoplasty using preserved bladder graft." J Urol **85**: 42-44.

van der Giessen, W. J., A. M. Lincoff, et al. (1996). "Marked inflammatory sequelae to implantation of biodegradable and nonbiodegradable polymers in porcine coronary arteries." Circulation **94**(7): 1690-1697.

VandeVord, P. J., H. W. Matthew, et al. (2002). "Evaluation of the biocompatibility of a chitosan scaffold in mice." J Biomed Mater Res **59**(3): 585-590.

Wallis, M. C., H. Yeger, et al. (2008). "Feasibility study of a novel urinary bladder bioreactor." Tissue Eng Part A **14**(3): 339-348.

Waters, S. L., L. J. Cummings, et al. (2006). "Tissue growth in a rotating bioreactor. Part I: mechanical stability." Math Med Biol **23**(4): 311-337.

Weston, M. W., D. V. LaBorde, et al. (1999). "Estimation of the shear stress on the surface of an aortic valve leaflet." Ann Biomed Eng **27**(4): 572-579.

Wood, D. and J. Southgate (2008). "Current status of tissue engineering in urology." Curr Opin Urol **18**(6): 564-569.

Wu, X., Y. Liu, et al. (2010). "Preparation of aligned porous gelatin scaffolds by unidirectional freeze-drying method." Acta Biomater **6**(3): 1167-1177.

Xue, L. and H. P. Greisler (2003). "Biomaterials in the development and future of vascular grafts." J Vasc Surg **37**(2): 472-480.

Zeltinger, J., J. K. Sherwood, et al. (2001). "Effect of pore size and void fraction on cellular adhesion, proliferation, and matrix deposition." Tissue Engineering **7**(5): 557-572.

CHAPTER III

CHARACTERIZATION OF POLYCAPROLACTONE MATRICES GENERATED IN AQUEOUS MEDIA

3.1. Introduction.

Polycaprolactone (PCL) is biocompatible polyester with a low melting point (60°C). It has been explored for forming various medical devices (van der Giessen, Lincoff et al. 1996), templates for tissue regeneration (Htay, Teoh et al. 2004; Li, Cooper et al. 2006) and drug delivery systems (Aliabadi, Mahmud et al. 2005). Apart from its low melting point, the ability to tailor the mechanical properties and non-enzymatic degradation (by hydrolysis) rate of PCL by altering the molecular chain length are very attractive features (Engelberg and Kohn 1991); PCL matrices formed after dissolution in chloroform show elongation up to 1000% before breaking (Averous, Moro et al. 2000). However, the poor wettability of the prepared matrices prevents uniform distribution of proteins and cell adhesion, thus compromising their application in biomedical devices (Lee, Kim et al. 2004).

To enhance the bioreactivity of the PCL surface and to modulate cell survival, a number of studies have evaluated the effect of the solvents used during matrix generation process (Tang, Black et al. 2004). Typically used halogenated hydrocarbon solvents such

as chloroform and dichloromethane have been shown to generate a hydrophobic surface with smooth surface characteristics. To reduce the surface hydrophobicity, grafting hydrophilic fragments of synthetic or natural polymers such as acrylates, collagen and chitosan has also been explored (Jones, Djokic et al. 2002; Cheng and Teoh 2004; Jones, McLaughlin et al. 2005; Chung, Wang et al. 2006; Williamson, Black et al. 2006). Alternatively, etching the surface at the nanoscale using sodium hydroxide is also proposed (Serrano, Portoles et al. 2005). Further, melt molding techniques have used molds with different surface features (Hanson, Jamshidi et al. 1988). Nevertheless, the effect of these modifications on the resulting polymer is not completely understood.

In this study, a novel process of dissolving PCL in acetic acid (AA) was explored which allows self-assembly of PCL in an aqueous environment. To understand the utility of these matrices in biomedical applications, their surface characteristics, effect of neutralizing in alkaline solution, tensile properties and stress relaxation properties were investigated. Matrices formed by dissolving in chloroform and air drying, an method that has been widely investigated (Cheng and Teoh 2004; Tang, Black et al. 2004), were used as control. In addition, the cytocompatibility and cytoskeletal organization of well-characterized fibroblasts were tested in serum-free medium. The results showed a significant benefit of the modified process relative to casting matrices with chloroform.

3.2. Materials and Methods.

PCL of 80 kDa (in number Mn) and gelatin (type-A) were purchased from Sigma–Aldrich (St. Louis, MO). Glacial AA was purchased from Pharmco Products Inc. (Brookfield, CT). Pure ethanol was from AAPER (Shelbyville, KY). Human

foreskin fibroblast cells (HFF-1, cell line) were purchased from the American Type Culture Collection (Walkersville, MD). All other chemicals were of reagent grade.

3.2.1 Preparing solutions and forming blends.

PCL solution (10% (w/v)) was prepared in glacial AA, and the same percentage of PCL solution was prepared in chloroform. Gelatin solution (5% (w/v)) was prepared in distilled water. All solutions were prepared fresh or stored for no longer than 4 days. Long-term storage is deleterious to self-assembly of PCL matrix.

3.2.2. Forming matrices.

PCL matrices were made in 5 cm diameter Teflon dishes for tensile testing and surface analysis using two methods:

• Method 1: dispensing 2-3 mL PCL solution dropwise on top of a water bath.

• Method 2: layering 2 mL PCL solution on the bottom of the dish and dipping the entire dish into a larger container of water.

Although matrices formed spontaneously in both the modes, they were undisturbed for 5 min to allow the process of matrix formation to complete. Generated matrices were allowed to air dry. Some of those PCL matrices were incubated in gelatin solution for 30 min, and were then allowed to air dry. Both gelatin-coated and uncoated matrices were removed from the dish, and placed in an ethanol bath for 15 min. These matrices were used for tensile testing measurements and surface analysis. Chloroform–cast matrices were made in the same Teflon dishes by layering 2 mL PCL solution and air drying.

To form porous matrices, the water bath was replaced with $NaHCO_3$ solutions which react with AA to form CO_2. To evaluate the effect of concentration of $NaHCO_3$ solution on matrix formation, experiments were performed using 2%, 5% and 8% (w/v) $NaHCO_3$ solutions. The formed matrices were dipped in a 1 N sodium hydroxide solution for 10 min to test the effect of etching on surface roughness and charge.

For surface analysis of formed matrices, samples were incubated in ethanol for 10 min and allowed to dry overnight in a vacuum desiccator. Dry matrices were attached to aluminum stubs with carbon paint and sputter coated with gold for 1 min. The surface architecture of the matrices was analyzed by scanning electron microscopy (SEM, JEOL 6360, JEOL USA Inc., Peabody, MA) at an accelerating voltage of 21 kV.

3.2.3. Surface roughness and charge analysis.

Surface roughness analysis of matrices was done by atomic force microscopy (AFM) using a DI Nanoscope V Multimode Scanning Probe Microscope (Digital Instruments, Veeco Metrology Group, Santa Barbara, CA) at ambient conditions, as described previously (Sarasam, Krishnaswamy et al. 2006) In brief, at least triplicate samples were prepared per condition. Each sample was split into four, and each of the four samples was attached to iron substrates using double-sided tape (for the roughness test) and conductive tape (for the charge test). In each sample, AFM analysis was performed by randomly choosing 10 different locations, with a field size of 5 μm × 5 μm. Topographic images were obtained in tapping mode at a scan rate of 1 Hz and 256 scanning lines using commercial silicon micro-cantilever probes (MikroMasch, Portland, OR) with a tip radius of 5-10 nm and a spring constant of 2-5

N/m. Height images were captured at the probe oscillation resonance frequency of 160 kHz. The roughness factor, Rq, is the root mean square average of the number, n, of height deviations (Zi) taken from the mean data plane, calculated using the equation:

$$Rq = \sqrt{Z_i^2 / n} \tag{3.1}$$

For surface charge, topographic images were obtained in tapping mode using micro-cantilever probes coated with platinum–iridium with a tip radius of 20 nm. Then topographic images were rescanned in electrical force mode. Surface potential charges were recorded using the associated software (Nanoscope, version 7).

3.2.4. Tensile testing.

Tensile testing was performed by the method previously described (Raghavan, Kropp et al. 2005; Sarasam and Madihally 2005). In brief, 30 mm × 10 mm rectangular strips were cut from each matrix and strained to break at a constant crosshead speed of 10 mm/min using and Instron 5842 (Instron Inc., Canton, MA). Tensile stress and strain were determined using the associated software Merlin (Instron Inc.). Samples were tested either in the dry state at 25 °C or in the wet state at 37 °C by immersion in phosphate-buffered saline (PBS) using a custom-built environmental chamber. The elastic modulus was calculated from the slope of the linear portion (0.1-5% strain range) of the stress–strain curve. To measure the thickness of the matrices, digital micrographs were obtained at various locations through an inverted microscope (Nikon TE2000U, Melville, NY) equipped with a CCD camera, as described previously (Raghavan, Kropp et al. 2005). These images were quantified for the thickness using image the analysis software Sigma Scan Pro

(SPSS Science, Chicago, IL), calibrated using a micrograph of a hemocytometer at the same magnification. Four or five images were obtained per sample with at least 20 points per image. The calculated minimum thicknesses were used to determine the stress values in each sample.

3.2.5. Stress relaxation testing.

Stress relaxation testing was performed using the previously described procedure (Mirani, Pratt et al. 2009). In brief, 30 mm × 10 mm rectangular matrices were tested using the Instron 5542 mechanical testing machine. The load limits were predetermined by the linear portion of the stress–strain curves obtained previously under tensile testing. Samples were subjected to a constant step tensile strain applied at the rate of 1.0% s^{-1} for 50 s and the sample was allowed to relax for 100 s. Each single test had five steps of ramp-hold cycles.

3.2.6. Evaluating cell adhesion.

HFF-1 cells were seeded onto each sample and maintained in serum-free FGM medium purchased from Lonza (Walkersville, MD). The cultures were maintained in 5% CO_2/95% air at 37 °C with medium changes every 48 h. Cells were detached with 0.01% trypsin–10 μM EDTA, obtained from Invitrogen Corp. (Carlsbad, CA). Viable cell numbers were determined using the Trypan Blue dye exclusion assay. Ten thousand viable cells were seeded onto the control, and 25,000 cells were seeded uniformly onto the scaffolds. Growth medium (2 mL) was added and the cells were incubated for 48 h.

After 2 days, samples were fixed in 3.7% formaldehyde for 30 min at room temperature. Samples were washed three times with PBS, and permeabilized with -

20 °C ethanol overnight at 4°C (Huang, Onyeri et al. 2005). The samples were stained with Alexa Fluor 546 phalloidin (Molecular Probes, Eugene, OR) for 3 hours at -4 °C in the dark. Samples were counterstained with DAPI following the vendor's protocol (Invitrogen) and observed under a fluorescence microscope (Nikon TE2000), and digital micrographs were collected from different locations using the attached CCD camera. Surface architecture of matrices was also analyzed by SEM to observe changes in the architecture due to incubation with cells.

3.2.7. Statistical analysis.

All cell culture experiments were repeated three or more times with quadruplicate samples. All tensile testing and compliance testing were repeated four or more times and average and standard deviations were calculated. Significant differences between two groups were evaluated using a one way analysis of variance (ANOVA) with 99% confidence interval. When $P < 0.01$, the differences were considered to be statistically significant.

3.3. Results.

3.3.1. Macroscopic properties of matrices.

Dispersion of PCL solution in a water bath formed matrices quickly in both methods. However, dropwise dispersion (method 1) of PCL solutions formed a uniform matrix (**Figure 3.1-B**) unlike spreading PCL solution (method 2) (**Figure 3.1-C**); matrices generated using method 1 had more uniform thickness, and these matrices were used for the subsequent analyses described below. When PCL solution stored for more than 4 days was used, no spontaneous matrix formation was observed. This could probably be due to the acid hydrolysis decreasing the molecular weight of

the polymer and the inability to form an interpenetrating network. All solutions for subsequent testing were freshly prepared for forming matrices.

To test the possibility of incorporating porous architecture into the matrices, solutions were dispersed in 8% (w/v) sodium bicarbonate solution. Matrices formed much faster in these baths than in a water bath and formation of bubbles due to the release of CO_2 was also observed. These bubbles created pores in the formed matrices (**Figure 3.1-D**). When self-assembled matrices were immersed in gelatin solution, macroscopically their characteristics were identical to **Figure 3.1-B** (data not shown).

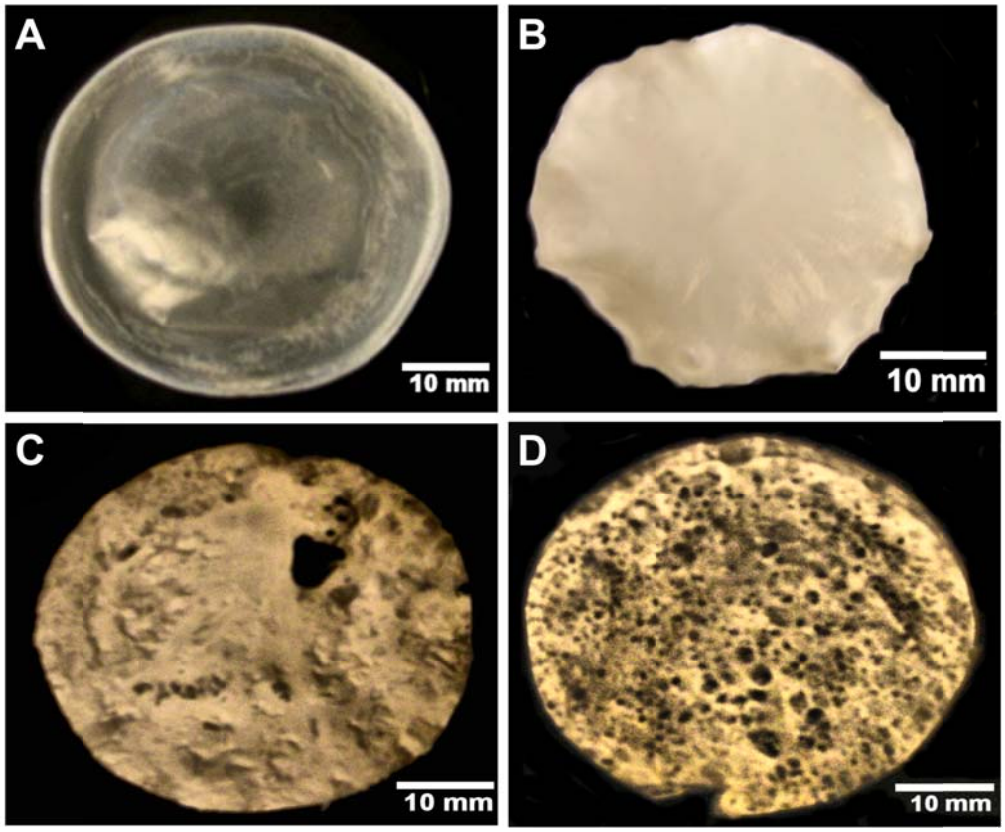

Figure 3.1. Macroscopic view of the PCL matrices. (A) Matrix formed in chloroform, (B) Matrix formed in Acetic Acid by Method 1, (C) Matrix formed in Acetic Acid by Method 2, (D) Matrix formed using 8% (wt/v) $NaHCO_3$.

Next, formed matrices were analyzed using SEM to better understand the microarchitecture. Chloroform–cast matrices had a smooth surface and appeared like a fused network of crystals (**Figure 3.2-A**) with no porosity on both sides of the matrix. However, self-assembled PCL matrices had a rougher surface architecture and the surface facing the air had a number of micropores (**Figure 3.2-B**). Matrices formed in $NaHCO_3$ bath showed a number of micropores although the walls appeared smooth. Upon immersion in gelatin solution, self-assembled matrices (**Figure 3.2-D**) had a reduction in pore size and surface roughness, probably due to the presence of gelatin. However, no significant change was observed in chloroform–cast PCL samples after dipping in gelatin solution.

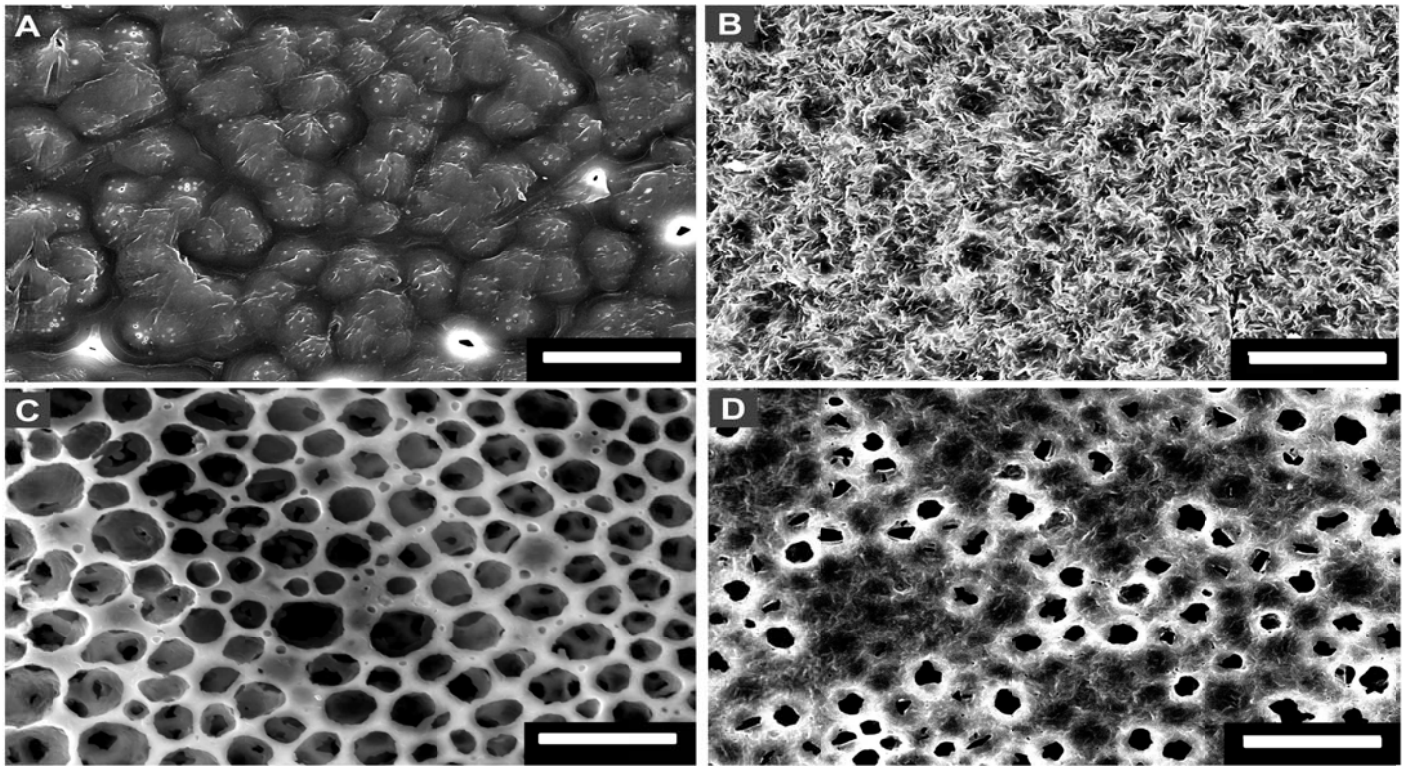

Figure 3.2. Comparison of surface characteristics of PCL matrices. Micrographs of matrices formed by dissolving (A) PCL in chloroform; (B) PCL in AA; (C) PCL in AA and reaction with $NaHCO_3$; (D) PCL in AA and incubation in gelatin solution. Scale bar = 50 μm..

3.3.2. Analysis of surface roughness.

Next, the effectiveness of generating matrices on the surface roughness was compared with the chloroform-cast PCL matrices. AFM analysis of formed matrices in AA (**Figure 3.3-A**) showed a statistically significant increase in roughness relative to chloroform–cast matrices (**Figure 3.3-C**). While average roughness factor of PCL matrices formed in AA was 150 nm, employing chloroform resulted in an average roughness factor of 30 nm (**Figure 3.3-E**).

To assess the effect of incubation in an alkaline solution for neutralization of AA bound to self-assembled matrix, PCL matrices were immersed in 1 N NaOH for 10 min. These results showed a significant reduction in the roughness (referred as etching in Figure 3) of self-assembled PCL matrices. After 10 min of incubation in NaOH at room temperature, the roughness factor decreased to 75 nm. There was only a marginal reduction in chloroform-cast PCL matrices (**Figure 3.3-D**). Thus while neutralizing the remaining AA in self-assembled PCL matrices; one has to consider the effect of alkaline solution concentration and the incubation time.

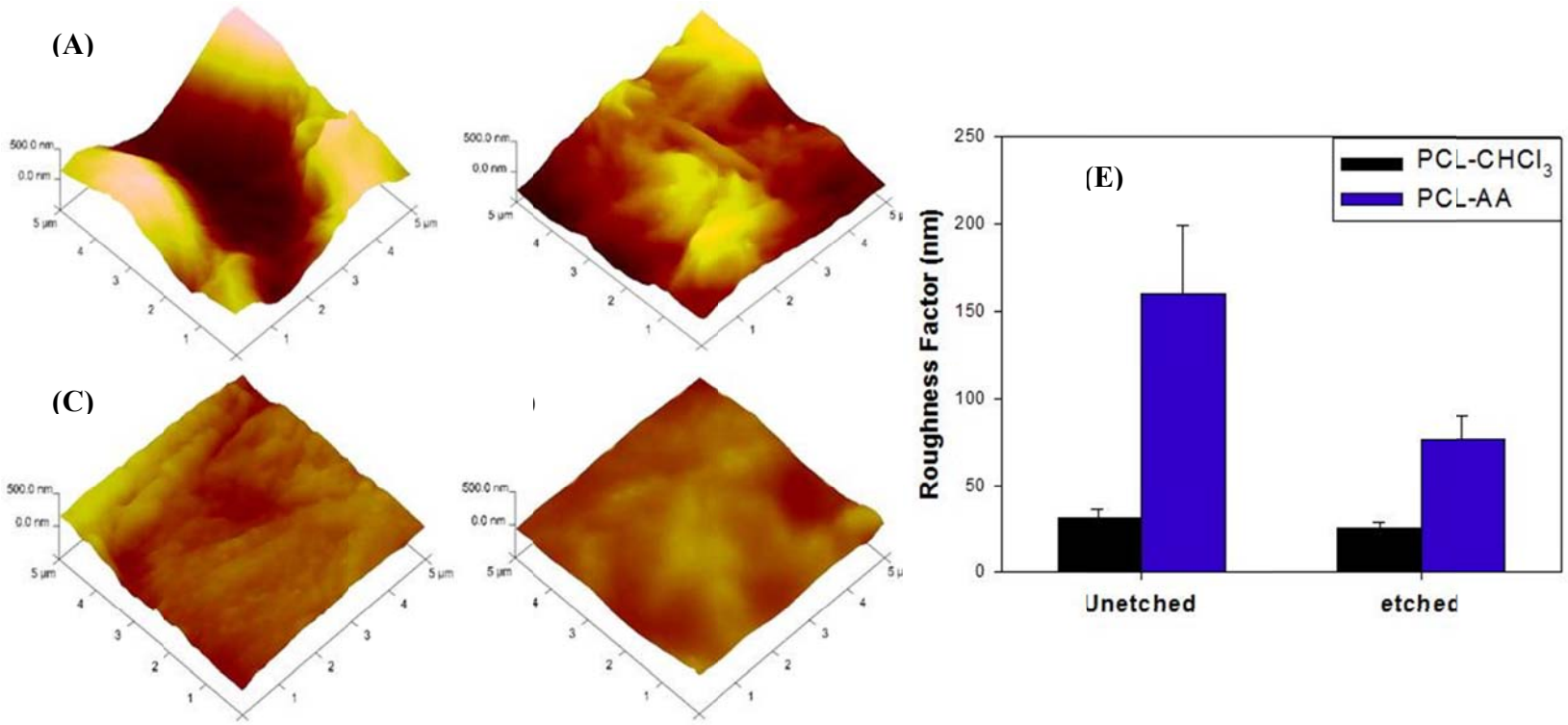

Figure 3.3. Surface roughness characteristics. (A) PCL in AA; (B) PCL in AA after etching; (C) PCL in chloroform; (D) PCL in chloroform after etching; (E) variation in roughness values. Average and standard deviations from at least four samples for each condition are shown. Micrographs correspond to 5 μm × 5 μm area and the roughness coordinate is 500 nm.

3.3.3. Alteration in surface charge.

Next, we investigated whether the self-assembled PCL matrix shows a different surface charge relative to chloroform-cast matrices. For this purpose, formed matrices were assessed for surface charge using AFM. The analyzed surface in contact with the probe was that in contact with the water bath. These results showed (**Figure 3.4**) that self-assembled matrices had a net positive surface charge (+9.988), whereas chloroform-cast matrices had a negative surface charge (-9.998). Since gelatin has a net negative charge in acidic conditions, immersion in gelatin solution resulted in ionic binding of gelatin to the PCL surface. The surface charge of gelatin-coated self-assembled PCL matrix changed to negative. This suggested the possibility of immobilizing gelatin via ionic interactions. Interestingly, the alkaline etching did not alter the surface charge characteristics in both processes

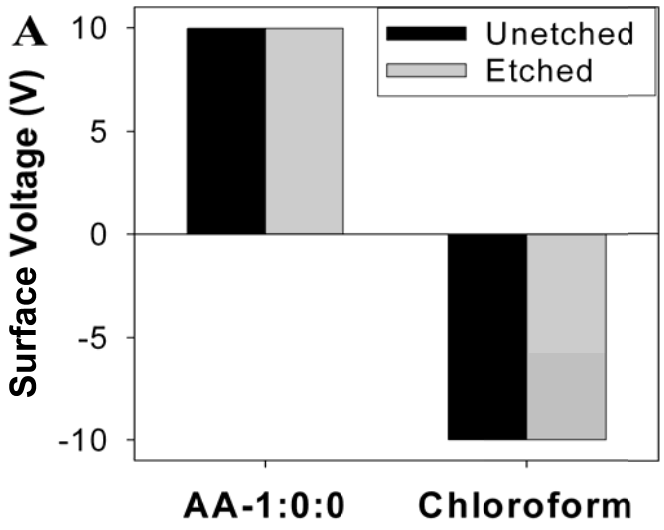

Figure 3.4. Surface charge characteristics. Matrices formed by different solvents, and one of the samples were coated with gelatin

3.3.4. Effect on tensile properties.

Next, alterations in the tensile strength of matrices were evaluated. These results (**Figure 3.5-A**) showed that chloroform-cast matrix had a higher tensile stress and strain than self-assembled matrix. The break strain of chloroform–cast matrix was more than 700%, and the break stress was 12 MPa. The break strain of self-assembled matrix was 230%, and its break stress was between 3.0 and 3.5 MPa. Elastic modulus was estimated using the initial linear range (0.1–5%) of the stress-strain curve. These results showed that self-assembled matrices were more elastic than chloroform–cast matrices (**Figure 3.5-B**). The elastic modulus of the self-assembled matrix was 40 MPa, relative to 140 MPa in chloroform–cast matrices. Both scaffolds had a similar thickness (100 μm). However, this does not mean that the packing density of the two conditions is the same. This observed difference in elastic modulus could be due to reduced packing of polymer chains with an interpenetrated network formation during self-assembly.

When matrices were tested in the hydrated condition (**Figure 3.5-A**), break stress was similar to dry conditions but break strain increased in self-assembled matrices. However, in chloroform-cast matrices both break stress and break strain decreased slightly. Elastic modulus (**Figure 3.5-B**) decreased in both cases by nearly 50%.

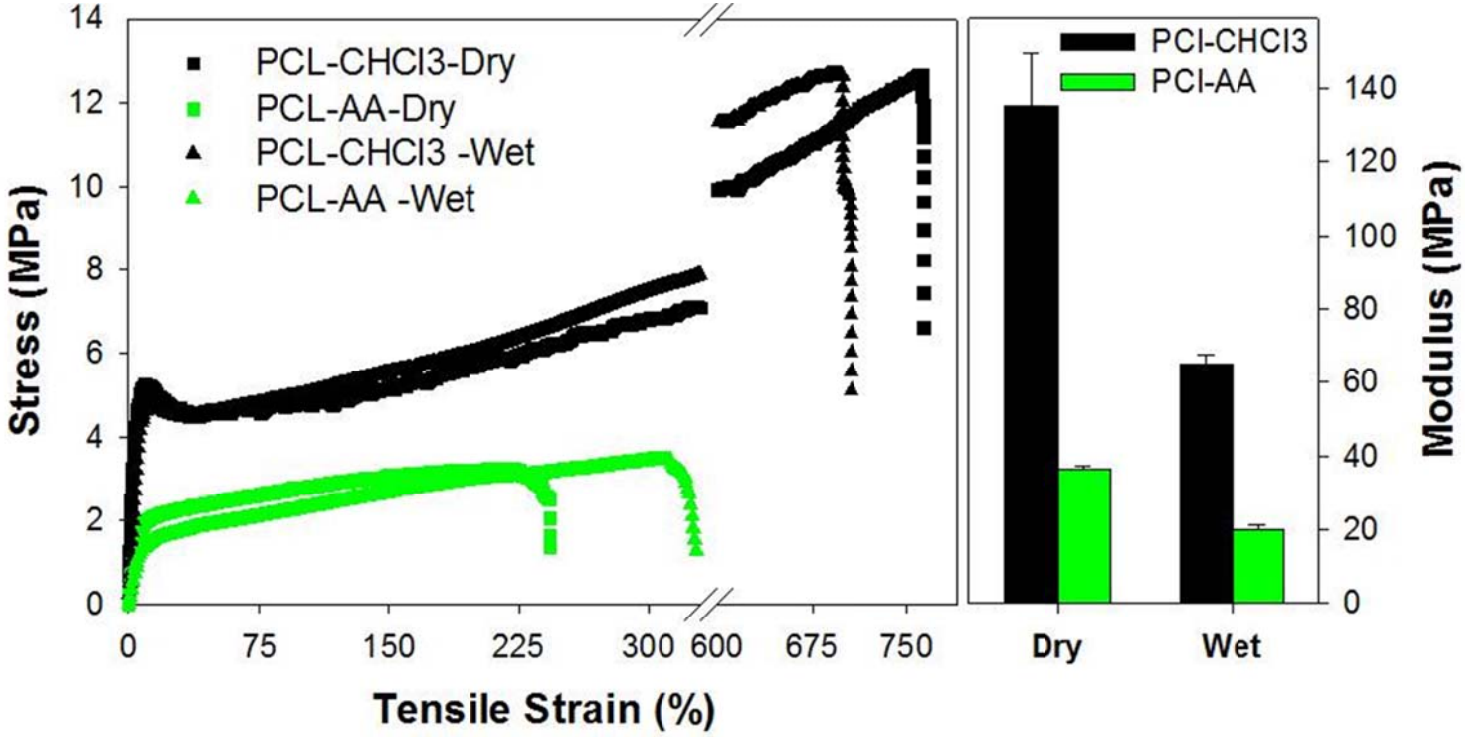

Figure 3.5. Effect of different solvents on stress-strain behavior of PCL matrices. (A) Stress-strain behavior, (B) Elastic modulus of matrices calculated from the linear region of stress-strain curve.

3.3.5. Effect on stress relaxation properties.

PCL is known to behave like a viscoelastic material which stores and dissipates energy within the complex molecular structure, producing hysteresis and allowing creep and stress relaxation to occur (Duling, Dupaix et al. 2008). Hence, a full description of the mechanical response of materials requires nonlinear viscoelastic behavior. To understand the effect of self-assembly on the polymeric matrix, stress relaxation was tested. These results (**Figure 3.6**) showed that both self-assembled and chloroform-cast matrices showed similar behavior in ramp and hold cycles. In the first ramp and hold cycle, both matrices showed high stress values for the same amount of strain. However, in the successive ramp-hold conditions, there were no significant differences. After the first ramp-hold, successive ramp-hold tests showed similar stress levels, suggesting that the hysteresis loss could be negligible and hence that it might be possible to use these matrices in applications where tissues will be subjected to cyclical loading conditions. Electrospun PCL fibers have been shown to have similar behavior (Duling, Dupaix et al. 2008). Thus, one could refer to the first cycle as the preconditioning cycle. Nevertheless, self-assembled matrices experienced nearly half the stress relative to chloroform–cast matrices for the same strain range in all the cycles. This supported the fact that chloroform–cast matrices were harder than self-assembled matrices.

One interesting difference between the two types of matrices was the level of stress experienced during the loading part of each cycle. Chloroform–cast matrices showed an initial surge in stress which reduced to a lower level despite further application of strain. This behavior was not observed in self-assembled matrices. One could attribute this difference in behavior to the alteration in the interpenetrating

network architecture which accumulates and disperses the stress during loading. Importantly, preconditioning and relaxation allowed the self-assembled matrices to go beyond the break strain range observed in linear tensile loading, particularly in self-assembled PCL matrices.

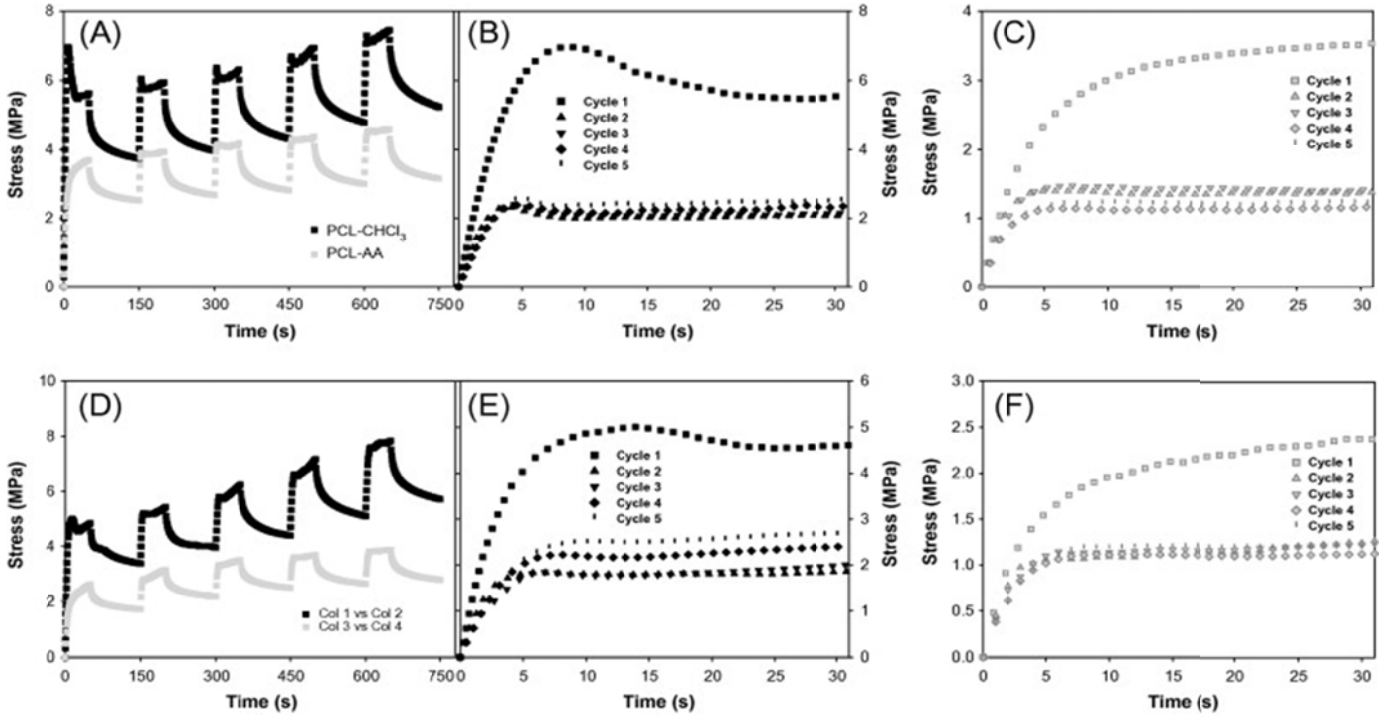

Figure 3.6. Stress relaxation behavior of different materials. (A) Effect of casting process; (B) loading behavior of chloroform–cast matrix in different cycles at the rate of 1.0% s^{-1} for 30 s; (C) loading behavior of self-assembled matrix in different cycles at the rate of 1.0% s^{-1} for 30 s; (D) effect of casting process at wet condition (37 °C); (E) loading behavior of chloroform–cast matrix in different cycles at the rate of 1.0% s^{-1} for 30 s at wet condition (37 °C); (F) loading behavior of self-assembled matrix in different cycles at the rate of 1.0% s^{-1} for 30 s at wet condition (37 °C).

3.3.6. Effect on cellular activity.

Microarchitecture analysis along with surface charge showed the possibility of immobilizing gelatin directly onto PCL. To understand the functional implications of these changes, the cell morphologies of HFF-1 were evaluated in serum-free conditions. These results (**Figure 3.7**) showed increased presence of HFF-1 cells on self-assembled PCL matrices, with well spread spindle shape. Self-assembled matrices immersed in gelatin showed a qualitative improvement in the retention of seeded cells on the surface. Further, HFFs showed peripheral distribution of actin filaments, similar to cells on tissue culture plastic (TCP) surface. On the other hand, chloroform-cast matrices showed very few cells with and without gelatin coating. This significant difference suggests that forming self-assembled matrices in aqueous medium helps improve cell adhesion to PCL even in the absence of serum proteins. Counterstaining with DAPI confirmed the presence of nuclei, along with the actin fiber, suggesting that the PCL structure promotes cell attachment.

To understand the cellular interactions better, samples were evaluated using SEM (**Figure 3.8**). The morphology of self-assembled matrices was similar to those observed prior to cell seeding; PCL-only matrices showed increased surface roughness and the presence of gelatin reduced the roughness. Cells attached and spread throughout matrix despite the presence of micropores in the matrix on self-assembled matrices. On chloroform-cast matrices, not many cells were detected, probably due to loss of weakly adherent cells during the sample preparation.

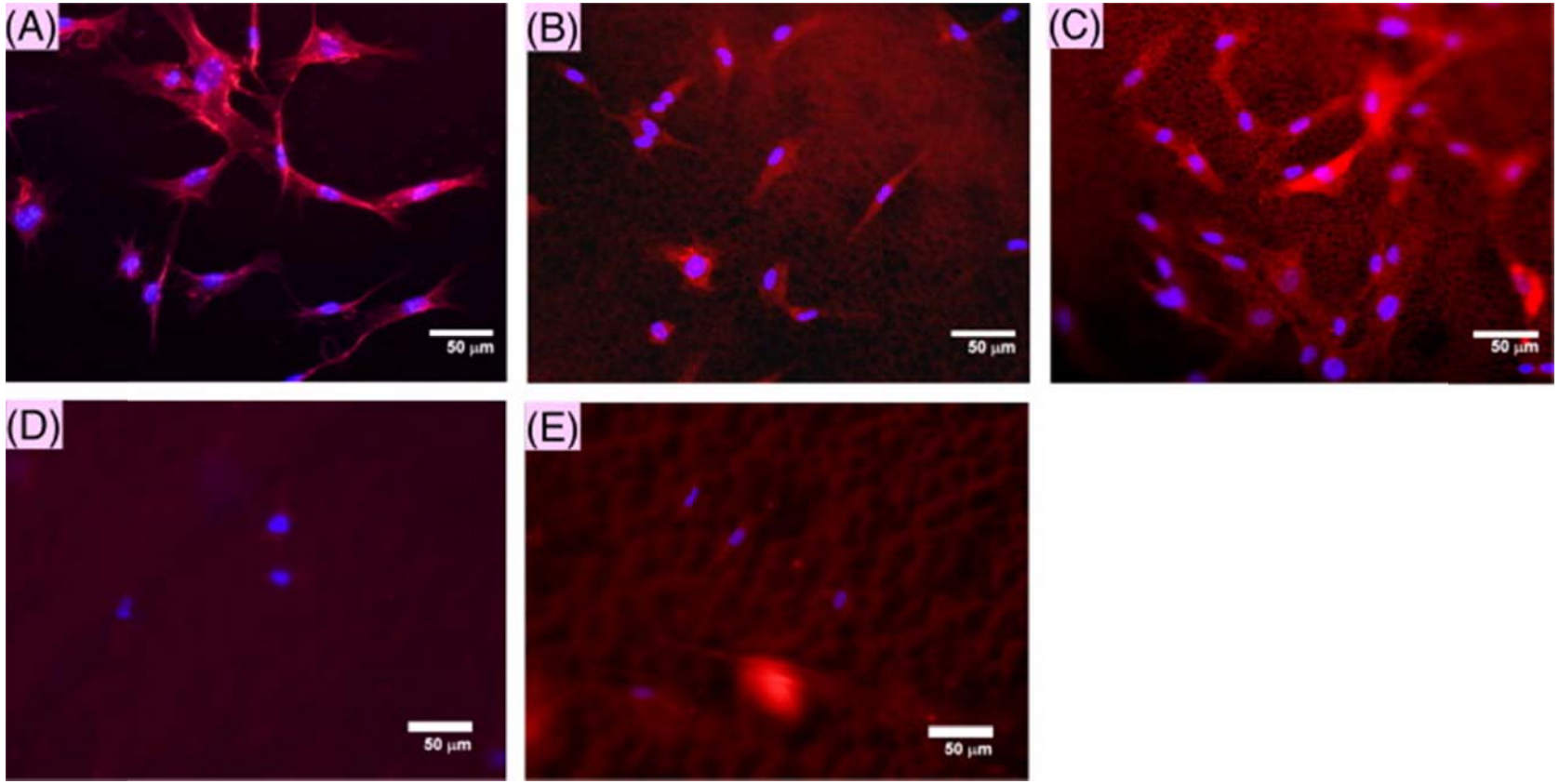

Figure 3.7. Cell spreading of fibroblasts. Fluorescence micrographs of cells stained for actin and nucleus after 48 hrs of incubation. (A) Tissue Culture Plastic, (B) PCL-AA, (C) PCL-AA + gelatin, (D) PCL-chloroform, (E) PCL-chloroform + gelatin.

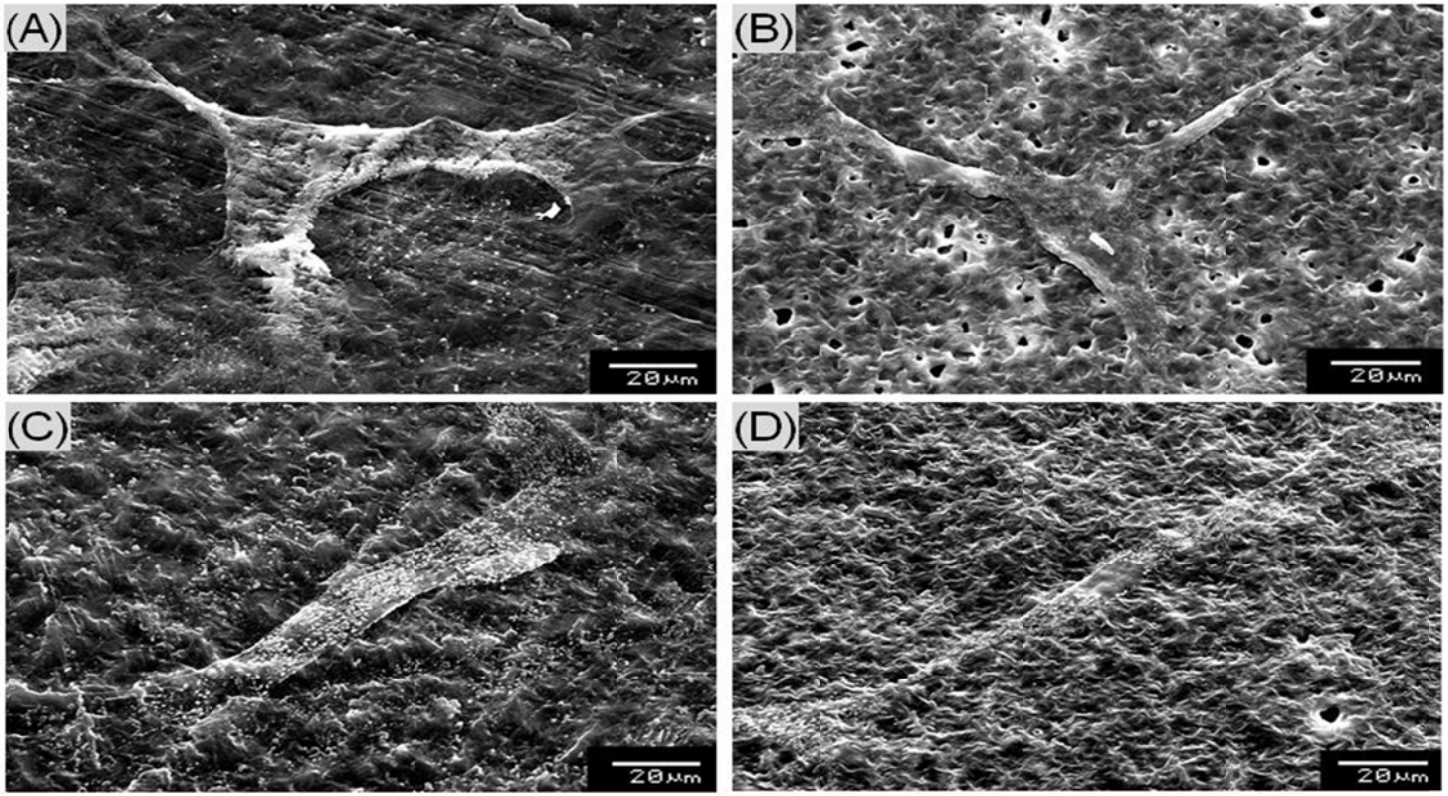

Figure 3.8. Cell spreading of fibroblasts analyzed by SEM (A) Chloroform-casted matrix, (B) PCL-AA, (C) Chloroform-casted matrix and incubated in gelatin solution, (D) PCL-AA + gelatin.

3.4. Discussion.

In this study, a novel method of generating PCL-based matrices in an aqueous environment was evaluated. The self-assembly of PCL into matrices was observed in concentrated (>5%) solutions of PCL upon contact with water. This precipitation into stable matrices did not occur with PCL of 10 kDa Mn, probably due to the lack of stable interpenetrating network formation. The matrices that formed had increased roughness relative to chloroform-cast matrices. Other researchers have measured the surface roughness of chloroform–cast PCL matrices and reported a roughness of less than 100 nm (Cheng and Teoh 2004).

Assessed tensile properties showed a reduction in self-assembled matrix relative to chloroform–cast matrix. However, the self-assembled matrices had a break stress that is comparable to that of small intestinal submucosa (3 MPa) (Lawrence, Maase et al. 2009), a natural matrix utilized in tissue regeneration. Further, the calculated elastic modulus was comparable to that of small intestinal submucosa. Hence, the reduction in elastic modulus is advantageous in tissue regeneration strategies as it reduces the mismatch in mechanical properties with the surrounding tissues. Measured stress relaxation characteristics showed less accumulation of stress in self-assembled matrices relative to chloroform-cast materials. A significant difference between self-assembled matrix and chloroform-cast matrix was relaxation during the loading phase of chloroform–cast matrix. This was not observed in self-assembled matrices, which could be attributed to alteration in the packing of the polymeric chains. However, one has to perform experiments with varying loading and relaxation times to better understand the viscoelastic behavior as viscoelastic behavior significantly depends on the loading and

relaxation times. Further, one has to test the effect of temperature on the viscoelastic behavior.

Previously, our laboratory has shown the possibility of blending PCL with chitosan uniformly at low concentrations (<2%) using 70% AA solution (Sarasam and Madihally 2005; Sarasam, Krishnaswamy et al. 2006). When crystalline properties were evaluated (using wide-angle X-ray diffraction, melting temperature and glass transition temperature), no significant changes were observed in PCL crystalline properties. The increased roughness could be attributed to the different mode of assembly of PCL, similar to results reports by others using different solvents (Tang, Black et al. 2004). One possibility for different assembly is that the dissolution of PCL in acidic environment could introduce a charge in the PCL backbone. This could create an affinity for water on one side while the nonfunctionalized regions still retain hydrophobicity. Thus the hydrophobic regions could randomly aggregate, forming a rough architecture. Interestingly, surface formed in contact with water was hydrophilic as water uniformly distributed when added dropwise onto the dry matrix. However, there could be a change in the surface characteristics on the side exposed to air. One has to explore the differences in the characteristics of the matrix on both sides and understand the mechanism of self-assembly.

When cellular activity was measured, increased cell adhesion was observed on self-assembled matrices. Further, cell spreading was similar to TCP, unlike other reports in which cell spreading was shown to be minimal on chloroform–cast PCL matrices (Serrano, Pagani et al. 2004). In the absence of serum, adhesion to chloroform–cast PCL was minimal. Thus the new simple technique shows a significant improvement in

cellular interactions. Since matrix topography affects cell spreading characteristics (Huang, Siewe et al. 2006), the observed variation in cellular activity could be attributed to the significant increase roughness. A number of previous studies have investigated systematically the effect of surface porosity and roughness on cell proliferation rates (Walboomers, Croes et al. 1998) and (Degirmenbasi, Ozkan et al. 2009). Further, this increase may be required to observe the marked effect as nanoscale (100 nm) variation in surface roughness showed no significant difference in cellular activity (Serrano, Pagani et al. 2004). Alternatively, the observed differences could also be due to the changes in the surface energy along with the changes in the adhesion of proteins present in the medium. However, detailed cell colonization studies, such as growth characteristics and alteration in secretion of matrix elements, have to be analyzed. In addition, analysis of cellular activity needs to be extended to include other types of cells. These findings open a new set of possibilities to understand the influence of charge and roughness separately on macromolecular interactions and cell colonization, which has not been well understood in tissue regeneration.

This study assessed only the formation of matrices in an aqueous environment. To utilize this technique, one has to explore the possibility of easy layering onto various devices in an aqueous environment. The utility of this technique in forming three dimensional porous structures needs to be explored and compared to other techniques (Coombes, Rizzi et al. 2004). In addition, the three-dimensional matrices formed via a reaction to generate CO_2 had pores with a wide distribution in size. Further studies are necessary to improve the method of forming porous structures with better control of pore size. Nevertheless, there are many approaches to incorporating the porous architecture.

For example, one could use the self-assembled PCL matrix to support porous structures formed using natural polymers (Lawrence, Maase et al. 2009).

In summary, the results show that PCL matrices can be generated using the novel technique in aqueous media. Self-assembled matrices showed an increase in roughness, which was decreased after immersion in NaOH solution. Measured tensile properties showed a reduction in elastic modulus but with similar stress relaxation behavior relative to chloroform–cast matrices. Cell adhesion and spreading were significantly improved on the self-assembled matrix. Thus, this technique offers a significant opportunity to enhance the use of PCL in biomedical applications.

3.5. References.

Aliabadi, H. M., A. Mahmud, et al. (2005). "Micelles of methoxy poly(ethylene oxide)-b-poly(epsilon-caprolactone) as vehicles for the solubilization and controlled delivery of cyclosporine A." J Control Release **104**(2): 301-311.

Averous, L., L. Moro, et al. (2000). "Properties of thermoplastic blends: starch-polycaprolactone." Polymer **41**(11): 4157-4167.

Cheng, Z. and S.-H. Teoh (2004). "Surface modification of ultra thin poly (epsilon-caprolactone) films using acrylic acid and collagen." Biomaterials **25**(11): 1991-2001.

Cheng, Z. and S. H. Teoh (2004). "Surface modification of ultra thin poly (epsilon-caprolactone) films using acrylic acid and collagen." Biomaterials **25**(11): 1991-2001.

Chung, T. W., Y. Z. Wang, et al. (2006). "Poly (epsilon-caprolactone) grafted with nano-structured chitosan enhances growth of human dermal fibroblasts." Artif Organs **30**(1): 35-41.

Coombes, A. G. A., S. C. Rizzi, et al. (2004). "Precipitation casting of polycaprolactone for applications in tissue engineering and drug delivery." Biomaterials **25**(2): 315-325.

Degirmenbasi, N., S. Ozkan, et al. (2009). "Surface patterning of poly(L-lactide) upon melt processing: In vitro culturing of fibroblasts and osteoblasts on surfaces ranging from highly crystalline with spherulitic protrusions to amorphous with nanoscale indentations." Journal of Biomedical Materials Research Part A **88A**(1): 94-104.

Duling, R. R., R. B. Dupaix, et al. (2008). "Mechanical characterization of electrospun polycaprolactone (PCL): a potential scaffold for tissue engineering." J Biomech Eng **130**(1): 011006.

Engelberg, I. and J. Kohn (1991). "Physico-mechanical properties of degradable polymers used in medical applications: a comparative study." Biomaterials **12**(3): 292-304.

Hanson, S. J., K. Jamshidi, et al. (1988). "Mechanical evaluation of resorbable copolymers for end use as vascular grafts." ASAIO Trans **34**(3): 789-793.

Htay, A. S., S. H. Teoh, et al. (2004). "Development of perforated microthin poly(epsilon-caprolactone) films as matrices for membrane tissue engineering." J Biomater Sci Polym Ed **15**(5): 683-700.

Huang, Y., S. Onyeri, et al. (2005). "In vitro characterization of chitosan-gelatin scaffolds for tissue engineering." Biomaterials **26**(36): 7616-7627.

Huang, Y., M. Siewe, et al. (2006). "Effect of spatial architecture on cellular colonization." Biotechnol Bioeng **93**(1): 64-75.

Jones, D. S., J. Djokic, et al. (2002). "Poly(epsilon-caprolactone) and poly(epsilon-caprolactone)-polyvinylpyrrolidone-iodine blends as ureteral biomaterials: characterisation of mechanical and surface properties, degradation and resistance to encrustation in vitro." Biomaterials **23**(23): 4449-4458.

Jones, D. S., D. W. McLaughlin, et al. (2005). "Physicochemical characterisation and biological evaluation of hydrogel-poly(epsilon-caprolactone) interpenetrating polymer networks as novel urinary biomaterials." Biomaterials **26**(14): 1761-1770.

Lawrence, B. J., E. L. Maase, et al. (2009). "Multilayer composite scaffolds with mechanical properties similar to small intestinal submucosa." Journal Of Biomedical Materials Research. Part A **88**(3): 634-643.

Lee, J. W., Y. H. Kim, et al. (2004). "Importance of integrin beta1-mediated cell adhesion on biodegradable polymers under serum depletion in mesenchymal stem cells and chondrocytes." Biomaterials **25**(10): 1901-1909.

Li, W. J., J. A. Cooper, Jr., et al. (2006). "Fabrication and characterization of six electrospun poly(alpha-hydroxy ester)-based fibrous scaffolds for tissue engineering applications." Acta Biomater **2**(4): 377-385.

Mirani, R. D., J. Pratt, et al. (2009). "The stress relaxation characteristics of composite matrices etched to produce nanoscale surface features." Biomaterials **30**(5): 703-710.

Raghavan, D., B. P. Kropp, et al. (2005). "Physical characteristics of small intestinal submucosa scaffolds are location-dependent." J Biomed Mater Res A **73A**(1): 90-96.

Sarasam, A. and S. V. Madihally (2005). "Characterization of chitosan-polycaprolactone blends for tissue engineering applications." Biomaterials **26**(27): 5500-5508.

Sarasam, A. R., R. K. Krishnaswamy, et al. (2006). "Blending chitosan with polycaprolactone: effects on physicochemical and antibacterial properties." Biomacromolecules **7**(4): 1131-1138.

Serrano, M. C., R. Pagani, et al. (2004). "In vitro biocompatibility assessment of poly([var epsilon]-caprolactone) films using L929 mouse fibroblasts." Biomaterials **25**(25): 5603-5611.

Serrano, M. C., M. T. Portoles, et al. (2005). "Vascular endothelial and smooth muscle cell culture on NaOH-treated poly(epsilon-caprolactone) films: a preliminary study for vascular graft development." Macromol Biosci **5**(5): 415-423.

Tang, Z. G., R. A. Black, et al. (2004). "Surface properties and biocompatibility of solvent-cast poly epsilon-caprolactone films." Biomaterials **25**(19): 4741-4748.

Tang, Z. G., R. A. Black, et al. (2004). "Surface properties and biocompatibility of solvent-cast poly[-caprolactone] films." Biomaterials **25**(19): 4741-4748.

van der Giessen, W. J., A. M. Lincoff, et al. (1996). "Marked inflammatory sequelae to implantation of biodegradable and nonbiodegradable polymers in porcine coronary arteries." Circulation **94**(7): 1690-1697.

Walboomers, X. F., H. J. E. Croes, et al. (1998). "Growth behavior of fibroblasts on microgrooved polystyrene." Biomaterials **19**(20): 1861-1868.

Williamson, M. R., R. Black, et al. (2006). "PCL-PU composite vascular scaffold production for vascular tissue engineering: attachment, proliferation and bioactivity of human vascular endothelial cells." Biomaterials **27**(19): 3608-3616.

CHAPTER IV

EFFECT OF BLENDING DIFFERENT MOLECULAR WEIGHT OF POLYCAPROLACTONE AND IMMOBILIZATION OF THE NATURAL POLYMER ON BIOLOGICAL PROPERTIES

4.1. Introduction.

Polycaprolactone (PCL) is semi-crystalline linear aliphatic polyester formed from ring opening polymerization of caprolactone. Due to biocompatibility and excellent tensile strength, PCL is explored in forming various medical devices (van der Giessen, Lincoff et al. 1996), templates in tissue regeneration (Htay, Teoh et al. 2004; Li, Cooper et al. 2006), and drug delivery systems (Aliabadi, Mahmud et al. 2005). Membranes of PCL formed by air drying chloroform show elongation up to 1000% before break. Further, its low melting point (60°C) allows processing into various forms by variety of techniques. However, wide use of PCL in biomedical applications in hindered by two properties: i) bioregulatory activity and ii) direct relationship of resorption rate with molecular weight.

Formed PCL surfaces are typically hydrophobic and show poor wettability, which prevents uniform distribution of proteins. There has been a significant effort to improve bioactivity of PCL via co-polymerization (Park, Wu et al. 1998), grafting RGD peptides

(necessary for cellular attachment) (Eid, Chen et al. 2001), blending with other hydrophilic polymers (Wei, Gong et al. 2009), or surface treatment (Cheng and Teoh 2004). Previously, we reported a novel process of generating PCL flat matrices in aqueous medium, which decreased hydrophobic surface properties (Pok, Wallace et al. 2010). Immobilizing gelatin on to these surfaces was also possible, which promoted cell adhesion even in the absence of serum.

PCL is subjected to biodegradation because of the susceptibility of its aliphatic ester linkage to hydrolysis. Resorption of PCL matrices is considerably slower than other aliphatic polyesters due to its hydrophobic character and high crystallinity. However, using high MW PCL in forming structures for biomedical applications has been a common strategy since structures formed with low MW PCL are unstable (Baker, Rohman et al. 2009; Guarino, Taddei et al. 2009). High MW PCL is biostable for nearly two years (Pitt, Gratzl et al. 1981) as the degradation rate is a function of MW. Interestingly, combining structural integrity while altering the degradation of PCL is not well investigated. In particular, influence of blending different molecular weights of PCL in forming structures has not been explored.

For tissue engineering to be successful, building scaffolds of the shape similar to the tissue to be replaced is important. Current techniques utilize porous sheets and the surgeon molds the sheets into required shape (Atala, Bauer et al. 2007). However, they have uneven thickness due to wrinkling and overlap. Further, the quality of the regenerated tissue is dependent on the surgeons' ability to mold. Thus, it is important to develop anatomical relevant scaffolds appropriate to regenerating a specific tissue.

The objective of this study was to evaluate the possibility of blending different MW (80 kDa, 46 kDa and 10 kDa Mn) in the same solvent. Self assembled matrices were evaluated for degradation characteristics, tensile properties, effect of neutralization using alkaline solution and cell adhesion. Further, ability to assemble in anatomically relevant tubular and spherical shapes was also investigated. In addition, incorporating the porous structure of gelatin-chitosan mixture, known to support cell colonization (Huang, Onyeri et al. 2005), was evaluated. Formed composite matrices were evaluated for surface characteristics and tensile properties. These results showed significant potential for using PCL self assembly in tissue regeneration.

4.2. Materials and Methods.

PCL of 80 kDa, 10 kDa (in number Mn), chitosan of low molecular weight, and type A porcine skin gelatin were purchased from Sigma Aldrich (St. Louis, MO). PCL of 46 kDa (in number Mn) was purchased from Polysciences (Warrington, PA). Glacial acetic acid was purchased from Pharmco Products Inc (Brookfield, CN). Pure ethanol was from AAPER (Shelbyville, KY). $NaHCO_3$ was purchased from EMD Chemicals Inc (Gibbstown, NJ). Human Foreskin Fibroblasts (HFF-1, cell line) was purchased from American Type Culture Collection (Walkersville, MD). All other chemicals were of reagent grade.

4.2.1. Preparing Solutions and Forming Blends.

From each MW PCL, 10% (wt/v) solutions were prepared in glacial acetic acid. Blend solutions containing different MW PCL were prepared by mixing equal volumes of individual solutions using factorial design of experiments 1:0:0, 1:0:1, 1:1:1, 0:1:0 (all

abbreviations are in the order of 80:46:10 kDa Mn). A solution of 0.5% chitosan and 0.5% gelatin composite was prepared in water with 1 M acetic acid. All solutions were prepared fresh or stored and used within 2 days. Long-term storage is deleterious to membrane formation.

4.2.2. Forming Matrices.

PCL matrices were made using the previously described procedure (Pok, Wallace et al. 2010). In brief, 5 cm diameter Teflon dishes containing 10 mL water were used for water baths. Two to three milliliter of the PCL solution was dropped on the top of a water bath. Although matrices formed spontaneously by contacting with water, they were undisturbed for 5 minutes to allow the process of matrix formation to complete. Generated matrices were allowed to air dry. These matrices were used for mechanical testing measurements, surface roughness, degradation and cellular activity analysis.

Some of the formed matrices were dipped in a 1 N sodium hydroxide solution for 10 minutes to test the effect of neutralizing the acetic acid in an alkaline solution.

Silicone rods of 6 mm outer diameter were used to make tubular shapes useful in vascular graft application. Rods were immersed in PCL solution for few seconds and immersed in water bath immediately. This step was repeated three times in fresh PCL solution and water to form thicker matrices. Self assembled PCL tubes were analyzed for surface characteristics using SEM by following the procedure described for 2-D matrices. In addition, matrices of bladder shape (spherical shape) were made using latex balloons with the same method of the tubular self assembly.

Self-assembled 2-D PCL matrices of 1:0:1 sample was sandwiched with gelatin-

chitosan porous structure by the previously reported method (Lawrence, Maase et al. 2008) with modifications. In brief, approximately 5 mL of 0.5 % (w/v) chitosan containing 0.5 % gelatin were poured into 5 cm diameter Teflon dishes. Formed PCL matrices were laid down on the solutions, and 5 mL of solution were poured onto surfaces of PCL matrices. These samples were frozen at -80°C for 6 hours and lyophilized at -80°C for 24 hours.

4.2.3. Surface Analysis by SEM.

All self assembled samples were incubated in ethanol for ten minutes and allowed to dry overnight in a vacuum desiccator. Dry matrices were attached to aluminum stubs with carbon paint and sputter-coated with gold for one minute. Surface architecture of matrices was analyzed using a scanning electron microscope (JOEL 6360, Jeol USA Inc., Peabody, MA) at an accelerating voltage of 15kV.

4.2.4. Surface Roughness Analysis.

Surface analysis of membranes was done by atomic force microscopy (AFM) using a DI Nanoscope V Multimode Scanning Probe Microscope (Digital Instruments, Veeco Metrology Group, Santa Barbara, CA) at ambient conditions, as described previously (Pok, Wallace et al. 2010). In brief, sample films were attached onto iron substrates using double-sided tape. Topographic images were obtained in tapping mode using commercial silicon microcantilever probes (MikroMasch, Portland, OR) with a tip radius of 5-10 nm and spring constant 2-5 N/m. The size of analyzed field was 5 μm × 5 μm at a scan rate of 1 Hz and 256 scanning lines. Height images were captured at the probe oscillation resonance frequency was ~160 KHz. Images of each sample were

captured at different locations, and then the roughness factors were calculated using associated software (Nanoscope, Version 7). The roughness factor R_q is the root mean square average of 'n' number of height deviations (Z_i) taken from the mean data plane

$$Rq = \sqrt{Z_i^2 / n} \tag{4.1}$$

4.2.5. Evaluating Cellular Activity.

Human Foreskin Fibroblasts (HFF-1, cell line) was purchased from American Type Culture Collection (Walkersville, MD, USA) and maintained in Dulbecco's modified Eagle medium supplemented with 4 mM L-glutamine, 4.5 g/L sodium bicarbonate, 0.1 mM β-mercaptoethanol, 100 U/mL penicillin-streptomycin, 2.5 g/mL amphotericin, and 10% fetal bovine serum (Invitrogen Corp., Carlsbad, CA, USA). The cultures were maintained in 5% CO_2 /95% air at 37°C with medium changes every 48 hours. Cells were detached with 0.01% trypsin - 10 μM EDTA, obtained from Invitrogen Corp., (Carlsbad, CA, USA). Viable cell numbers were determined using trypan blue dye exclusion assay. 10,000 cells were seeded onto the tissue culture plastic, and 25,000 cells were seeded uniformly onto the scaffolds. All cells were incubated in 0.5 mL of growth medium for 72h.

After two days, samples were fixed in 3.7% formaldehyde for 30 min at room temperature. Samples were washed thrice with phosphate buffered saline (PBS), and permeabilized with -20 °C ethanol overnight at 4 °C (Huang, Onyeri et al. 2005). The samples were stained with Alexa Fluor 546 phalloidin (Molecular Probes, Eugene, OR) for 3h at -4 °C in the dark. Samples were counterstained with DAPI following vendor's protocol (Invitrogen Corp., Carlsbad, CA, USA) and observed under a fluorescence

microscope (Nikon TE2000, Melville, NY) and digital micrographs were collected from different locations using the attached CCD camera.

4.2.6. Tensile Testing of Matrices.

Tensile testing was performed by the method previously described (Pok, Wallace et al. 2010). In brief, 30 mm × 10 mm rectangular strips were cut from each matrix and strained to break at a constant crosshead speed of 10 mm/min using INSTRON 5842 (INSTRON Inc., Canton, MA). Using the associated software Merlin (INSTRON Inc.) break stress and strain were determined. Samples were tested either in dry state at 25 °C or in the wet state at 37 °C by immersing in PBS (pH=7.4) using a custom-built environmental chamber. While testing at 37 °C, samples were immersed in PBS. The elastic modulus was calculated from the slope of the linear portion (0.1% to 5% strain range) of the stress-strain curve. To measure the thickness of the matrices, digital micrographs were obtained at various locations through an inverted microscope (Nikon TE2000U, Melville, NY) equipped with a CCD camera. These images were quantified for the thickness using image analysis software Sigma Scan Pro (SPSS Science, Chicago, IL), calibrated using a micrograph of a hemocytometer at the same magnification. Four to five images were obtained per sample with at least ten points per image. The calculated minimum thicknesses were used for determining the stress values in each sample.

4.2.7. Degradation Characterization.

Degradation of the formed matrices was analyzed using the previously described procedure with minor modifications (Sarasam, Krishnaswamy et al. 2006). In brief, 15 mm ×15 mm samples were cut from each matrix, washed with deionized water, sterilized in absolute alcohol for 30 minutes and washed thoroughly in sterile Krebs Henseleit buffer solution prior to incubating in 10 mL Krebs Henseleit buffer solution (pH = 7.4). Samples were placed in 20mL vials with a 15 mm diameter hole drilled in the caps and covered on the inside with 0.45 μm filters. Incubation was carried out in an incubator maintained at 37°C and 5% CO_2/95% Air. The media was replaced once every six days. During the incubation pH of the buffer was also monitored.

At ten day intervals, three samples per group were retrieved for determining the weight. Digital images of samples were also obtained to assess dimensional changes. Collected samples were washed with deionized water, dehydrated using absolute alcohol and briefly dried in a vacuum desiccator at ambient conditions prior to final weight determination. Samples were also analyzed by SEM to characterize structural changes.

4.2.8. Statistical Analysis.

All cell culture experiments were repeated three or more times with quadruplicate samples. All tensile testing were repeated four or more times and average and standard deviations were calculated. Significant differences between two groups were evaluated using a one way analysis of variance (ANOVA) with 99% confidence interval. When $P<0.01$, the differences were considered to be statistically significant.

4.3. Results.

4.3.1. Macroscopic Properties of Matrices.

Dispersion of PCL solution in water bath formed matrices quickly in 80 kDa and 46 kDa samples. However, 10 kDa PCL and mixture of 46 kDa and 10kDa PCL solutions did not produce a stable matrix despite precipitation, suggesting that MW of PCL plays a role in the matrix formation. Further, higher MW PCL solutions stored for more than four days also showed no matrix formation, probably due to the acid hydrolyses decreasing the MW of the polymer. Hence, all solutions were freshly prepared for generating matrices. No further testing was done with the ratio of 10 kDa PCL and mixture of 46 kDa and 10kDa PCL solutions.

Since temperature of water bath could influence matrix formation, other water temperatures were tested apart from room temperature solution (~ 25 °C). Decreasing the bath temperature to ~ 10 °C did not have a significant effect on the ease of formation of the matrices. Interestingly, PCL solution froze at 4 °C (refrigerator) and the MW did influence how fast the solution froze, probably due to freezing of acetic acid (melting point=16 °C).

4.3.2. Surface Properties of Matrices.

First, we questioned whether there is any difference in the surface characteristics of the side exposed to water-air interface (referred as top surface) compared to the side submerged in water (referred as bottom surface). For this purpose, both sides were evaluated by SEM. These results showed significant differences between the top side **(Figure 4.1)** and the bottom side **(Figure 4.2)** of the matrices have different characteristic.

Top side of all matrices showed porous structure, while the bottom side had rough surfaces with significantly less number of pores. Top side of blended matrices had larger pores compared to pure components. In addition, 1:0:1 blended matrix showed perforations on the surface, and microdomains appeared like indentation on the top side. This could be due to large difference in the chain size of the two molecular weights. Matrices containing the intermediate MW PCL showed no microdomains in the top surface. On the bottom side, 1:0:1 blended matrix showed a smooth surface compared to all other compositions but no microdomains were observed. No significant differences were observed between 0:1:0 and 1:1:1 blends.

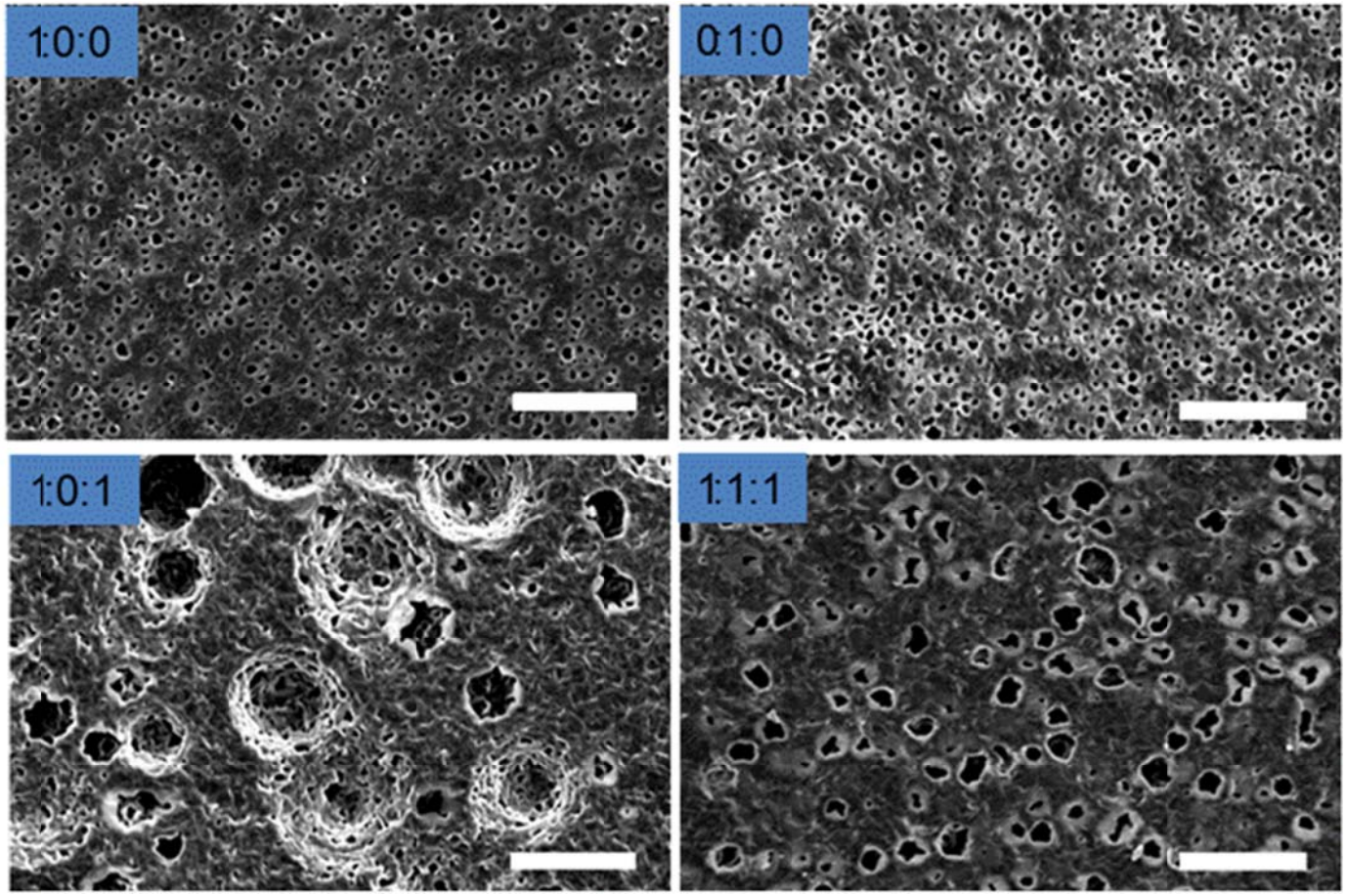

Figure 4.1. **Surface morphology of the top sides of matrices.** Scale bar corresponds to 50 μm.

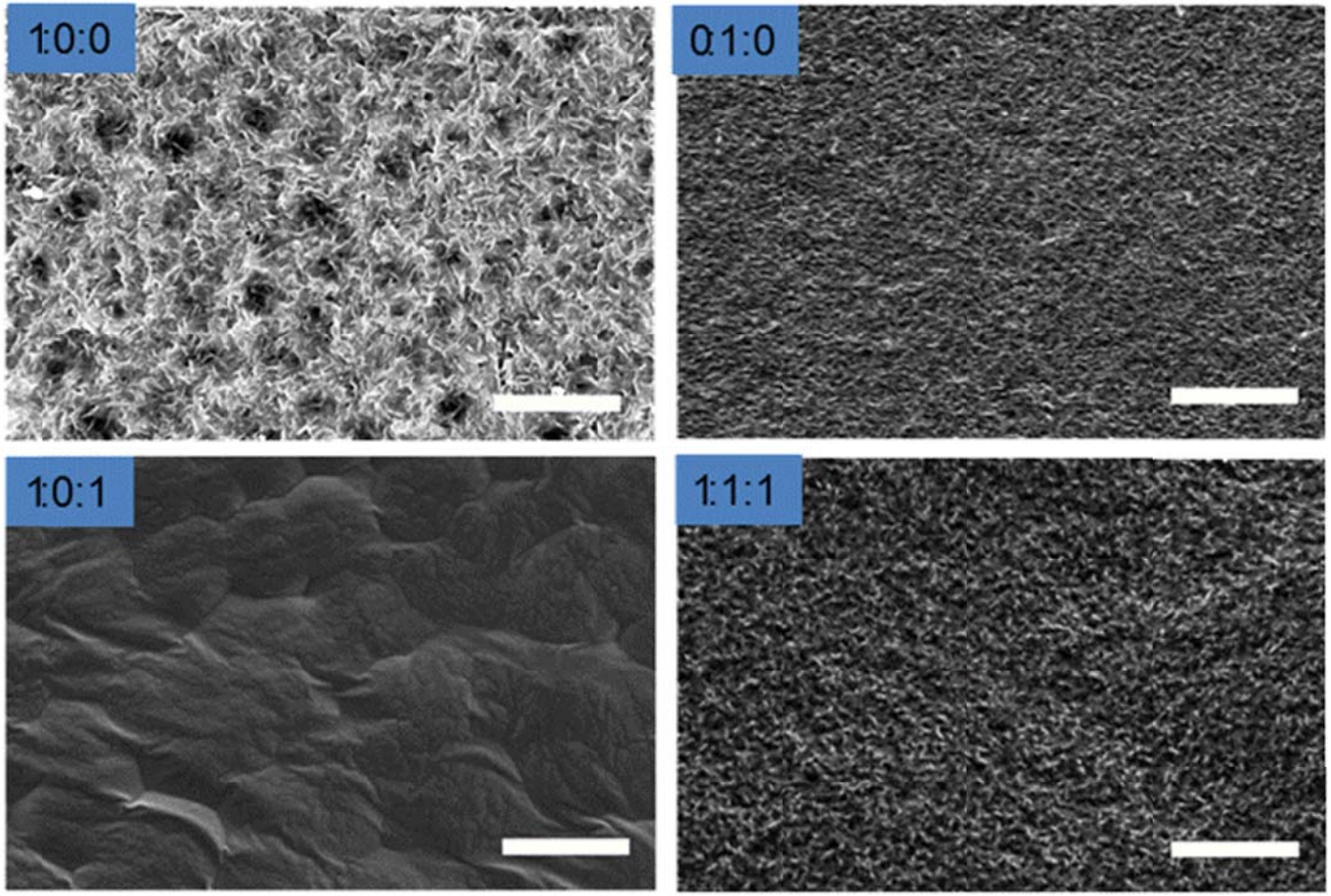

Figure 4.2. Surface morphology of the bottom sides of matrices. Scale bar corresponds to 50 μm.

4.3.3. Analysis of Surface Roughness.

The surface roughness was evaluated using AFM to better understand the effect of blending different MW of PCL on the roughness of the bottom side of the matrices. These results showed (**Figures 4.3-A**) a reduction in the surface roughness characteristics with decreased MW; matrices formed with 1:0:0 showed the highest roughness. Blending 10 kDa Mn PCL reduced roughness characteristics and presence of 46 kDa showed an increase in roughness factor. Quantitative analysis of roughness factor (**Figures 4.3-C**) confirmed statistically significant differences between 1:0:0 and 1:0:1 surfaces. This could be probably due to the packing of low MW PCL within the high MW structure during self assembly.

4.3.4. Effect of NaOH Neutralization on Surface Roughness.

Prior to using the formed matrices in biomedical applications, reminiscent acetic acid has to be removed. One option is to neutralize the surface with NaOH solution. To assess the effect of alkaline solution on the surface of PCL, surface topographies were analyzed by AFM. Neutralization process was carried out with 1N NaOH for 10 min. These results (**Figures 4.3-B**) showed a significant difference between neutralized and non-neutralized samples in 1:0:0 samples; non-neutralized 1:0:0 matrices had an average roughness factor of ~160 nm and after neutralization, the roughness factor decreased to ~75 nm (**Figures 4.3-C**). Mixtures of different MW showed no significant effect of neutralization process on the surface roughness, even in presence of 10 kDa PCL.

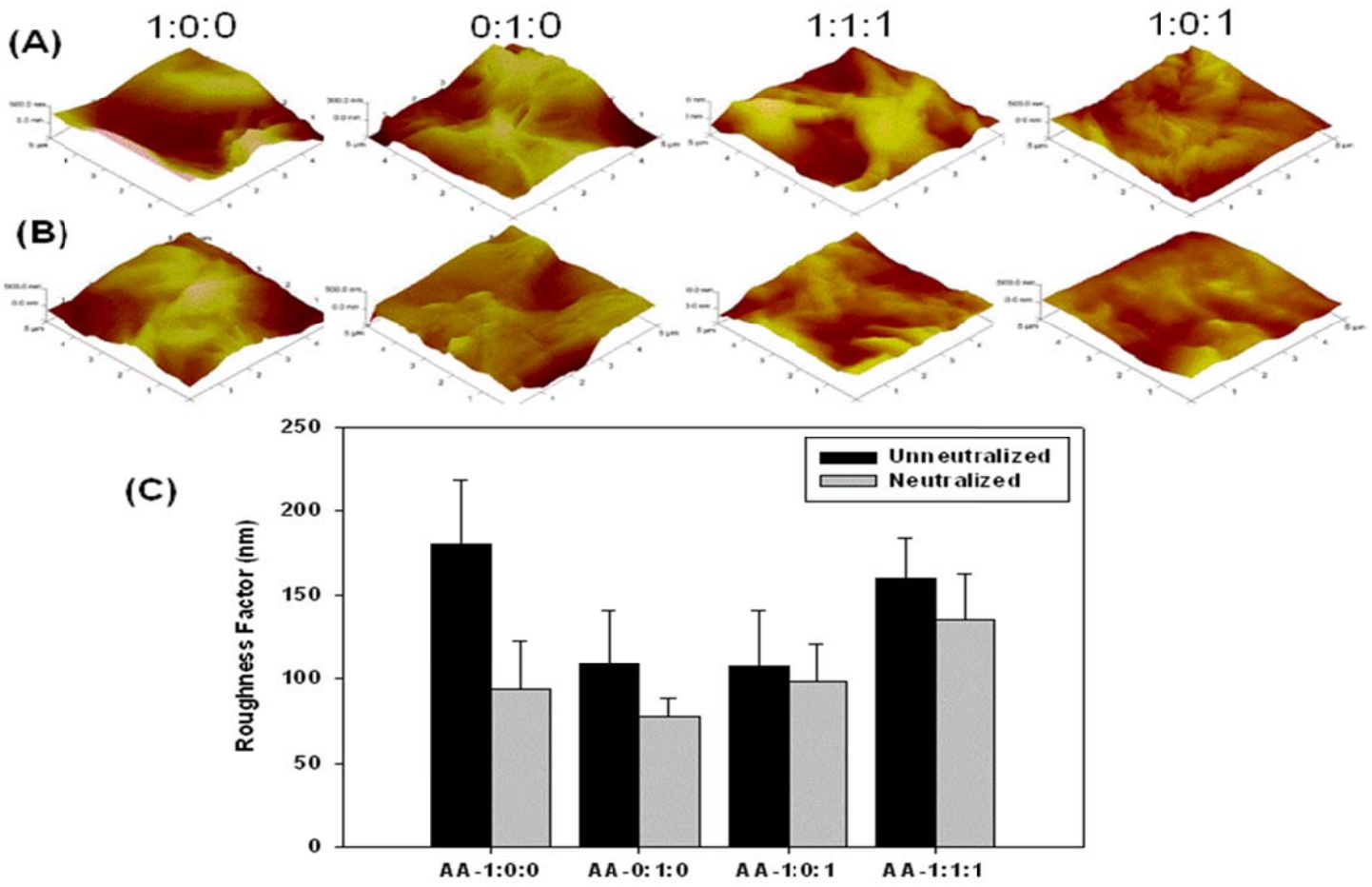

Figure 4.3. Surface roughness characteristics. (A) Surface morphology of fresh matrices. (B) Surface morphology after neutralization in NaOH. (C) Roughness changes in different blends.

4.3.5. Effect on Cellular Activity.

Cell morphologies were evaluated to understand whether PCL matrices support cell colonization. Cytoskeletal organization of HFF-1 was probed via actin staining. These results (**Figure 4.4**) showed that HFFs PCL matrices had spindle shape, similar to previous publications (Huang, Onyeri et al. 2005; Lawrence, Maase et al. 2008). HFFs showed peripheral distribution of actin filaments, similar to cells on TCP surface. However, there was a reduction in cell spreading characteristics relative to tissue culture plastic. There was no significant difference in the cell spreading on different blended matrices. Counterstaining with DAPI confirmed the presence of nuclei, along with the actin fiber, suggesting that the PCL structure promotes cell attachment.

4.3.6. Surface Properties of Composite-layered Matrices.

Gelatin-chitosan composite scaffolds were attached to PCL matrices to improve its bioactivity. These results showed **(Figures 4.5)** that the composite matrix was attached on the both sides of 1:0:1 PCL matrix through the perforations. Since 1:0:1 PCL sample had natural perforations by self assembly, gelatin-chitosan solution was penetrated through the perforations and formed multilayer on PCL matrix. Multilayer was not separated while the samples were neutralized in ethanol and incubated in PBS for the mechanical test. This confirmed that gelatin-chitosan matrices were fastened through the perforations of PCL matrix.

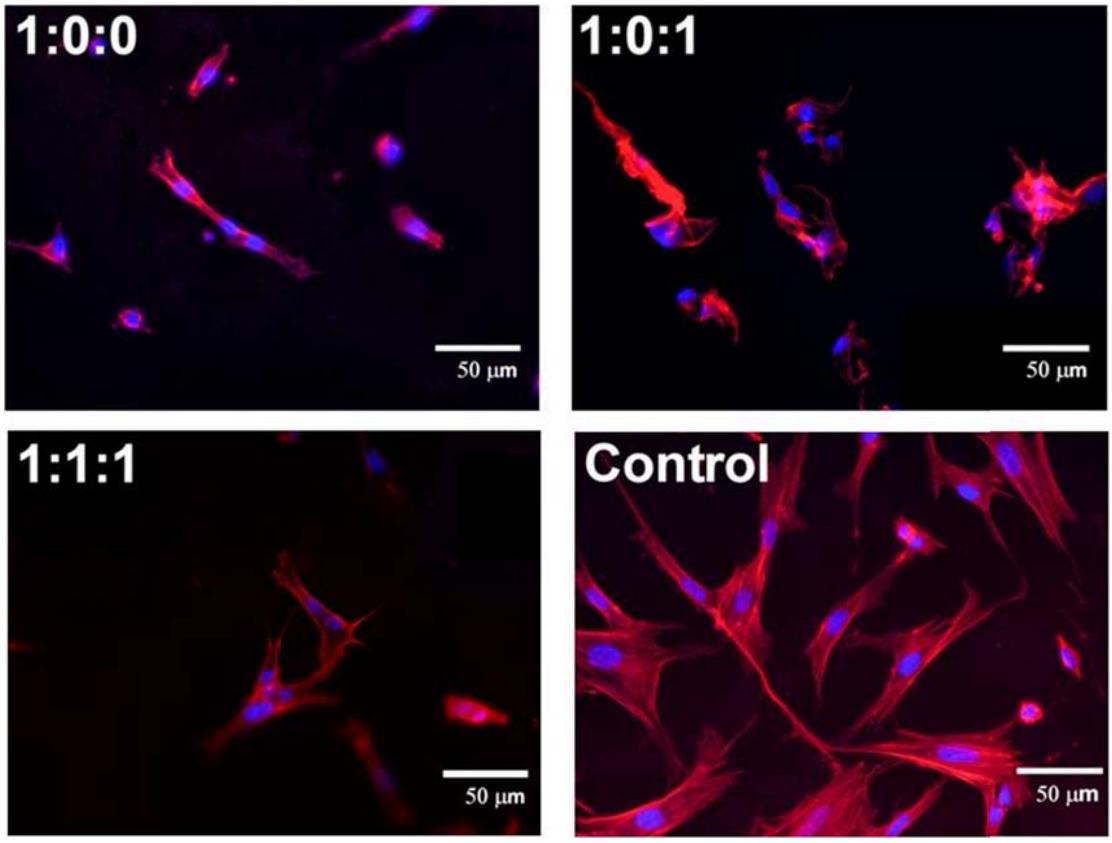

Figure 4.4. Effect of blending on the spreading of fibroblasts. Fluorescence micrographs obtained after staining with actin and nucleus after 48 hrs of incubation.

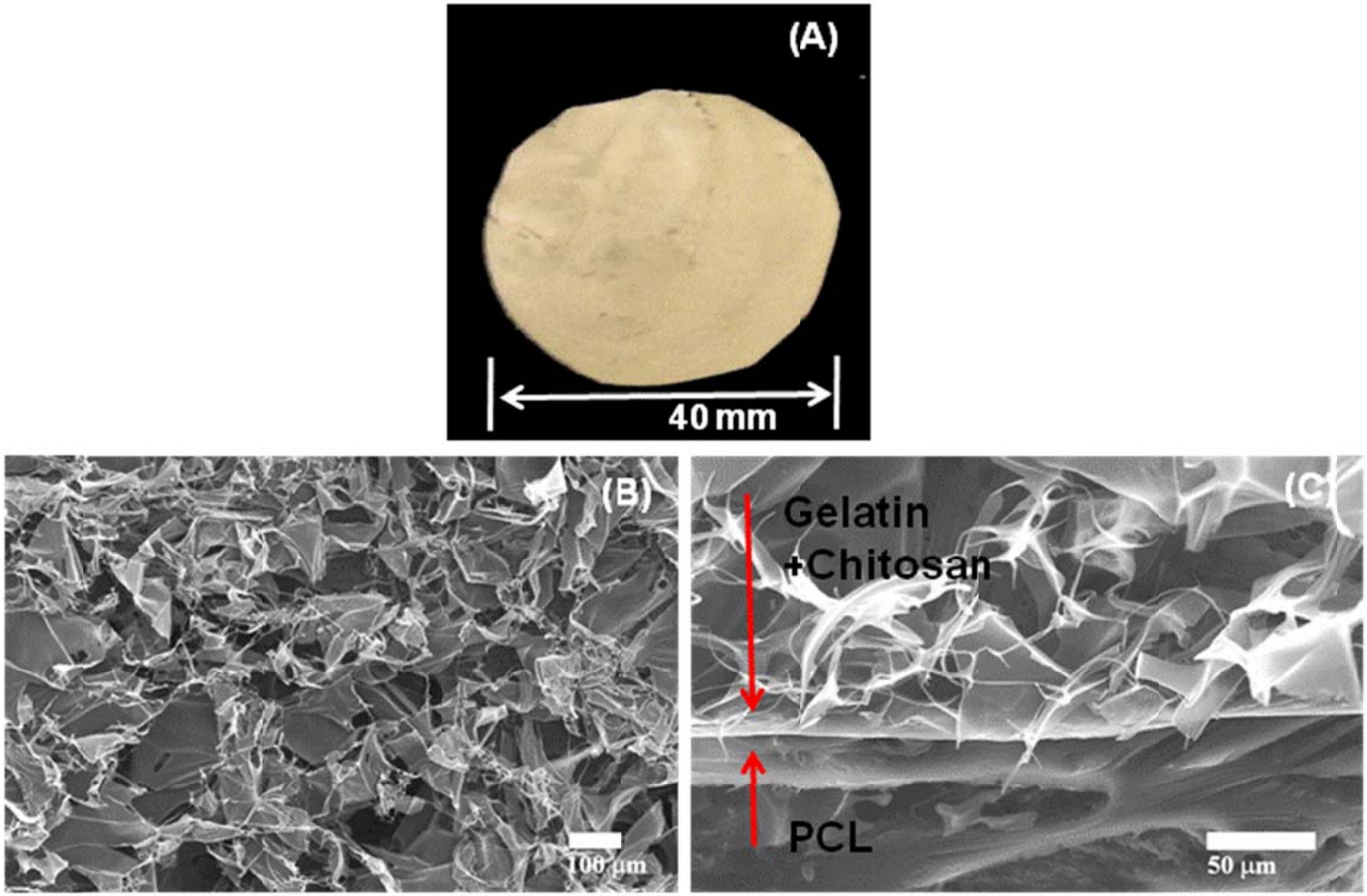

Figure 4.5. Effect of grafting gelatin-chitosan on porous stucture. (A) Photographs of gelatin-chitosan grafted 1:0:1 PCL matrix, Micrographs of (B) gelatin-chitosan coated PCL (top view), and (C) gelatin-chitosan coated PCL (cross-sectional view).

4.3.7. Effect on Tensile Properties.

Tensile properties were assessed in dry condition to understand the effect of blending on mechanical characteristics. These results (**Figure 4.6-A**) showed a significant decrease in the ultimate tensile stress of blended matrices; ultimate tensile stress was 1 to 2 MPa for 1:0:1 blended matrix relative to 1:0:0 (80 kDa) matrices which were in the range of 3 to 4 MPa. Further, strain range also decreased with blending; 1:0:1 blended matrix had 5 to 10% strain range whereas 1:0:0 (80 kDa) matrix had 320 to 370% strain range.

When matrices were tested in hydrated conditions at 37°C (**Figure 4.6-B**), ultimate tensile stress did not change significantly in both 80 kDa PCL and mixture. However, tensile strain range increased remarkably in all the samples; 46 kDa PCL showed the highest increase in the tensile strain. In addition, gelatin-chitosan coated 1:0:1 sample showed no differences in stress vs. strain curves and elastic modulus in both conditions **(Figures 4.6-A-C)**.

Elastic modulus was (**Figure 4.6-C**) calculated using the linear range (0.1%-5%). These results showed that 80 kDa matrices had the highest modulus in both dry and wet conditions. Elastic modulus was less in all the blended matrices relative to 80 kDa PCL, suggesting an increase in the elastic properties of the matrix. In addition, elastic moduli of all samples decreased in wet condition. This could be due to hydration of the polymers in the wet condition.

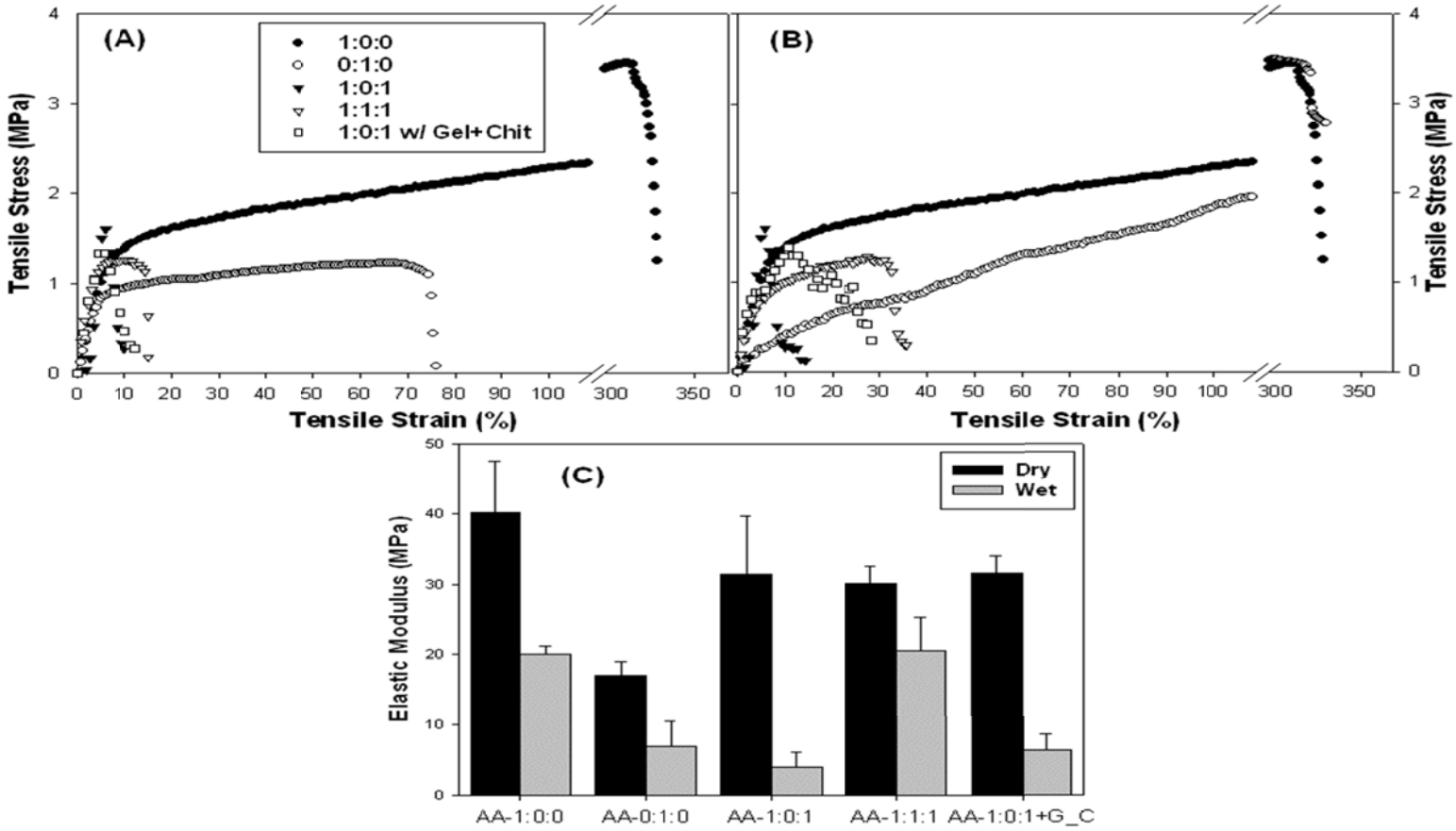

Figure 4.6. Effect of blending on stress-strain behavior. (A) Dry matrices assessed at room temperature. (B) Wet matrices assessed at 37°C in PBS. (C) Elastic modulus of matrices calculated from the linear region of stress-strain curve. Average and standard deviations from at least four samples for each condition are shown.

4.3.8. Effect on Degradation Characteristic.

Matrices were incubated in Krebs Henseleit buffer solution to understand the effect of blending on degradation characteristics. These results showed that presence of low MW PCL increased the degradation rate **(Figure 4.7-A)**. Weight loss calculations showed that 1:0:1 PCL matrices had 10% of weight loss after 50 days incubation. There was no significant difference in the weight of 1:0:0 and 0:1:0 PCL matrices, confirming that the weight loss is primarily due to 10 kDa Mn PCL. This suggests polymers were present individually in the matrices without combining. However, pH of the incubation medium did not change, probably due to the buffering capacity of Krebs Henseleit buffer, unlike phosphate buffered saline.

When dimensions of the matrices were analyzed, no significant change in width and length of formed matrices were observed. All matrices appeared intact during the study period except 1:0:1 matrix **(Figure 4.7-B),** which ruptured around 50 days. Further, 1:0:1 matrix also showed an increase in number of holes in the matrix during 30 days. This could correspond to the microdomains observed in the top side of the 1:0:1 matrix.

To understand the changes in surface architecture during degradation, samples were analyzed by SEM. Since 1:0:1 sample showed significant differences, only those samples were selected. These results showed no significant alteration during first ten days in both top side and bottom side of the matrix **(Figure 4.7-C)**. The surface features were still present on both sides of the matrix. Generally, samples retrieved after thirty days of incubation showed similar bottom side features as that of day zero samples. Samples retrieved after fifty days showed similar top side features as that of day zero

samples. This suggests that self assembled matrices of high MW PCL are stable despite dissolution in acetic acid. Degradation was localized to the regions containing 10 kDa PCL.

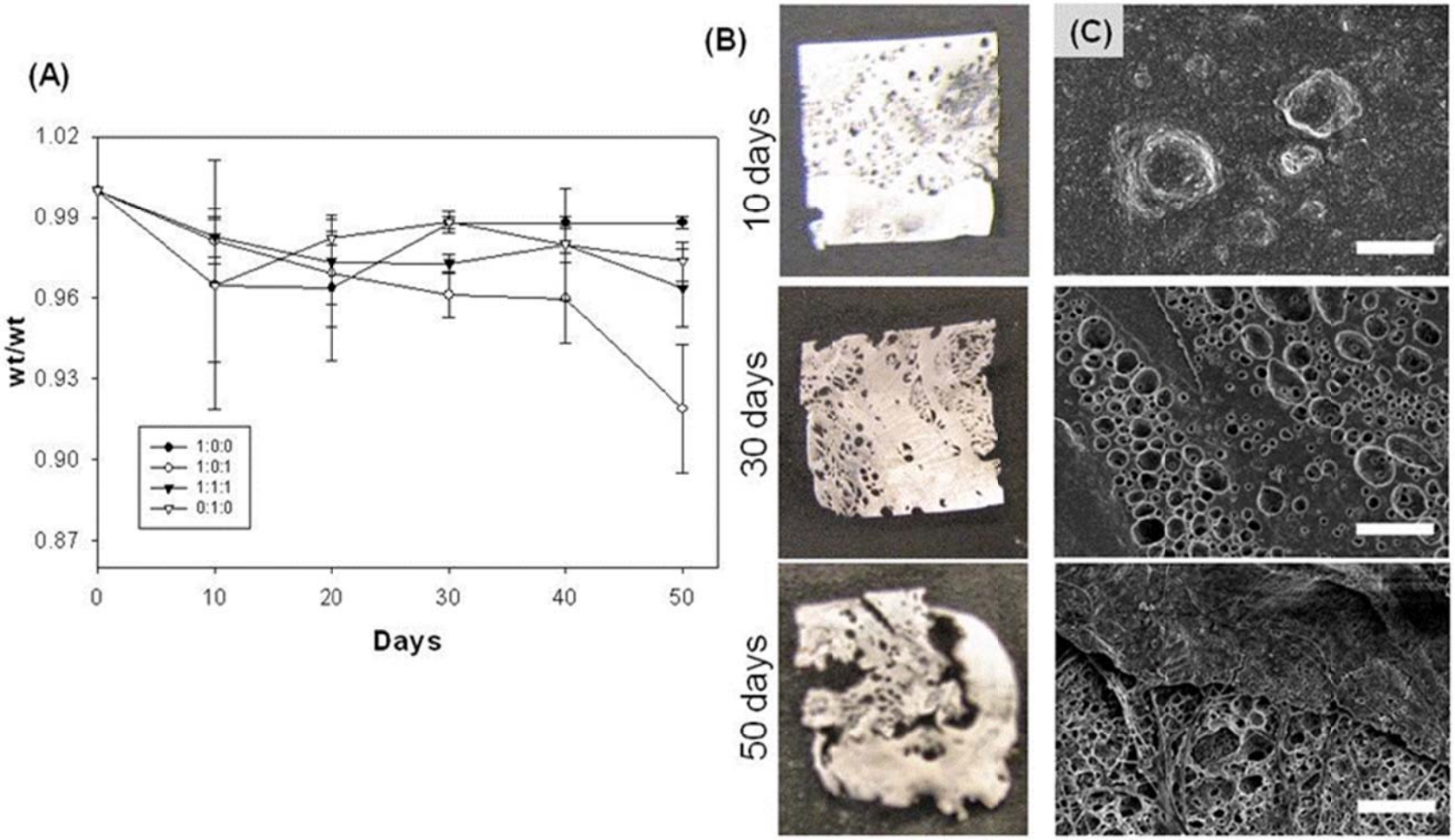

Figure 4.7. Degradation characteristics. (A) Changes in the weight relative to day zero values. (B) Photographs of 1:0:1 samples at different time points. (C) Micrographs of 1:0:1 samples at different time points. Scale bar corresponds to 50 μm.

4.3.9. Surface Properties of Anatomically Relevant Matrices.

Self assembly of PCL also occurred in tubular and spherical shapes on the solid supports **(Figure 4.8-A & D)**. However, one time self assembly was very thin and porous, which caused difficulty in removing from the mold. Hence, three layers were formed to improve the thickness. Since self assembly removes significant amount of PCL from the solution and water becomes very acidic, every time fresh solutions were used. If increased thickness is necessary, additional layers could be formed. Formed pure 80kDa PCL matrices had no structural changes compared to 2-D matrix, where as 1:0:1 blended PCL matrices had a reduced number of perforations by multiple layering. Further, layers could not be clearly identified by SEM, suggesting strong intermeshing of new layers to the previous self assembled layers. Thus, mechanical failure due to weak layer-by-layer interaction is not anticipated. However, these results **(Figure 4.8)** showed that matrices of the anatomical structures had different surface characteristics relative to 2-D matrices. Both inside and outside surfaces of tubular shape matrices had the similar surface characteristics **(Figures 4.8-B & C)** where as 2-D matrices had different surface architectures between top and bottom side. In addition, matrices of spherical shape showed non-porous structures outside of matrices where as inside of matrices had porous structures without microdomains **(Figures 4.8- E~F)**. These structural changes could be attributed to i) multiple layering and ii) contact with a solid surface rather air while assembling.

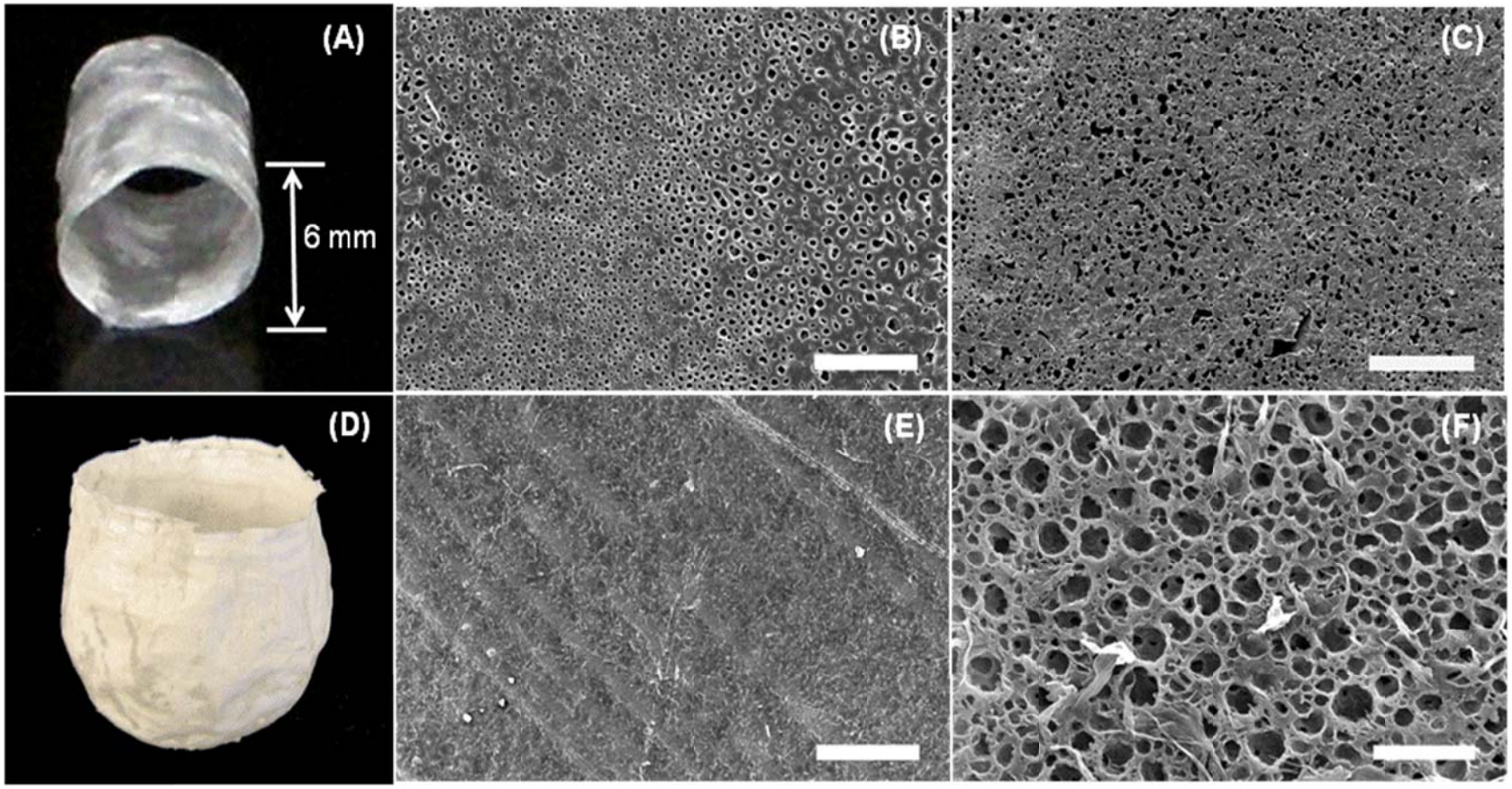

Figure 4.8. Surface morphology of the 3-D scaffolds. (A) Photographs of tubular shape of 1:0:1 sample. Micrographs of (B) outside of tubular shape, (C) inside of tubular shape, (D) photographs of bladder shape of 1:0:1 sample, (E) outside of bladder shape, and (F) inside of bladder shape. Scale bar corresponds to 50 μm.

4.4. Discussion.

Previously, we demonstrated the spontaneous aggregation of PCL dissolved in acetic acid upon contact with water (Pok, Wallace et al. 2010). Formed PCL matrices were hydrophilic as water uniformly distributed when added drop-wise onto the bottom side of the dry matrix. Surface energy estimation of 80 kDa PCL matrices showed different charge distribution on the bottom side of the PCL matrix. This facilitated immobilization of gelatin via electrostatic interactions. Previous reports show that dissolution of PCL in acetic acid does not alter the melting point and glass transition temperature of PCL (Sarasam and Madihally 2005; Sarasam, Krishnaswamy et al. 2006).

This study explored the possibility of blending different molecular weights of PCL and forming matrices in different shapes, suitable for tissue engineering applications. Equal amounts of different molecular weights were blended and other blend ratios were not investigated. Similar to 80 kDa, spontaneous aggregation of PCL into matrices was observed upon contact with water. Although precipitation into self assembled matrices did not occur with 10 kDa Mn PCL, blending 10 kDa Mn PCL with 80 kDa MW PCL allowed formation of matrices. Blending the low MW PCL helps in regulating the degradation rate. Nevertheless, one has to test the optimum ratio of low MW PCL to high MW PCL since low MW PCL alone cannot form self assembled matrices and stable structures by other methods such as electrospinning. Further, the same concept can be adapted in other processing techniques such as electrospinning (Ghasemi-Mobarakeh, Prabhakaran et al. 2008). Majority of the electrospun fibers for tissue engineering applications are formed using high MW PCL. However, if degradation rates have to be altered based on tissue type, then blending low MW is an option. In these studies, one

has to assess the changes in surface properties and degradation behavior.

Surface analysis showed different morphology on both sides of the matrices. Bottom side of the matrix had increased roughness relative to chloroform casted membranes, probably due to the different aggregation mode as reported by others using different solvents (Tang, Black et al. 2004). Top side had more perforations than bottom side. We did not measure the alteration in surface charges with the addition of different MW PCL. We speculate that the charge distribution will be similar to 80 kDa PCL matrices.

When cellular activity was measured, cell spreading was significantly less compared to tissue culture plastic surface. Since PCL alone does not have cell binding domain, cellular attachment is probably due to serum proteins. To alter cellular activity, blending natural polymers such as gelatin needs to be explored similar to previous studies. Previously, cells adhered to self assembled PCL matrices in the absence of serum (Pok, Wallace et al. 2010). Also, analysis of cellular activity needs to be extended to include other types of cells and functionalities.

Measured tensile properties showed a reduction in ultimate tensile strength and strain upon blending low MW PCL. These reductions could be due to the microdomains observed in the surface, clearly visible in 80 kDa and 10 kDa mixtures. Similar domain could exist in other blend combinations. Thus, while blending different molecular weights, one has to consider the effect on mechanical properties. An option is making thicker matrices which could have reduced pores on one side of the surface. Alternative option to improve the distribution is by heat annealing or solvent annealing techniques.

These strategies have to be investigated.

Since porous structures are necessary for three-dimensional colonization of cells, porous structures were generated using gelatin-chitosan combination. Previously, we have shown that gelatin-chitosan- supports proliferation of many cell types including fibroblasts and smooth muscle cells. There was no difficulty in distributing gelatin-chitosan solution on to the self assembled PCL matrix. There was no need to perforate the self-assembled PCL matrix while ensuring the adhesion of the porous structure, unlike previously reported PLGA-based composite (Coombes, Rizzi et al. 2004). Further, the uniform distribution of perforations in PCL matrix also showed less separation between the gelatin-chitosan porous structures. It was observed that the entire composite failed together during tensile tests, suggesting continuity between different phases. Nevertheless, one has to test the tissue regeneration in these composite matrices.

In summary, blending different molecular weights to alter degradation characteristics is an efficient approach which minimizes issues related to cross-linking and presence of other functional groups. When matrices are generated by self assembly in aqueous medium, roughness decreased in blended matrices. Surface roughness was not altered in blended matrices after treatment with NaOH solution to neutralize acetic acid. No significant alteration in cellular activity was observed. Further, tensile properties also decreased by blending. Elastic modulus decreased with decreased MW, validating the observed trend in compliance measurement. Significant alteration in degradation rate was observed. Self assembled PCL matrices can be generated in different shapes by using appropriate shapes. Gelatin-chitosan composite scaffolds were attached to surface of blended PCL matrices and composite solution penetrated through

the perforations. Freez-drying did not alter the tensile properties of self assembled PCL. In summary, this self assembled PCL matrices show significant potential in tissue engineering applications.

4.5. References.

Aliabadi, H. M., A. Mahmud, et al. (2005). "Micelles of methoxy poly(ethylene oxide)-b-poly(epsilon-caprolactone) as vehicles for the solubilization and controlled delivery of cyclosporine A." J Control Release **104**(2): 301-311.

Atala, A., S. B. Bauer, et al. (2007). "Tissue-engineered autologous bladders for patients needing cystoplasty." Journal of Urology **177**(4): 66-66.

Baker, S. C., G. Rohman, et al. (2009). "The relationship between the mechanical properties and cell behaviour on PLGA and PCL scaffolds for bladder tissue engineering." Biomaterials **30**(7): 1321-1328.

Cheng, Z. and S. H. Teoh (2004). "Surface modification of ultra thin poly (epsilon-caprolactone) films using acrylic acid and collagen." Biomaterials **25**(11): 1991-2001.

Coombes, A. G., S. C. Rizzi, et al. (2004). "Precipitation casting of polycaprolactone for applications in tissue engineering and drug delivery." Biomaterials **25**(2): 315-325.

Eid, K., E. Chen, et al. (2001). "Effect of RGD coating on osteocompatibility of PLGA-polymer disks in a rat tibial wound." J Biomed Mater Res **57**(2): 224-231.

Ghasemi-Mobarakeh, L., M. P. Prabhakaran, et al. (2008). "Electrospun poly([var epsilon]-caprolactone)/gelatin nanofibrous scaffolds for nerve tissue engineering." Biomaterials **29**(34): 4532-4539.

Guarino, V., P. Taddei, et al. (2009). "The Influence of Hydroxyapatite Particles on in vitro Degradation Behaviour of PCL based Composite Scaffolds." Tissue Eng Part A.

Htay, A. S., S. H. Teoh, et al. (2004). "Development of perforated microthin poly(epsilon-caprolactone) films as matrices for membrane tissue engineering." J Biomater Sci Polym Ed **15**(5): 683-700.

Huang, Y., S. Onyeri, et al. (2005). "In vitro characterization of chitosan-gelatin scaffolds for tissue engineering." Biomaterials **26**(36): 7616-7627.

Lawrence, B. J., E. L. Maase, et al. (2008). "Multilayer composite scaffolds with mechanical properties similar to small intestinal submucosa." J Biomed Mater Res A.

Li, W. J., J. A. Cooper, Jr., et al. (2006). "Fabrication and characterization of six electrospun poly(alpha-hydroxy ester)-based fibrous scaffolds for tissue engineering applications." Acta Biomater **2**(4): 377-385.

Park, A., B. Wu, et al. (1998). "Integration of surface modification and 3D fabrication techniques to prepare patterned poly(L-lactide) substrates allowing regionally selective cell adhesion." J Biomater Sci Polym Ed **9**(2): 89-110.

Pitt, C. G., M. M. Gratzl, et al. (1981). "Aliphatic polyesters II. The degradation of poly (DL-lactide), poly (epsilon-caprolactone), and their copolymers in vivo." Biomaterials **2**(4): 215-220.

Pok, S. W., K. N. Wallace, et al. (2010). "In vitro characterization of polycaprolactone matrices generated in aqueous media." Acta Biomaterialia **6**(3): 1061-1068.

Sarasam, A. and S. V. Madihally (2005). "Characterization of chitosan-polycaprolactone blends for tissue engineering applications." Biomaterials **26**(27): 5500-5508.

Sarasam, A. R., R. K. Krishnaswamy, et al. (2006). "Blending chitosan with polycaprolactone: effects on physicochemical and antibacterial properties." Biomacromolecules **7**(4): 1131-1138.

Tang, Z. G., R. A. Black, et al. (2004). "Surface properties and biocompatibility of solvent-cast poly[-caprolactone] films." Biomaterials **25**(19): 4741-4748.

van der Giessen, W. J., A. M. Lincoff, et al. (1996). "Marked inflammatory sequelae to implantation of biodegradable and nonbiodegradable polymers in porcine coronary arteries." Circulation **94**(7): 1690-1697.

Wei, X., C. Gong, et al. (2009). "Biodegradable poly([var epsilon]-caprolactone)-poly(ethylene glycol) copolymers as drug delivery system." International Journal of Pharmaceutics **381**(1): 1-18.

CHAPTER V

BIOREACTOR DESIGN CONFIGURATIONS FOR REGENERATING HUMAN BLADDER

5.1. Introduction.

Several approaches have been explored to colonize cells within a porous scaffold necessary for *in vitro* tissue regeneration. Using traditional tissue culture plastic, porous templates are inserted into wells and cells are seeded in a growth medium. However, adapting the technique to thicker structures is limited by the diffusion of nutrients as the primary mode of nutrient distribution within the porous structure is dictated by Fick's first law. The thickness of the tissue grown in static cultures is not comparable to that necessary for transplantation. Bioreactors have been widely utilized to continuously replenish the nutrients by convection (Gooch et al. 2001; Gray et al. 1988; Huang et al. 2005; Martin and Vermette 2005). In addition to improving the nutrient distribution, fluid flow can also introduce shear force on the cells. This shear force stimulates cells and alters the secretion characteristics which could affect the quality of the regenerated tissue. Cells respond to stress by altering their ECM biosynthesis (Gooch et al. 2001) and change the tissue composition (Chatzizisis et al. 2007; Cooper et al. 2007). Using

various bioreactor designs, some studies reported an improvement in the quality of the regenerated tissue (Niklason et al. 1999). However, other studies have reported deterioration in the quality (Heydarkhan-Hagvall et al. 2006). Overall outcome of regenerated tissue using bioreactors is of poor quality (Chen and Hu 2006; Martin et al. 2004; Niklason et al. 1999). This could be attributed to incomplete consideration of reactor design.

A number of studies have been performed to model bioreactor fluid dynamics (Brown and Meenan 2007; Cioffi et al. 2006; Hutmacher and Singh 2008; Porter et al. 2005; Sander and Nauman 2003; Williams et al. 2002). Simulations have simplified mathematical models and reduced scaffold size due to increased computational demand in simulating reactors suitable for clinical transplantation. Also, the kinetic models are over-simplified by ignoring the mass and structural complexities. Further, tissue regeneration is a dynamic process where the porous characteristics change due to matrix deposition and tissue maturation. Assembly and maturation of ECM elements in tissue regeneration play a significant role in determining the quality of the regenerated tissue. These changes affect the transport characteristics and nutrient distribution. Also, in vitro regeneration strategies are not characterized for high aspect ratio tissues which have large surface area relative to the thickness (Heydarkhan-Hagvall et al. 2006). Among different reactor configurations, the flow through reactor is better suited for regenerating high aspect ratio tissues due to following advantages (Lawrence et al. 2009): (a) uniformly supports or constrains the scaffold to prevent deformation, (b) continuous flow replenishes the nutrients while providing better control on hydrodynamic shear stress induced by the fluid flow, and (c) easy scaled-up to clinical requirement.

Increasing computational capabilities and advances in the application of numerical techniques has opened up possibilities to include complex transport steps in modeling. Our laboratory previously reported on the analysis of fluid flow characteristics along with nutrient distribution in growing tissues (Devarapalli et al. 2009; Lawrence et al. 2009). We evaluated the effect of various factors including i) reactor shapes (rectangular, circular), ii) flow rate, iii) inlet-outlet location, iv) inlet-outlet size which regulate velocities, v) changing pore architecture, vi) nutrient consumption (particularly oxygen and glucose) characteristics, and vii) different types of cells (smooth muscle cells, chondrocytes, and hepatocytes) in flat bioreactor configurations. The bioreactor shape and position of inlets and outlets affected to flow distribution and shear stress in high aspect ratio reactors containing porous structures.

Many tissues in the body are three-dimensional in nature. In this study, we aimed to simulate a bioreactor suitable for regenerating a human bladder by selecting appropriate dimensions. Two different shapes of inlets were simulated to minimize shear stress at the inlet area. Mimicking bladder shape of inlet was also tested. Within the reactor, the importance of locating the porous structure was also evaluated in conditions mimicking tissue regeneration i.e., changes in cell number and permeability.

5.2. Materials and Methods.

5.2.1. Preparation of Porous Scaffolds.

1%-1% (wt/v) gelatin-chitosan, chitosan with 190-310 kDa MW and gelatin Type-A (300 Bloom) were obtained from Sigma Aldrich Chemical Co. (St. Louis, MO), solutions were prepared in 0.1M acetic acid using deionized water. A well of 10cm diameter was prepared on Teflon dishes using silicon glue and 25mL of respective solutions were poured in the well and frozen overnight at -80^{0}C. The frozen solution was lyophilized overnight (Virtis, Gardiner, NY). When porous scaffolds are formed by lyophilization technique a thin non-porous film forms at the surface. This skinny layer hinders access to the underlying porous structure if not removed. For removing the skinny layer from scaffolds of 1%-1% (wt/v), a wet paper was placed on the top of the solution once it was poured inside the well and frozen along with the solution. After lyophilizing the paper was peeled off to generate scaffold without the skinny layer. Since acetic acid remaining in the scaffold has to be removed, dried samples were first incubated with pure ethanol for ten min and washed four times with phosphate buffered saline (PBS). Wet samples were analyzed using an inverted microscope outfitted with a CCD camera. Obtained digital micrographs were was analyzed using Sigma Scan Pro software (Systat Software, Inc., Point Richmond. CA) for pore size and number of pores.

5.2.2. Bioreactor Designs.

The spherical shape of the bioreactor was designed for bladder tissue regeneration. Based on the human bladder size, the volume of the reactor was set to 820 mL. The volume of scaffold was chosen to be 755 mL with a thickness of 3 mm, similar to the

human bladder.

Different inlet shapes: Simulations were performed in three different shapes of inlets to assess shear stress distribution (**Figure 1**):

Design 1: Single cylindrical inlet and outlet with 28 mm high and 6 mm diameter at the center of top and bottom of the reactor.

Design 2: Funnel shape inlet and outlet with 28 mm high, 6 mm diameter at the center of top and bottom of the reactor.

Design 3: Double cylindrical inlet and single outlet with the same size of Design 1.

Different location of scaffolds: Since funnel shape inlet (Design 2) showed minimal shear stress at the inlet area and uniform oxygen distribution throughout the reactor, Design 2 was selected for further analysis. Three different locations of the scaffold within the reactor were investigated using Design 2 (**Figure 3**):

Design 2-A: A 3-mm thick porous scaffold attached to the interior wall of the spherical reactor. There was an additional 3mm open channel above the porous structure which did not have any porous structure..

Design 2-B: A 3-mm thick porous structure was the annular region through which medium was circulated.

Design 2-C: A 3-mm thick scaffold was suspended in the middle with 1.5 mm open channel on either side.

5.2.3. Fluid Flow Simulation.

The steady state analysis of the fluid flow was performed using the COMSOL 3.5a Multiphysics. Three dimensional (3D) reactor models were created by drawing spheres of different radius in 3D (Geom1) and then using the "difference" tab in COMSOL for getting the desired annular region. To add inlet and the outlet to this annular region, a rectangular shape was drawn in 2D (Geom2) and then revolving it 360 degree along the axis. Next, the sub-domain and boundary conditions were set in the Physics tab. The geometry was meshed one by one on all the edges using the *constrained edge element distribution* in the *free mesh parameters* tab. Subsequently the surfaces and the sub-domain were meshed using the triangular method and keeping the maximum elemental size as 0.005. The number of mesh points was 12099~15673, and the number of elements was 51417~68479. The flow rate was set at 0.5 mL/min initially. Then, the flow rate was increased to 1 mL/min and then to 7.5 mL/min to determine the minimum flow rate at which the nutrients were consumed fully. The simulation was performed using the previously described procedure with modifications(Devarapalli, Lawrence et al. 2009), the velocity profiles were determined by solving a) the incompressible Navier – Stokes equation on the non-porous regions and b) the Brinkman equation on the porous regions. The nonporous sections of the reactor were modeled solving incompressible Navier-Stokes equation which is given by

$$\rho(u \bullet \nabla)u = -\nabla \bullet \left[-\tau + p\delta_{ij}\right] \tag{5.1}$$

$$\nabla \bullet u = 0 \tag{5.2}$$

where u is the flow velocity (m/s), ρ is the fluid's density (kg/m^3), p is the pressure (Pa),

δ_{ij} is the Kronecker delta function. The Brinkman equation is given by

$$\mu\nabla^2 u_s - \frac{\mu}{\kappa} u_s = \nabla p \tag{5.3}$$

$$\nabla \bullet u_s = 0 \tag{5.4}$$

where κ is the permeability of the porous medium (m^2), u_s denotes the fluid superficial velocity vector (m/s), p is the fluid pressure (Pa), and μ is the effective viscosity in the porous medium (kg/m.s). The permeability (κ) of the porous medium is a geometric characteristic of the porous structure at several length scales. Based on the pore architecture of chitosan porous structures utilized in experimental analysis, the permeability was calculated using an average pore size of 85 μm and 120 pores/mm^2 in the equation (Truskey, Yuan et al. 2004)

$$\kappa = \frac{\pi}{128} n_A d^4 \tag{5.5}$$

where n_A is the number of pores per unit area and d is the average pore diameter. Both the permeability (κ; m^2) and void fraction (ϕ, dimensionless) were incorporated into Eq.(3) in order to account for the porous characteristics of the matrix, yielding another form of the Brinkman equation (Truskey, Yuan et al. 2004) with the Navier-Stokes equation.

$$\frac{\eta}{k} u = -\nabla \cdot \left[\frac{-\tau}{\varepsilon_p} + p\delta_{ij} \right] \tag{5.6}$$

where ε_p is the porosity of the porous media, taken as 85% based on the chitosan porous structure characteristics. The shear stress was visualized as the viscous force per area in

the z direction, as calculated by

$$\tau \bullet n \tag{5.7}$$

The shear stress tensor is an integral part of the Navier-Stokes equations describing flow in a free channel While solving the incompressible Navier-Stokes equations, the perpendicular flow was given as 5 mL/min and the outlet boundary condition was set as pressure = 0.

Since the nutrient consumption is governed by diffusion rather than convection, it is important to accommodate the diffusive characteristics of nutrients through the porous structure. The change in effective diffusivity (D_{eff} in m^2/s) due to altered void fraction in the porous structure is calculated using Mackie-Meares relationship (Mackie and Meares 1955; Mackie and Meares 1955; Sengers, van Donkelaar et al. 2005).

$$\mathrm{D} = \mathrm{D}_{\infty} \left(\frac{\varepsilon_{\mathrm{p}}}{2-\varepsilon_{\mathrm{p}}}\right)^2 \tag{5.8}$$

where D_{∞} is the diffusion coefficient from Stokes-Einstein equation, and Φ is the porosity of the scaffold. Velocity profiles in the scaffolds were obtained, and *Peclet* number was calculated using the equation,

$$Pe = \frac{Vr}{D_{O_2}} \tag{5.9}$$

where V is the velocity, r is a radius of the scaffold, and D_{O2} is the diffusion coefficient of oxygen.

5.2.4. Reactions in the Porous Structure.

Reactions in the porous region were simulated by the method previously described(Devarapalli, Lawrence et al. 2009). Gelatin-chitosan scaffold was used for porous structure with SMCs. Oxygen and glucose consumptions were simulated independently for the reason that glucose concentration (5.5 moles/m^3) in the growth medium is in large excess relative to oxygen (0.2 moles/m^3) concentration (determined using the Henry's law constant at 37°C). The rate constants were obtained for SMCs based on the reaction rates reported in the literature (Motterlini, Kerger et al. 1998; Alpert, Gruzman et al. 2002; Sengers, Heywood et al. 2005; Fogler 2006). Using the steady state velocity profiles, the steady state concentration profiles of oxygen and glucose were obtained by solving the equation of continuity using the chemical reaction engineering module in COMSOL 3.5a Multiphysics. Nutrient consumption was included in the simulation via the rate law. The convective diffusion equation was used to obtain the concentration at varying position along the cross section of the reaction:

$$\nabla \cdot (-D\nabla C_A) + u \cdot \nabla C_A = r_A \qquad (5.10)$$

where c_A is the concentration of the species (mol/m^3), r_A is the rate of reaction of the species under consideration (mol/m^3.s), D is the diffusivity of the species (m^2/s), and u is velocity vector (m/s). Physical properties of water were used as it constitutes the bulk of the growth medium. The flow properties (i.e., viscosity and density) of the nutrient stream depend on the properties of the bulk fluid. Since the cells are present only in the porous scaffolds, nutrient consumption rate law was defined only in the porous region, the reaction term was zero in the non-porous regions. It is a typical practice to decouple

oxygen and glucose consumptions for the primary reason that glucose concentration (5.5 moles/m^3) in the growth medium is in large excess relative to oxygen (0.20 moles/m^3) concentration (the initial concentration of oxygen in the growth medium was determined using the Henry's law constant at 37°C for each cell type). In addition, for every mole of glucose consumed, six moles of oxygen is consumed according to the stoichiometry of aerobic metabolism. The rate constants were obtained for SMCs using Michaelis-Menten type rate law based on the reaction rates reported in the literature (Motterlini, Kerger et al. 1998; Alpert, Gruzman et al. 2002; Sengers, Heywood et al. 2005; Fogler 2006). The rate law is given by the expression

$$-r_A\left(mol/m^3.s\right)=\frac{V_m C_A}{K_m+C_A} \tag{5.11}$$

where r_A is the reaction rate, v_m is the maximum reaction rate, and k_m is the Michaelis constant. C_A was replaced by c_1 for the oxygen concentration, and C_A is replaced by c_2 for the glucose concentration. Both the rate laws were defined in the COMSOL to enable the visualization of both the oxygen and glucose profiles within the porous structure. Nutrient concentration profiles were obtained using "Slice Plot Parameter", and the minimum values were found using "Cross-Section Plot Parameters".

5.2.5. Statistical Analysis

Significant differences between two groups (T-test) and more than two groups (F-test) were evaluated using a one way analysis of variance (ANOVA) with 99% confidence interval. When $P<0.01$, the differences were considered to be statistically significant.

5.3. Results.

5.3.1. Effect of Inlet shape on shear stress.

To minimize shear stress at the inlet area, three different shapes of inlets were simulated. First, two different inlet shapes were simulated to evaluate shear stress distribution at the inlet area of the porous structure. To mimic bladder configuration, two inlets instead of one was also simulated. Based on our previous work (Devarapalli, Lawrence et al. 2009), minimum volumetric flow rate of 0.5 mL/min was selected using the relation $-r_{O_2}\big|_{inlet} = \upsilon \Delta C_{O_2} / V_R$ where V_R is the volume of the reactor and ΔC_{O2} medium concentration change at the outlet of the reactor. In Design 3, total volumetric flow rate is same as the other two designs. In other words, each inlet had half the total flow rate. Pressure drops through the reactor were simulated using Brinkman equation. These results (**Table 5.1**) showed that no significant difference was observed in pressure drop with different inlet shapes. Even though Design 3 had a half flow rate in each inlet, its pressure drop was similar to Design 2. Maximum shear stress at the inlet area of the scaffold was also evaluated. Maximum shear stresses of three designs increased constantly with increasing flow rate. However, Design 2 showed less increase in shear stress by increasing flow rate compared to Design 1 and 3. Maximum shear stress of Design 2 was ~161 µPa at 5 mL/min of flow rate where as Design 1 had 1160 µPa. Design 2 provided the uniform shear stress at the inlet while uniformly distributing sufficient amount of nutrients. This resulted in reduction in the shear stress at the wider inlet of Design 2 (**Figure 5.1**). In addition, the maximum shear stress and pressure drop of Design 3 was similar to Design 2 **(Table 5.1)**.

The effect of different inlet shapes on nutrient distribution was also evaluated. This result (**Figure 5.2**) showed that Design 1 and 2 had uniform distribution of oxygen through the bioreactor. However, Design 3 had reduction of oxygen concentration at the outlet area with non-uniform oxygen distribution because of two inlet flow from different directions. Since results of the pressure drop, shear stress, and nutrient distribution analysis showed that design 2 had the most favorable configuration, Design 2 was selected for further analysis in presence of porous.

Table 5.1. Effects of inlet shapes and flow rate on pressure drop through the reactor and shear stress at the inlet area.

	Design 1		**Design 2**		**Design 3**	
Flow Rate (mL/min)	**Δp (mPa)**	**Max. Shear Stress (μPa)**	**Δp (mPa)**	**Max. Shear Stress (μPa)**	**Δp (mPa)**	**Max. Shear Stress (μPa)**
0.5	12.07	44	8.32	17	8.22	31
1	24.19	99	16.73	35	16.56	64
5	127.55	1160	90.56	161	88.85	405

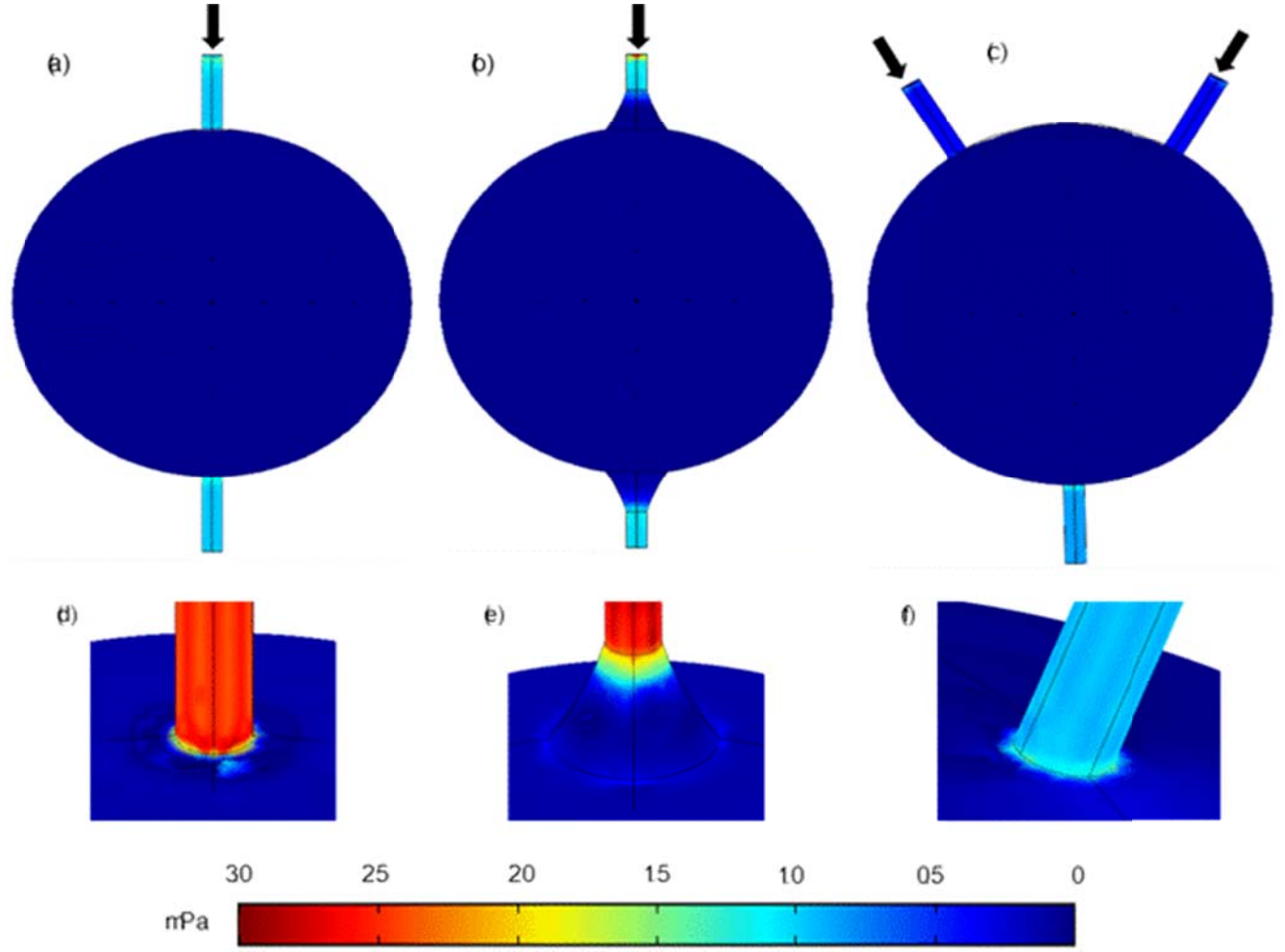

Figure 5.1. Shear stress distribution with different shapes of inlet. (a) cylindrical shape inlet, (b) funnel shape inlet, and (c) two cylindrical shape inlets.

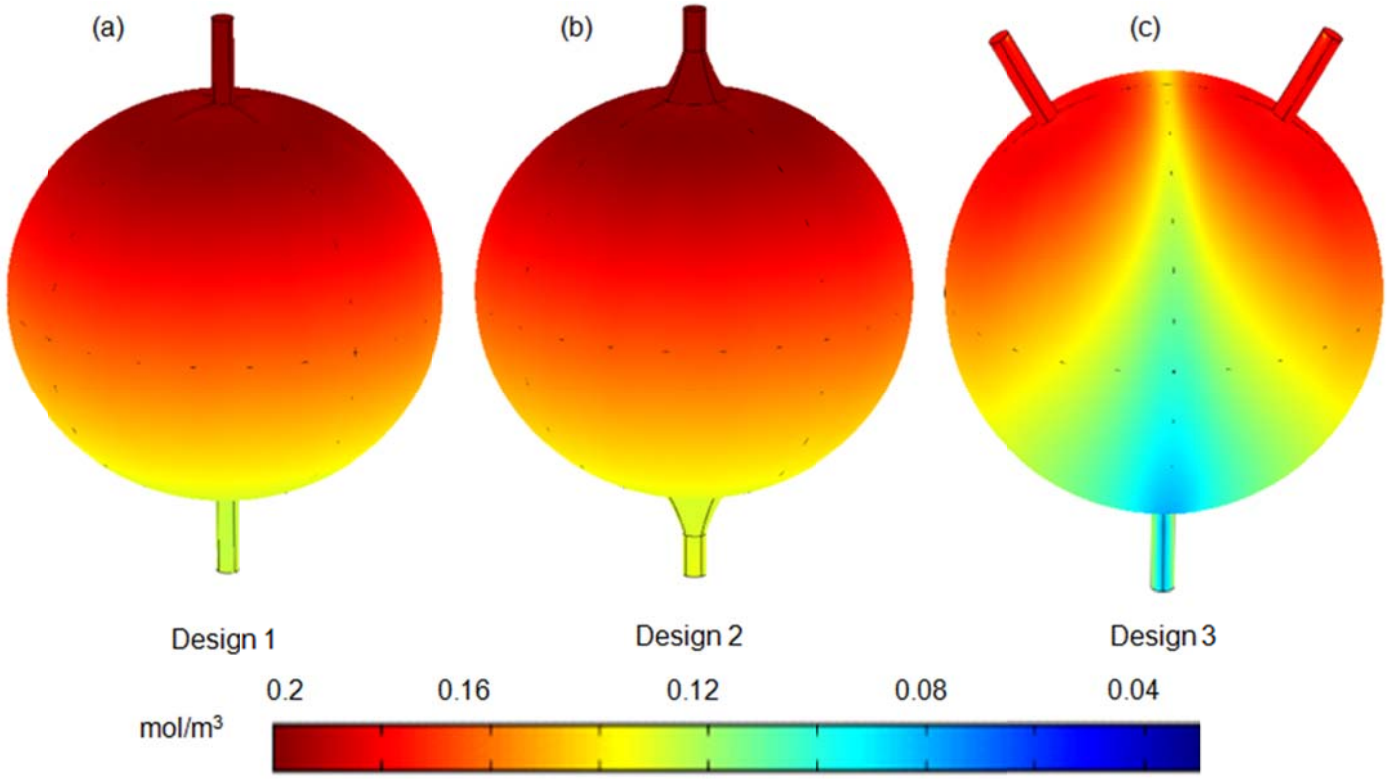

Figure 5.2. Oxygen distribution through the reactor with different shapes of inlet. (a) cylindrical shape inlet, (b) funnel shape inlet, and (c) two cylindrical shape inlets.

5.3.2. Effect of Location of the Scaffold on Velocity Profile.

Next, Oxygen mass transfer can be simply described as the movement of the molecule relatively to fixed references due to two main contributions: diffusion and convective flow(Martin and Vermette 2005). Based on this concept, three different locations of the scaffold within the reactor were investigated using Design 2 (**Figure 5.3. a-c**); i) Design 2-A: fluid flow within the scaffold occurred by diffusion, ii) Design 2-B: convective limited, and iii) Design 2-C: both diffusion and convection. Velocity profile within the scaffold was found using "Cross-Section Plot Parameters" with 5 mL/min of volumetric flow rate. These results showed (**Table 5.2 and Figure 5.4**) that reduced channel size with the same volumetric flow rate increases velocity. Design 2-B which has no channel between the reactor and porous structure had a higher average velocity (69000 mm/s) than Design 2-A (38 mm/s) and Design 2-C (82 mm/s). Further, velocity profile indicated that Design 2-C was the most favorable configuration with very low velocities across the scaffold. However, Design 2-A showed that the velocity reduced by reaching the inside wall of scaffold, and the velocity was zero at the end of scaffold.

In addition, the average *Péclet* number was calculated in the porous area using the equation 9. The velocity at the center of scaffold was used to calculate *Péclet* number with $1.1937*10^{-9}$ m^2/s of diffusivity of oxygen. These results showed that Design 2-A and C had *Péclet* number of less than 1 where as design 2-B had ~170 of dimensionless *Péclet* number (data was not shown). This suggested that Design-2 A and C had diffusion dominant characteristics where as Design 2-C was convective flow dominant.

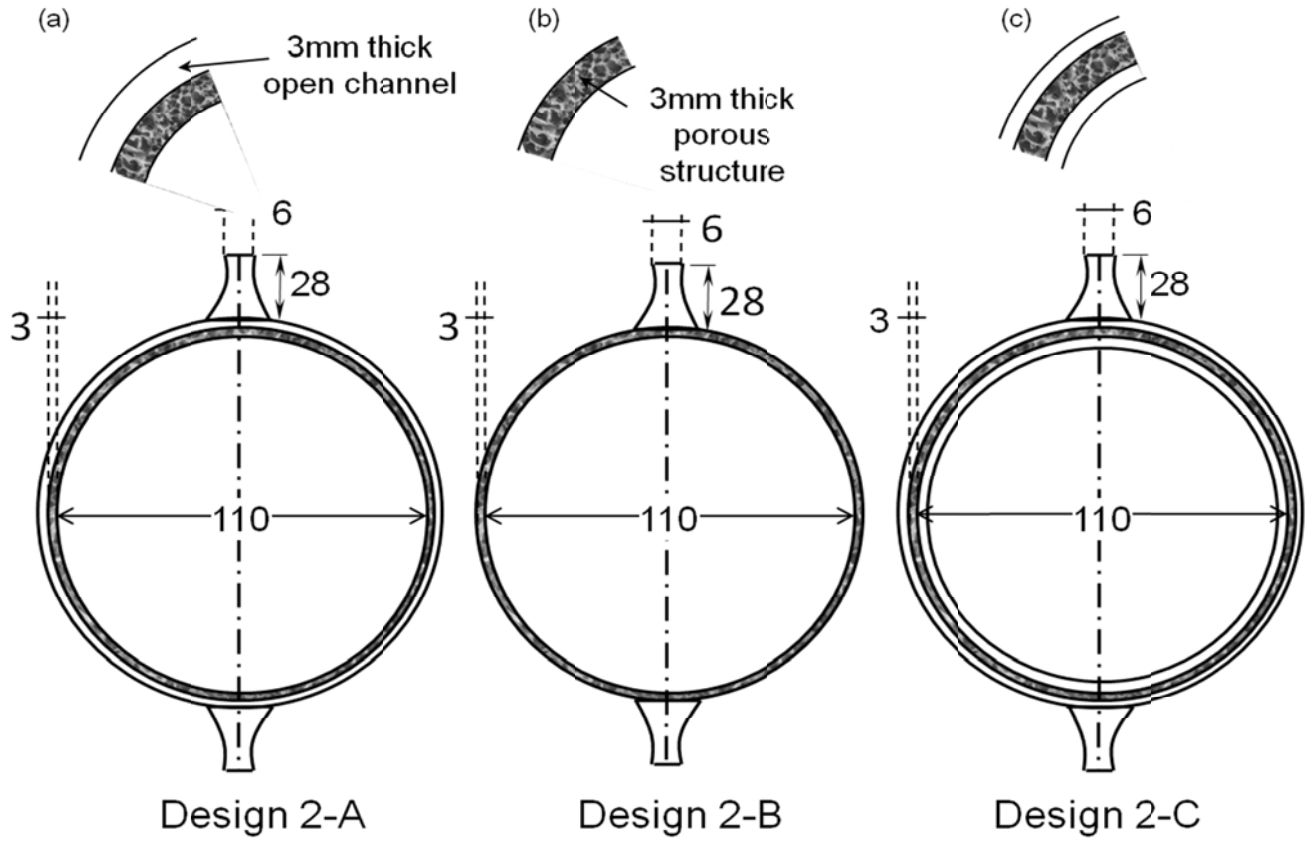

Figure 5.3. Designs of bioreactors with different location of scaffold.

Table 5.2. Effects of location of scaffold on *peclet number* and average velocity through the scaffold. Note that volumetric flow rate was 5 mL/min

	Peclet No.	Average Velocity (mm/s)
Design 2-A	0.096	38
Design 2-B	173.411	69000
Design 2-C	0.206	82

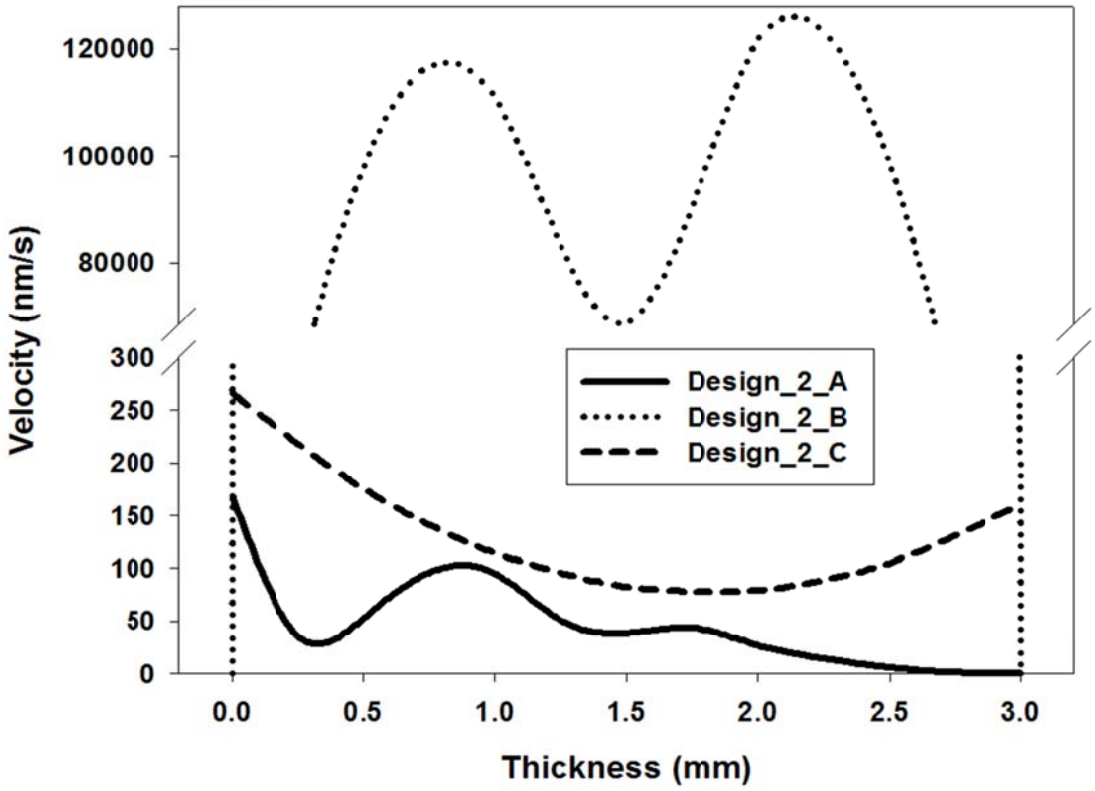

Figure 5.4. Velocity profile through the scaffold.

5.3.3. Effect of Location of the Scaffold and Flow rate on Pressure Drop and Shear Stress.

Pressure drop through the bioreactor and shear stress within the scaffold were analyzed with different scaffold locations and flow rates. Since pressure drop and shear stress were calculated by Brinkman equation, these values were not a function of the rate constants of SMCs. These results showed (**Table 5.3**) that pressure drop was increased by increasing the flow rate from 0.5 mL/min to 5 mL/min, and Design 2-B had the highest pressure drop compared to others.

Maximum shear stress ranges through the porous structure were evaluated using "Domain Plot Parameters" and "Surface" function. Since shear stresses at the inlet area were minimized from earlier simulation, shear stresses of inlet area were neglected. Maximum shear stresses showed a linear increase with increasing the flow rate (**Table 5.3**). Design 2-C showed a higher shear stress range relative to other designs. Maximum shear stress range of Design 2-A was 45~58 μPa, 90~200 μPa was for Design 2-B, and Design 2-C had 150~230 μPa. However, those values did not have significant difference.

Table 5.3. Effect of location of scaffold and flow rate on pressure drop through the reactor and shear stress through the scaffold.

	Design 2-A		Design 2-B		Design 2-C	
Flow Rate (mL/min)	Δp (mPa)	Max. Shear Stress (μPa)	Δp (mPa)	Max. Shear Stress (μPa)	Δp (mPa)	Max. Shear Stress (μPa)
0.5	8.32	4.5~6	10622	9~20	20.72	15~23
1	16.73	9~12	21249	18~40	41.54	30~46
5	90.56	45~58	106255	90~200	214.15	150~230

5.3.4. Oxygen and Glucose Concentration Profile at the Steady State.

To evaluate the effect of location of scaffold on nutrient consumptions of oxygen and glucose, simulations were performed with defined rate laws for smooth muscle cells. The simulations were performed at the same cell density (1.2×10^{12} cells/m^3). Nutrient concentration profiles were obtained using "Slice Plot Parameter", and the minimum values were found using "Cross-Section Plot Parameters". Most of minimum nutrient concentration was found at the outlet area of the porous structure. These results showed (**Table 5.4 and Figure 5.5**) that the location of the scaffold did not affect significantly to both minimum and outlet oxygen concentration at the low flow rate. Design 2-A showed a higher concentration with 0.5 mL/min of flow rate than Design 2-B and C. However, Design 2-B and C had higher minimum oxygen concentration at the higher flow rate than Design 2-A. In other words, Design 2-B and C showed a sharp increase of minimum oxygen concentration followed by increase of flow rate, whereas Design 2-A had a gradual increase. In addition, there was no significant difference in glucose consumption for three designs with lower flow rate. Along with a result of oxygen concentration, Design 2-B and C had a higher glucose concentration than Design 2-C. However, no significant difference was observed in glucose consumption by varying flow rate and location of scaffold.

Results of "Cross-Section Plot Parameters" analysis confirmed that oxygen distribution of three designs did not indicate significant differences at lower flow rates. Further, Design 2-B and C through the reactor and porous structure was fully saturated with oxygen by reaching at 5 mL/min of flow rate. Glucose was also highly saturated in every design (**Figure 5.6-5.7**).

Table 5.4. Effect of location of scaffold and flow rate on oxygen and glucose distributions.

	Design 2-A			Design 2-B			Design 2-C		
Flow Rate (mL/min)	Min. C_{oxygen} (mol/m^3)	Outlet C_{oxygen} (mol/m^3)	Min. $C_{glucose}$ (mol/m^3)	Min. C_{oxygen} (mol/m^3)	Outlet C_{oxygen} (mol/m^3)	Min. $C_{glucose}$ (mol/m^3)	Min. C_{oxygen} (mol/m^3)	Outlet C_{oxygen} (mol/m^3)	Min. $C_{glucose}$ (mol/m^3)
0.5	0.0352	0.0696	4.362	0.0274	0.0449	4.628	0.0262	0.0557	4.379
1	0.0666	0.1220	4.640	0.0745	0.1035	4.997	0.0590	0.1118	4.811
5	0.1076	0.1828	4.868	0.1553	0.1770	5.227	0.1314	0.1819	5.224

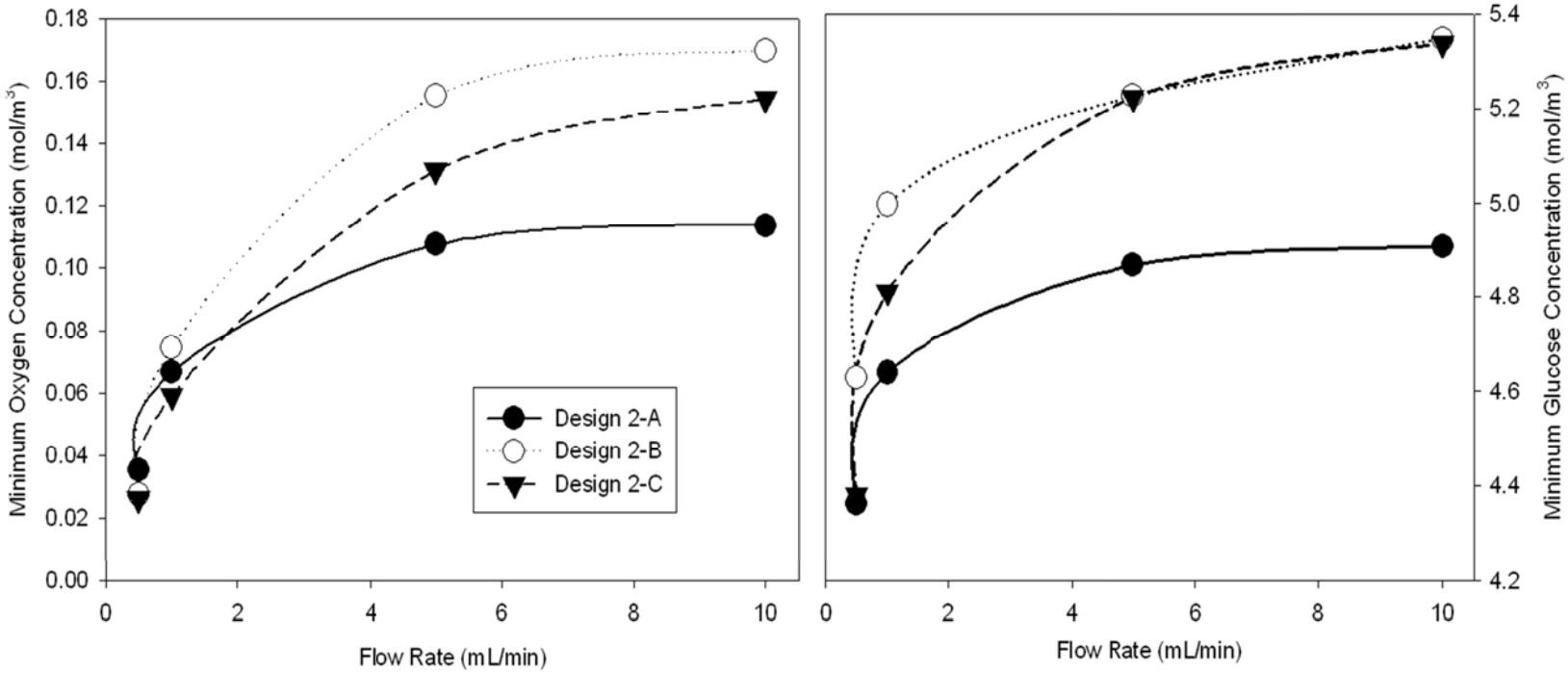

Figure 5.5. Effects of location of scaffold and flow rate on (a) oxygen concentration profile, and (b) glucose concentration profile.

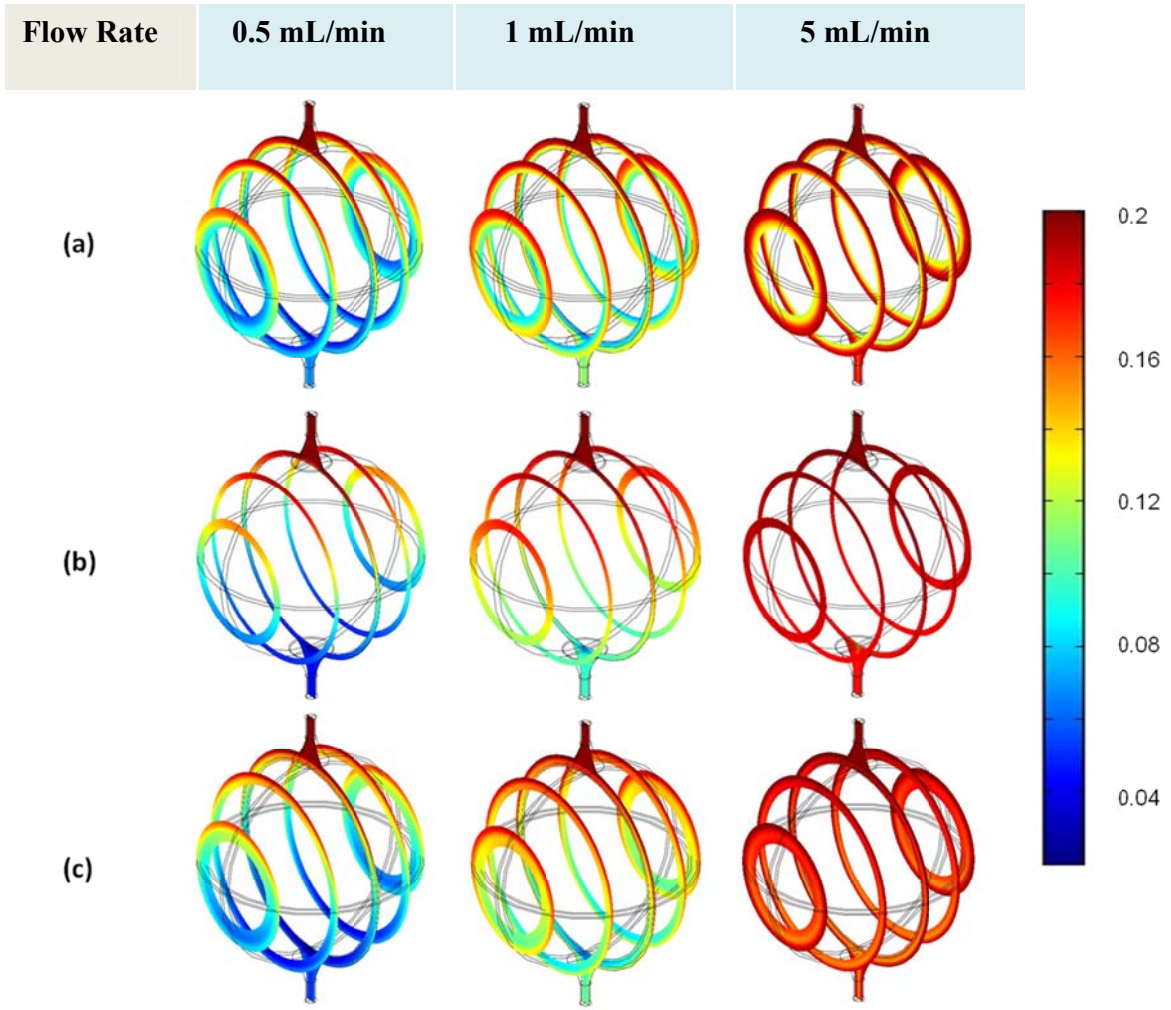

Figure 5.6. Effects of location of scaffold and flow rate on oxygen concentration profile.

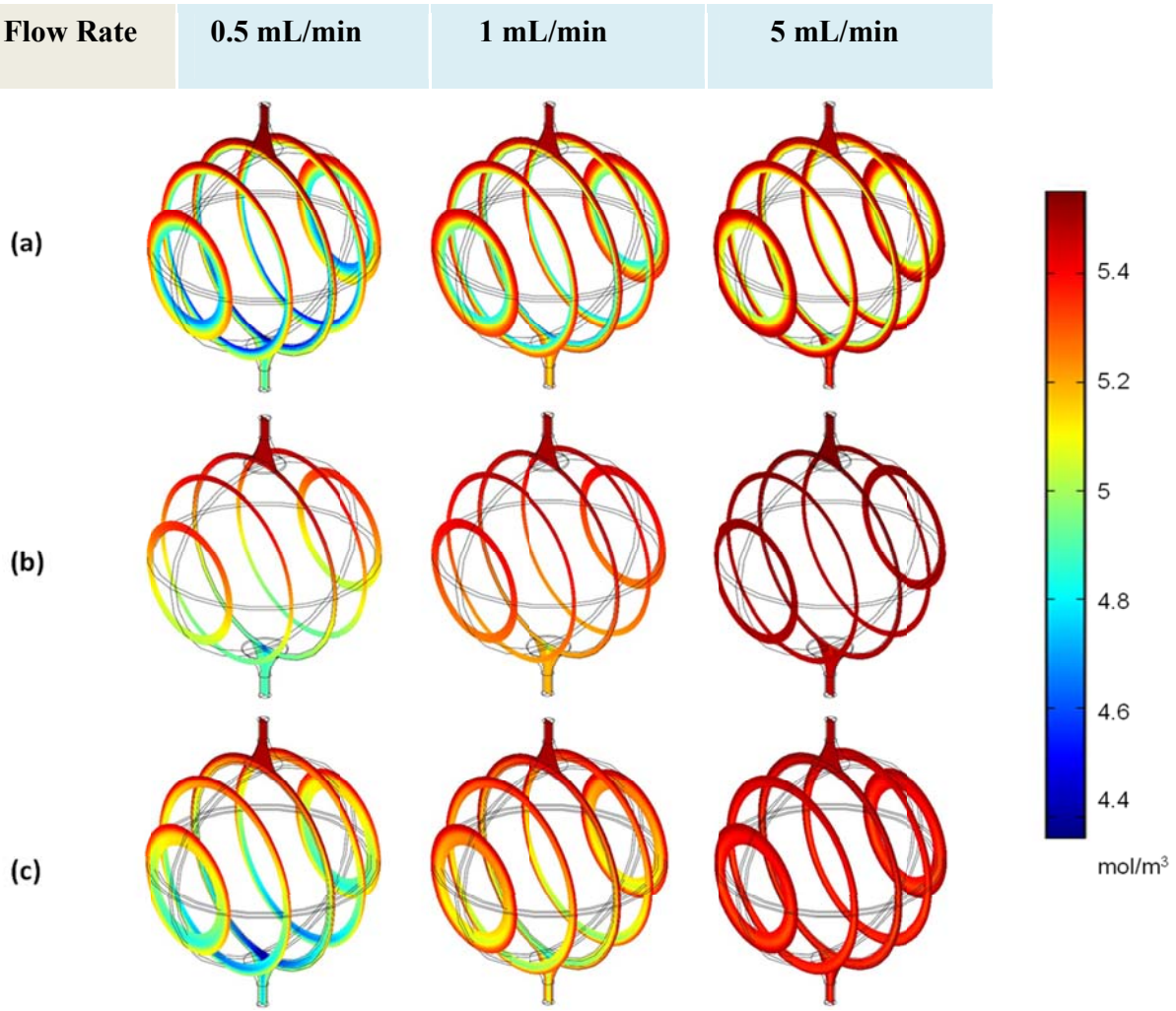

Figure 5.7. Effects of location of scaffold and flow rate on glucose concentration profile.

5.3.5. Effect of Cell Density and Permeability on Nutrients Consumption.

Since cells grow and populate through the scaffold, the number of cells can be increased or permeability of porous structure can be reduced by proliferation of cells without differentiation. To understand the effect of varying cell density and permeability on nutrient consumption, pressure drop, and shear stress, simulations were performed by increasing initial cell seeding density of SMCs or decreasing permeability. The flow rate was fixed with 5 mL/min. These results showed (**Table 5.5**) that minimum oxygen concentration reduced significantly with decreasing permeability at the constant cell number. Slice plot results for Design 2-C (**Figure 5.8-A**) also confirmed that insufficient oxygen concentration regions were observed within the porous structure with permeability of 4.7 μm^2. This result suggested that increasing the flow rate is necessary to adjust requirements to the cell proliferation. In addition, pressure drop of Design 2-A & C were increased slightly by reducing permeability where as design 2-B showed an increase of pressure drop. However, shear stress was not changed significantly by reducing permeability (data was not shown). This suggested that pressure and flow rate should be adjusted by decreasing permeability.

The number of cells was varied to evaluate the effect of cell density with constant permeability. These results showed **(Table 5.5 and Figure 5.8-B**) that minimum oxygen concentration decreased by increasing cell density of SMCs while outlet oxygen concentration decreased. Shear stresses were not altered significantly by increasing cell density at the constant permeability. Further, optimum flow rates for Design 2-C were evaluated to maintain the minimum oxygen concentration of 0.05 mol/m^3 followed by increasing cell density (**Figure 5.9**). The smooth muscle cell density of the human

bladder was calculated from the literature review. The number of cells was increased until it exceeds typical SMCs density of $1.3 * 10^{13}$ cells/m^3.

Table 5.5. Effects of varying cell density and changes in permeability on oxygen consumption rate.

			Design 2-A			Design 2-B			Design 2-C		
Cell Number	Pore Size (μm)	κ (μm^2)	Δp (mPa)	Min. C_{oxygen} (mol/ m^3)	Outlet C_{oxygen} (mol/ m^3)	Δp (mPa)	Min. C_{oxygen} (mol/ m^3)	Outlet C_{oxygen} (mol/ m^3)	Δp (mPa)	Min. C_{oxygen} (mol/ m^3)	Outlet C_{oxygen} (mol/ m^3)
1x	85	154	90.56	0.1076	0.1828	106255	0.1553	0.1770	214.15	0.1314	0.1819
1x	50	18	90.57	0.0398	0.1875	886240	0.1100	0.1773	229.74	0.0369	0.1861
1x	20	4.7	90.58	-0.0352	0.1944	34611082	-0.4448	0.1782	232.85	-0.0424	0.1939
2x	85	154	90.56	0.0595	0.1698	106255	0.1179	0.1565	214.15	0.1243	0.1610
4x	85	154	90.56	0.0226	0.1550	106255	0.0622	0.1198	214.15	0.0759	0.1368

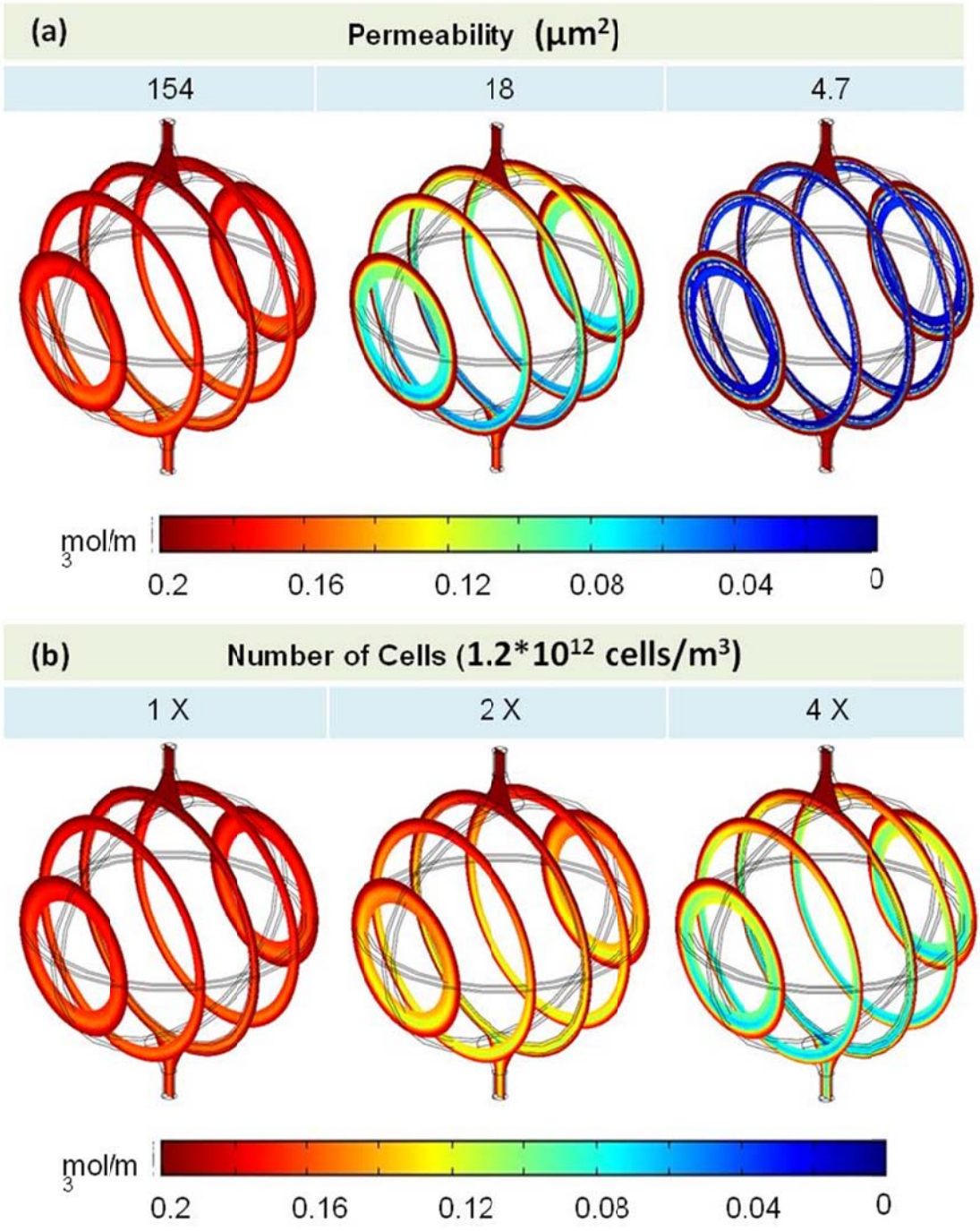

Figure 5.8. Effects of permeability and cell density on oxygen distribution. Note that volumetric flow rate was 5 mL/min.

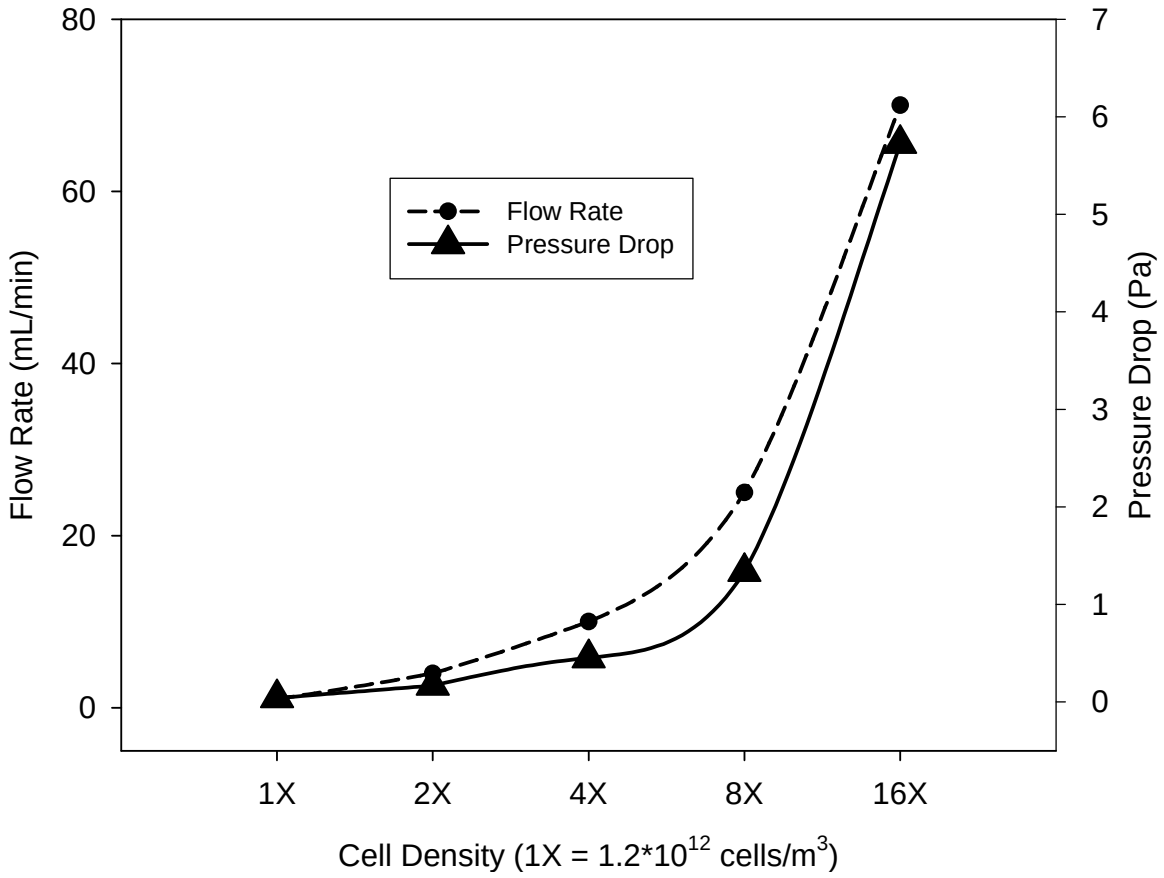

Figure 5.9. Optimal flow rate and pressure drop to maintain minimum oxygen concentration of 0.05 mol/m^3 followed by increasing cell density

5.4. Discussion.

Bladder contains a large number of SMCs and few layers of UCs. Static cultures relying on Fickian diffusion for distribution of nutrients cannot support the growth of thicker (>0.5-1.0 mm) tissues. Fluid is constantly replenished by recirculating in the porous structures to improve nutrients distribution by convection. Bioreactors of different configurations are explored for *in vitro* tissue regeneration, although no reactors are designed to support co-culturing of two cell types (Walther 2002; Martin, Wendt et al. 2004; Martin and Vermette 2005; Marolt, Augst et al. 2006; Cummings and Waters 2007). A popular design is a rotating reactor with simulated microgravity (Williams, Saini et al. 2002). However, these reactors are unsuitable for growing large thin bladder tissues as rotary motion tumbles and distorts the structure. Since, hydrodynamic shear force influences cellular alignment (Huang, Onyeri et al. 2005; Waters, Cummings et al. 2006) in the flow direction (Gray, Pizzanelli et al. 1988; Takahashi and Berk 1996; Huang, Onyeri et al. 2005), fluid path helps align the cell in the required direction. However, cellular constructs grown under hydrodynamic force shrink, due to suboptimal fluid flow, scaffold compression, premature washout of the *de novo* synthesized matrix elements prior to complete assembly, and cellular attachment and contraction. There is a need to understand the fluid flow characteristics within the bioreactor and evaluate the effect of the structure.

This study focused on understanding on the shapes of inlets, the location of scaffold, and what controls nutrient distribution with different conditions for large scale of tissue regeneration. Gelatin-chitosan system was selected as the model system for the following reasons: i) a significant work exist with chitosan-based tissue scaffolds ii) more

is known about its chemistry, degradation, iii) and host tissue response than most other tissue scaffolds. Scaffold degradation is enzyme-mediated. Hence, the dynamic changes in the porous scaffold due to degradation can be ignored in the absence of enzymes during the initial study period. Further, one could systematically study the role of degradation by adding enzymes and their reaction kinetics. The porosity and pore size distribution of these scaffolds in hydrated condition has been extensively characterized in our laboratory (Huang, Onyeri et al. 2005; Huang, Siewe et al. 2006; Tillman, Ullm et al. 2006). This combination promotes cell adhesion and increased secretion of ECM components in static cultures with very slow cell growth. Hence one could assess the effect of ECM maturation without considering dynamic changes in cell number.

Since it is widely known that cells respond to hydrodynamic shear stress, evaluation of optimized shear stress is essential for the design of bioreactors. In this study, shear stress at the inlet area was minimized by increase the size of connected area of inlet and reactor. Funnel shape inlet (Design 2) dispersed initial inlet flow, and showed a uniform distribution of shear stress through the scaffold. Maximum shear stress of Design 2 was significantly lower compared to Design 1 and Design 3. This could be attributed to the funnel shaped entrance, which provides a smooth expansion instead of sudden expansion of the fluid at the inlet, minimizing significant variation in shear stress. Minimized shear stress can give an advantage to increase flow rate, in case of insufficient nutrients consumptions.

Since nutrient transfer can be explained with diffusion and convective flow and their dominants can be changed by the location of scaffold and channel size in the reactor, three different types of designs were simulated to evaluate the effects on flow mechanism,

pressure drop, shear stress, and nutrients distribution. Diffusion or convection dominants were assessed by determining *Peclet number*. Design 2-A and C had *Peclet number* of less than 1 where as Design 2-B had *Peclet number* greater than 1. Especially, Design 2-C, fluid flow was occurred by both diffusion and convection, showed a shape increase of minimum nutrients concentrations by increasing flow rate rather than others. Hence, we could extend the current simulation results to include a 150-200 μm region with urothelial cell (UC) consumption kinetics. The flow through the UC layer should not be a significant factor as i) free diffusion is sufficient to distribute the nutrients without the need of convective flow and ii) Design 2-C can be adapted for this purpose.

To consider the changes in effective diffusivity with permeability, it was calculated for various void fractions using Mackie-Meares model (Mackie and Meares 1955; Mackie and Meares 1955; Sengers, van Donkelaar et al. 2005), which describes the diffusion of electrolytes in a resin membrane. Mackie-Meares model is based on the lattice model for liquids and assumes that the polymer fibers are of the same size as the solutes and the polymer network only blocks the pathway of solutes without affecting their mobility. Although Mackie-Meares model is shown to agree for a variety of conditions, it underestimates diffusivities with higher solute concentrations (based on water as the solvent) (Lai, Koseoglu et al. 2009). Mackie-Meares model ignores polymer-solute interactions such as adsorption effects. Thus, obtaining a better estimation of diffusivities and validating the Mackie-Meares model predictions is important. Further, structural changes due to fluid flow alter the nutrient distribution due to altered local convective flow and diffusivity.

Inner wall of the bladder is made up of 150-200 μm thick urothelial cells.

Bioreactor should allow regeneration of UCs for successful regeneration of bladder tissue. Design 2-C is ideally suited for this purpose. We could extend the current simulation results to include a with urothelial cell consumption kinetics. The flow through the UC layer should not be a significant factor as free diffusion is sufficient to distribute the nutrients without the need of convective flow. Nevertheless, these conditions need to be validated experimentally in presence of cells to determine whether those minimum flow rates are sufficient to ensure nutrient distribution. In addition, one has to determine the effect of flow rate on the quality of the regenerated tissue. Increased flow rate increases the shear stress in the microenvironment which could wash away de novo synthesized ECM components or alter cellular responses deleteriously. These changes could lead to poor quality of the regenerated tissue. Further, one has to generate 3D porous structure mimicking bladder shape, rather than suturing flat matrixes into a bowl-shape, which reduce the quality of the regenerated tissue due to the problems associated with the wrinkles (varied thickness) in the matrix (Atala, Bauer et al. 2006).

In summary, the new funnel shape of inlet decreased shear stress at the inlet area, and it showed uniform distribution of shear stress through the porous structure. The location of porous structure within the reactor affected to hydrodynamic forces and nutrient distributions significantly. Bioreactor with suspended porous structure in the middle with open flow area on either side had less pressure drop and shear stress distribution with retaining sufficient nutrients distribution. In addition, it is necessary for altering the volumetric flow rate and pressure to maintain constant nutrient distribution followed by cell proliferation and matrix deposition.

5.5. References.

Alpert, E., A. Gruzman, et al. (2002). "A natural protective mechanism against hyperglycaemia in vascular endothelial and smooth-muscle cells: role of glucose and 12-hydroxyeicosatetraenoic acid." Biochem. J. **362**(2): 413-422.

Brown, A. and B. J. Meenan (2007). "Investigating the effects of fluid shear forces on cellular responses to profiled surfaces in-vitro: a computational and experimental investigation." Conf Proc IEEE Eng Med Biol Soc **2007**: 5387-5390.

Chatzizisis, Y. S., A. U. Coskun, et al. (2007). "Role of endothelial shear stress in the natural history of coronary atherosclerosis and vascular remodeling: molecular, cellular, and vascular behavior." J Am Coll Cardiol **49**(25): 2379-2393.

Chen, H.-C. and Y.-C. Hu (2006). "Bioreactors for tissue engineering." Biotechnology Letters **28**(18): 1415-1423.

Chung, C. A., C. W. Chen, et al. (2007). "Enhancement of cell growth in tissue-engineering constructs under direct perfusion: Modeling and simulation." Biotechnology and Bioengineering **97**(6): 1603-1616.

Cioffi, M., F. Boschetti, et al. (2006). "Modeling evaluation of the fluid-dynamic microenvironment in tissue-engineered constructs: A micro-CT based model." Biotechnology and Bioengineering **93**(3): 500-510.

Cooper, J. A., Jr., W. J. Li, et al. (2007). "Encapsulated chondrocyte response in a pulsatile flow bioreactor." Acta Biomater **3**(1): 13-21.

Cummings, L. J. and S. L. Waters (2007). "Tissue growth in a rotating bioreactor. Part II: fluid flow and nutrient transport problems." Math Med Biol **24**(2): 169-208.

Devarapalli, M., B. J. Lawrence, et al. (2009). "Modeling nutrient consumptions in large flow-through bioreactors for tissue engineering." Biotechnol Bioeng **103**(5): 1003-1015.

Fogler, H. S. (2006). Elements of Chemical Reactor Engineering. Upper Saddle River, NJ, Prentice Hall.

Gooch, K. J., J. H. Kwon, et al. (2001). "Effects of mixing intensity on tissue-engineered cartilage." Biotechnology and Bioengineering **72**(4): 402-407.

Gray, M. L., A. M. Pizzanelli, et al. (1988). "Mechanical and physicochemical determinants of the chondrocyte biosynthetic response." Journal of Orthopaedic Research **6**(6): 777-792.

Heydarkhan-Hagvall, S., M. Esguerra, et al. (2006). "Production of Extracellular Matrix Components in Tissue-Engineered Blood Vessels." Tissue Engineering **12**(4): 831-842.

Huang, Y., S. Onyeri, et al. (2005). "In vitro characterization of chitosan-gelatin scaffolds for tissue engineering." Biomaterials **26**(36): 7616-7627.

Huang, Y., M. Siewe, et al. (2006). "Effect of spatial architecture on cellular colonization." Biotechnol Bioeng **93**(1): 64-75.

Hutmacher, D. W. and H. Singh (2008). "Computational fluid dynamics for improved bioreactor design and 3D culture." Trends Biotechnol **26**(4): 166-172.

Lai, C. Z., S. S. Koseoglu, et al. (2009). "Fluorous polymeric membranes for ionophore-based ion-selective potentiometry: how inert is Teflon AF?" J Am Chem Soc **131**(4): 1598-1606.

Lawrence, B. J., M. Devarapalli, et al. (2009). "Flow dynamics in bioreactors containing tissue engineering scaffolds." Biotechnol Bioeng **102**(3): 935-947.

Mackie, J. S. and P. Meares (1955). "Diffusion in a cation exchanger resin I." Proc. R. Soc **232**(A): 448-495.

Mackie, J. S. and P. Meares (1955). "Diffusion in a cation exchanger resin II." Proc. R. Soc **232**(A): 495-505.

Marolt, D., A. Augst, et al. (2006). "Bone and cartilage tissue constructs grown using human bone marrow stromal cells, silk scaffolds and rotating bioreactors." Biomaterials **27**(36): 6138-6149.

Martin, I., D. Wendt, et al. (2004). "The role of bioreactors in tissue engineering." Trends in Biotechnology **22**(2): 80-86.

Martin, Y. and P. Vermette (2005). "Bioreactors for tissue mass culture: Design, characterization, and recent advances." Biomaterials **26**(35): 7481-7503.

Motterlini, R., H. Kerger, et al. (1998). "Depression of endothelial and smooth muscle cell oxygen consumption by endotoxin." Am J Physiol Heart Circ Physiol **275**(3): H776-782.

Niklason, L. E., J. Gao, et al. (1999). "Functional Arteries Grown in Vitro." Science **284**(5413): 489-493.

Porter, B., R. Zauel, et al. (2005). "3-D computational modeling of media flow through scaffolds in a perfusion bioreactor." Journal of Biomechanics **38**(3): 543-549.

Sander, E. A. and E. A. Nauman (2003). "Permeability of musculoskeletal tissues and scaffolding materials: experimental results and theoretical predictions." Critical Reviews in Biomedical Engineering **31**(1): 1-26.

Sengers, B. G., H. K. Heywood, et al. (2005). "Nutrient Utilization by Bovine Articular Chondrocytes: A Combined Experimental and Theoretical Approach." Journal of Biomechanical Engineering **127**(5): 758-766.

Sengers, B. G., C. C. van Donkelaar, et al. (2005). "Computational study of culture conditions and nutrient supply in cartilage tissue engineering." Biotechnol Prog **21**(4): 1252-1261.

Takahashi, M. and B. C. Berk (1996). "Mitogen-activated protein kinase (ERK1/2) activation by shear stress and adhesion in endothelial cells. Essential role for a herbimycin-sensitive kinase." J Clin Invest **98**(11): 2623-2631.

Tillman, J., A. Ullm, et al. (2006). "Three-dimensional cell colonization in a sulfate rich environment." Biomaterials **27**(32): 5618-5626.

Truskey, G. A., F. Yuan, et al. (2004). Transport Phenomena in Biological Systems. Upper Saddle River, NJ, Pearson Prentice Hall**:** 317-321.

Walther, I. (2002). "Space bioreactors and their applications." Advances in space biology and medicine **8**: 197-213.

Waters, S. L., L. J. Cummings, et al. (2006). "Tissue growth in a rotating bioreactor. Part I: mechanical stability." Math Med Biol **23**(4): 311-337.

Williams, K. A., S. Saini, et al. (2002). "Computational Fluid Dynamics Modeling of Steady-State Momentum and Mass Transport in a Bioreactor for Cartilage Tissue Engineering." Biotechnol. Prog. **18**(5): 951-963.

CHAPTER VI

CONCLUSIONS AND RECOMMENDATIONS

6.1. Conclusions.

6.1.1. Characterization of a novel method to make scaffolds using the synthetic polymer polycaprolactone (PCL).

A novel process of dissolving PCL in acetic acid which allows spontaneous aggregation of PCL upon contacting with the water was investigated to develop a biocompatibility and environment friendly process. 80 kDa Mn PCL matrices formed from self assembly method were compared with chloroform-cast matrices (conventional method) to evaluate the effect of different solvents on the surface morphology and characteristics, effect of neutralization process, tensile properties, stress relaxation properties, and cellular activity.

The results showed that PCL matrices can be generated using the novel technique in aqueous media. Self-assembled matrices had rough and porous structures where as chloroform-cast matrices had smooth and non-porous surface characteristics. Self-assembled matrices showed an increase in roughness, which decreased after the neutralization process in NaOH solution. Measured tensile properties showed a reduction in elastic modulus but with similar stress relaxation behavior relative to chloroform–

casted matrices. Stress relaxation experiments showed less accumulation of stress in self-assembled matrices relative to chloroform–cast materials. A significant difference between self-assembled matrix and chloroform–cast matrix was a relaxation during the loading phase of chloroform–cast matrix. This was not observed in self-assembled matrices, which could be attributed to alteration in the packing pattern of the polymeric chains.

When cellular activity was measured, increased cell adhesion was observed on self-assembled matrices with a similar cell spreading to TCP. Thus the new simple technique shows an improvement in cellular interactions. Since matrix topography affects cell spreading characteristics, the observed variation in cellular activity could be attributed to the significant increase roughness. However, the number of cells attached to the matrix reduced significantly compared to TCP. Hence, immobilizing with naturally derived polymers was necessary to enhance cell adhesion with better control of pore size.

6.1.2. Effect of blending different molecular weight of PCL and multi-layered scaffolds on biological properties.

Self assembled PCL matrices needed an improvement in an ability to control degradation rate and cellular activity while sustaining suitable mechanical properties. Since degradability of PCL depends on its molecular weight, low molecular weights of PCL (47 and 10 kDa Mn) were blended and matrices were formed using the self assembly method. Further, gelatin-chitosan composite was hybridized to improve porous structure and to promote better cell adhesion.

Pure 10 kDa PCL was not formed a matrix, probably due to the lack of stable interpenetrating network formation. No significant differences in surface morphology and degradation characteristics were observed in between pure 80 kDa, 47 kDa, and mixtures of 80, 47, 10 kDa PCL matrices. The blended matrix of 80 and 10 kDa showed a distinguishable surface characteristic with perforations and larger pore size. Furthermore, percentages of weight loss was decreased significantly compared to others, due to the presence of low MW (10 kDa Mn) PCL. Although tensile properties decreased by 10 kDa PCL, comparing results with currently used materials showed suitable mechanical properties for tissue regeneration applications. The blended matrix of 80 and 10 kDa was used for further steps. The porous scaffold of chitosan-gelatin is known to support cell colonization.

Gelatin-chitosan composite scaffolds were sandwiched with PCL matrix, and formed multi-layered scaffolds. Gelatin-chitosan matrix was attached on the surface of PCL matrix and fastened through the perforations. There was no significant effect of multi layering on mechanical properties. In addition, the bladder and the blood vessel shapes of porous scaffold were formed by self assembly and multi-layering.

6.1.3. Design of a bioreactor for bladder tissue regeneration using computational fluid dynamic.

A bladder shape of scaffold was mimicked by self assembly and multi-layered scaffolds. Cell cultivation systems for large and 3-D scaffolds mimicking bladder shape have not been investigated yet. In this aim, fluid dynamics of the bioreactors for the bladder tissue regeneration were simulated using COMSOL multiphysics.

The bioreactor with an average volume size of human bladder was designed and simulated. These results showed that the funnel shape of inlet minimized the shear stress at the inlet area, and generated a uniform shear stress throughout the porous structure. Two inlets mimicked bladder configuration was also simulated. The shear stress at the inlet was decreased by splitting volumetric flow rate into two inlets. However, two inlet flows indicated non-uniform nutrient distributions through the bioreactor. Hence one funnel shape inlet was selected further investigations.

The location of porous structure within the reactor affected hydrodynamic forces and nutrient distributions significantly. Bioreactor with suspended porous structure in the middle with open flow area on either side had less pressure drop and shear stress distribution with retaining sufficient nutrients distribution. This result proved that nutrient transfer can be explained by diffusion and convection dominants by calculating *Peclet* number, and the diffusion dominant flow system with less convective effect had a better environment through the reactor and cell seeded scaffold.

Since cells grow and populate through the scaffold, the number of cells can be increased or permeability of porous structure can be reduced by proliferation of cells or matrix deposition. These results showed that the novel bioreactor provided sufficient nutrients for increased cell number, and there are no significant changes in the pressure drop and the shear stress. However, the volumetric flow rate and pressure need to be altered by decreasing permeability to maintain constant nutrient distribution. These results can be used as a criterion while developing bioreactors for the regeneration of human bladder.

6.2. Recommendations.

In this study, novel processing of the PCL matrix formation was characterized for suitability in tissue engineering. A significant advantage of this novel method is an easiness of forming scaffolds into desirable shapes and sizes. I focused on developing the methodology for the bladder tissue regeneration. However, there are many other applications such as vascular grafts in which this technique could be utilized. Further, a novel bioreactor configuration was designed and simulated to find optimized environments for a bladder tissue regeneration system. To see those studies for usefulness in clinical applications, several aspects need to be further evaluated.

6.2.1. Comparing scaffold characteristics with natural tissues.

The stress and relaxation property of self assemble matrices was analyzed. The relaxation during the loading phase was not observed in self-assembled matrices. However, one has to perform experiments with varying loading and relaxation times to better understand the viscoelastic behavior significantly depends on the loading and relaxation times. These results need to be considered compared to materials used, since different types of applications require different viscoelasticity. Further, one has to test the effect of temperature on the viscoelastic behavior.

Blending with low MW of PCL has indicated that the degradation rate was increased and they had a unique surface characteristic. However, this blended PCL had the same amount of PCL in each MW. Since the presence of more amounts of low MW PCL can affect or change its properties, one has to assess the effects of different ratio of blending on surface characteristics, mechanical strength, and biological properties.

In addition, effects of neutralization process in NaOH solution and blending different MW of PCL on the surface roughness factors were analyzed, and the results indicated the possibility of the control of the roughness factors. Most types of cells have their own desirable surface morphologies such as specific ranges of the roughness factor and the pore size (Nehrer, Breinan et al. 1997; Salem, Stevens et al. 2002). In this study, only HFF-1 cells were seeded, and their survivability was mainly focused. Hence, it is necessary to test the effects of different surface morphology characteristics of self assembled PCL matrices on different types of cellular activities.

6.2.2. Effects of Different Cell types and Kinetics.

In this study, cell adhesion and spreading were characterized on synthesized surfaces. Detailed cell colonization studies, such as growth characteristics and alteration in secretion of matrix elements such as collagen, elastin, proteoglycans, have to be analyzed extensively. In addition, cellular activity of other cell types needs to be performed. These findings open new possibilities to understand the influence of charge and roughness separately on macromolecular interactions and cell colonization, which has not been well understood in tissue regeneration.

Further, the kinetic parameters used in bioreactor simulation for nutrient consumption were obtained from the literature on tissue culture plastic condition (Motterlini, Kerger et al. 1998; Alpert, Gruzman et al. 2002). To improve the simulation, nutrient utilization constants for oxygen and glucose have to be evaluated in porous structure. Hence, detailed analysis of cell colonization should include nutrient kinetics as

well as secretion of matrix elements. One has to obtain the cell kinetic data of 3-D porous media to have better predictions in the bioreactor simulation.

6.2.3. Multiple Cell Lines of Bladder.

The human urinary bladder has a multilayer asymmetric architecture which means that the bladder has multi-cell lines consist of smooth muscle cells (SMCs) layer, urothelial cells layer, and extracellular components (Wallis, Yeger et al. 2008). In this study, only SMCs were seeded on the scaffold since SMCs layer consists of the most part of bladder layers, and urothelial cells layer has a thickness of 200 μm. Hence it was assumed that sufficient nutrients can be transferred by the diffusion. However, to consider reality, one has to simulate a co-culturing system which has two different inlet flows for the outer surface of scaffold and the inner surface of scaffold.

6.3. References.

Alpert, E., A. Gruzman, et al. (2002). "A natural protective mechanism against hyperglycaemia in vascular endothelial and smooth-muscle cells: role of glucose and 12-hydroxyeicosatetraenoic acid." Biochem J **362**(Pt 2): 413-422.

Motterlini, R., H. Kerger, et al. (1998). "Depression of endothelial and smooth muscle cell oxygen consumption by endotoxin." Am J Physiol **275**(3 Pt 2): H776-782.

Nehrer, S., H. A. Breinan, et al. (1997). "Matrix collagen type and pore size influence behaviour of seeded canine chondrocytes." Biomaterials **18**(11): 769-776.

Salem, A. K., R. Stevens, et al. (2002). "Interactions of 3T3 fibroblasts and endothelial cells with defined pore features." J Biomed Mater Res **61**(2): 212-217.

Wallis, M. C., H. Yeger, et al. (2008). "Feasibility study of a novel urinary bladder bioreactor." Tissue Eng Part A **14**(3): 339-348.

APPENDIX

APPENDIX A: COMSOL Multiphysics 3.5a

A.1. Creating Geometry.

1. **Start** > **All Programs** > **COMSOL 3.5 a** > Click on **COMSOL Multiphysics 3.5.a** Model.

2. In **Model Navigator** > Set **Space Dimension** as 3D.

3. In the **Application Modes** section, click on **Chemical Engineering Module** > **Fluid Chemical Reaction Interaction** > **Reacting Flow** > Select **Steady State Analysis**

4. In the **Dependent Variables** tab, type c1 and c2 > Click **Add** > **OK**.

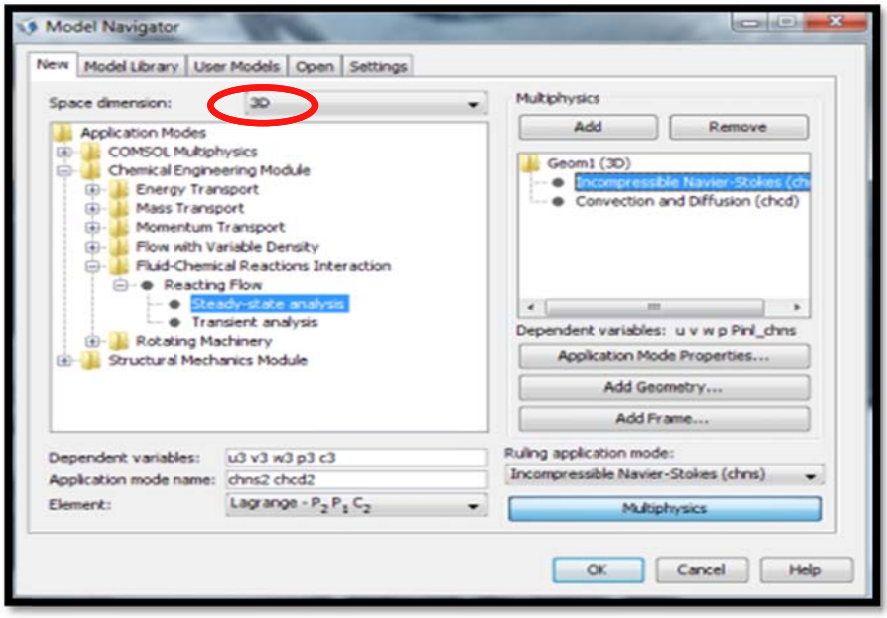

5. In the **Menu bar** go to **File** > **Save**. And save the file with a desired name, e.g. Bladder_reactor_design_1.

6. In the **Menu bar** go to **Draw** > Select **Sphere** > Set the radius as 5.5cm radius (SPH1)

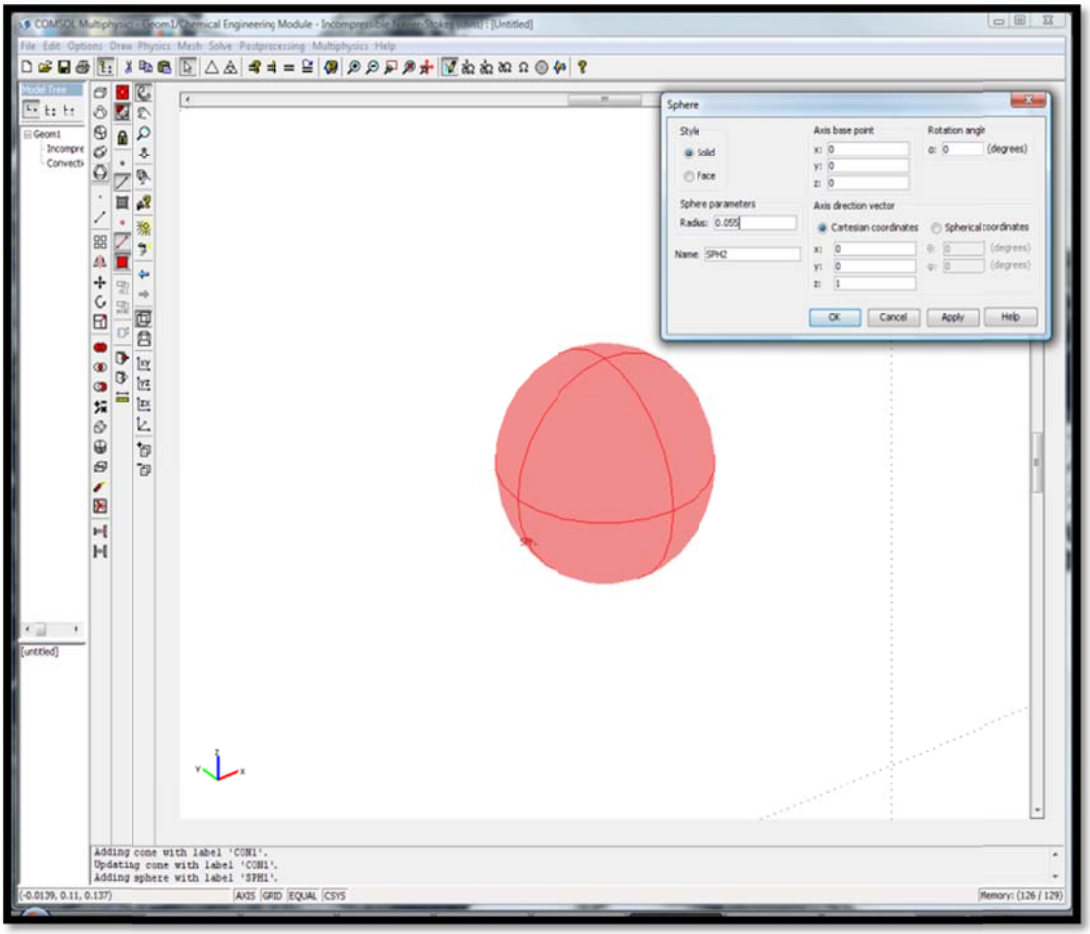

7. Repeat step 5, Draw spheres with 5.35 (SPH2) and 5.2 cm radius (SPH3)

8. Select SPH1 and SPH2 > click Difference tab to get the annular region between two sphere.

9. Repeat Step 7 for the SPH3

10. In the **Menu bar** go to **Multiphysics > Model Navigator > Click Add Geometry >** Set **Space dimension** as **2D** > click **OK**.

11. For inserting the funnel shape inlet and outlet, Click **Geom2** > Draw lines shown in the figure below.

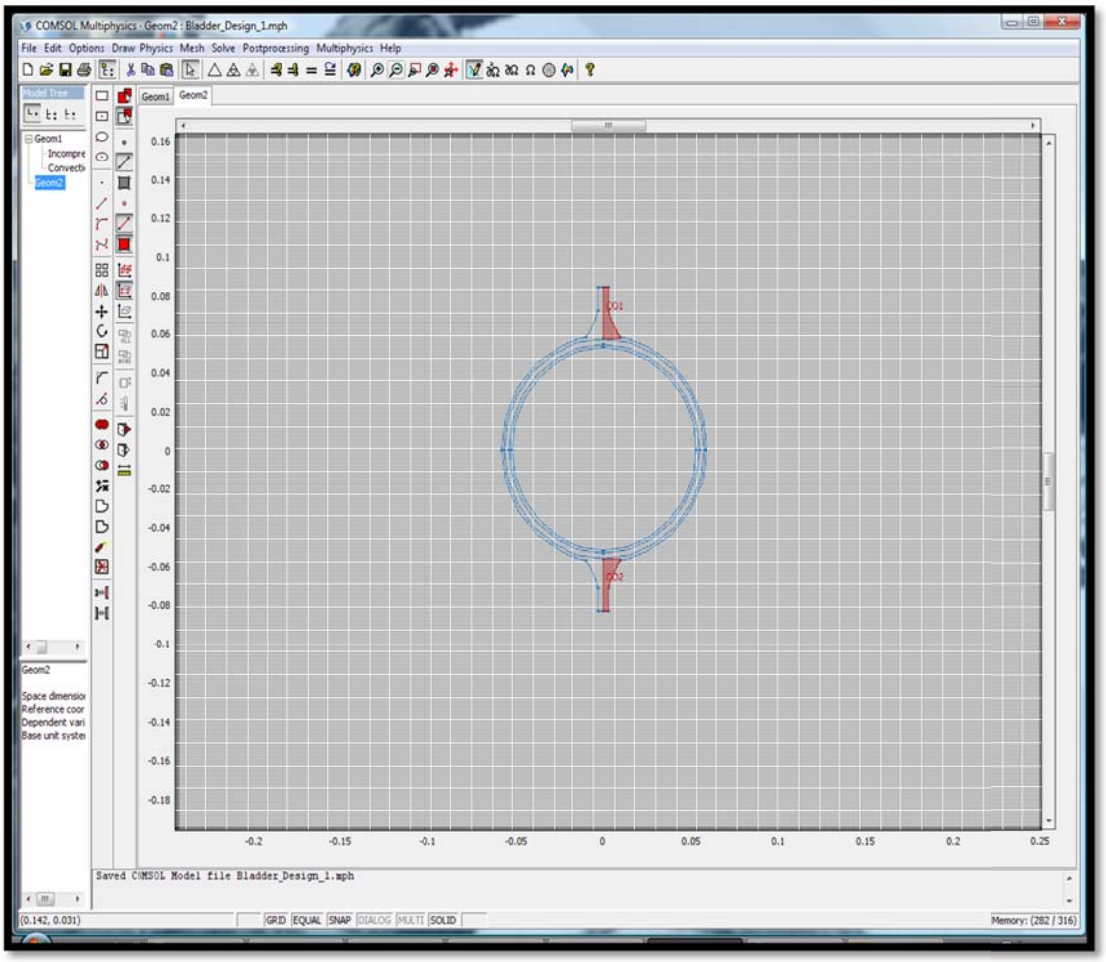

12. In the **Menu bar** go to **Draw** > **Revolve** > Set **a2 degree** as 360°

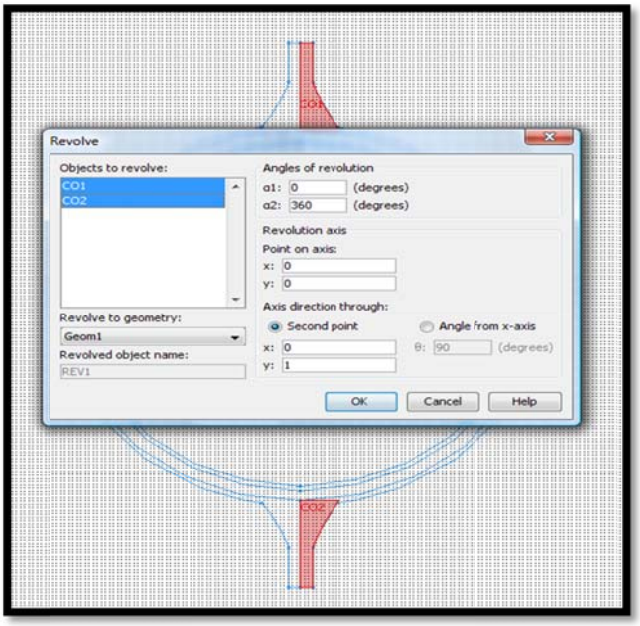

13. To unify Geometry 1 and 2, Select sphere, inlet, and outlet > In the **Menu bar** go to **Draw** > **Create Composite Object** > Unclick **Keep interior boundaries** > Click **OK**.

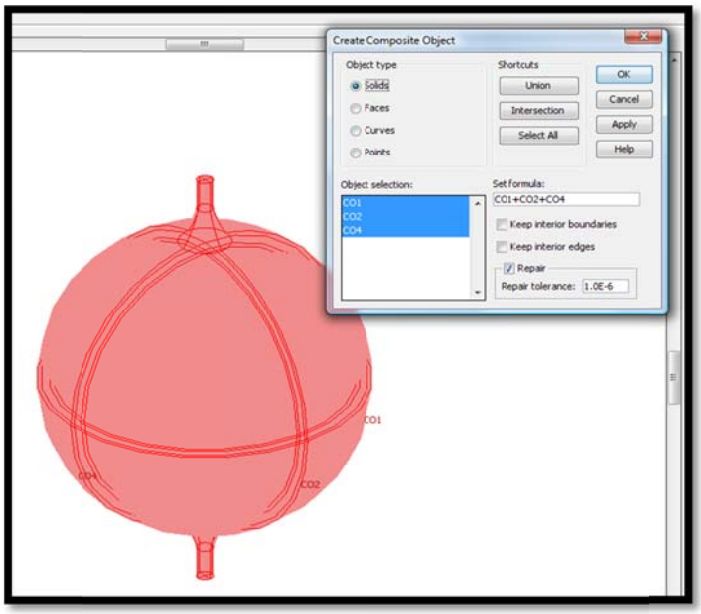

A.2. Meshing Geometry.

1. In the **Menu bar** go to **Mesh** > **Free Mesh Parameter** > **Edge** > **Distribution** > Set **Number of edge elements** accordingly > Click **Mesh Selected** > **OK**.

2. In the **Menu bar** go to **Mesh** > **Free Mesh Parameter** > **Boundary** > **Distribution** > Set **Maximum element size** accordingly > Click **Mesh Selected** > **OK**.

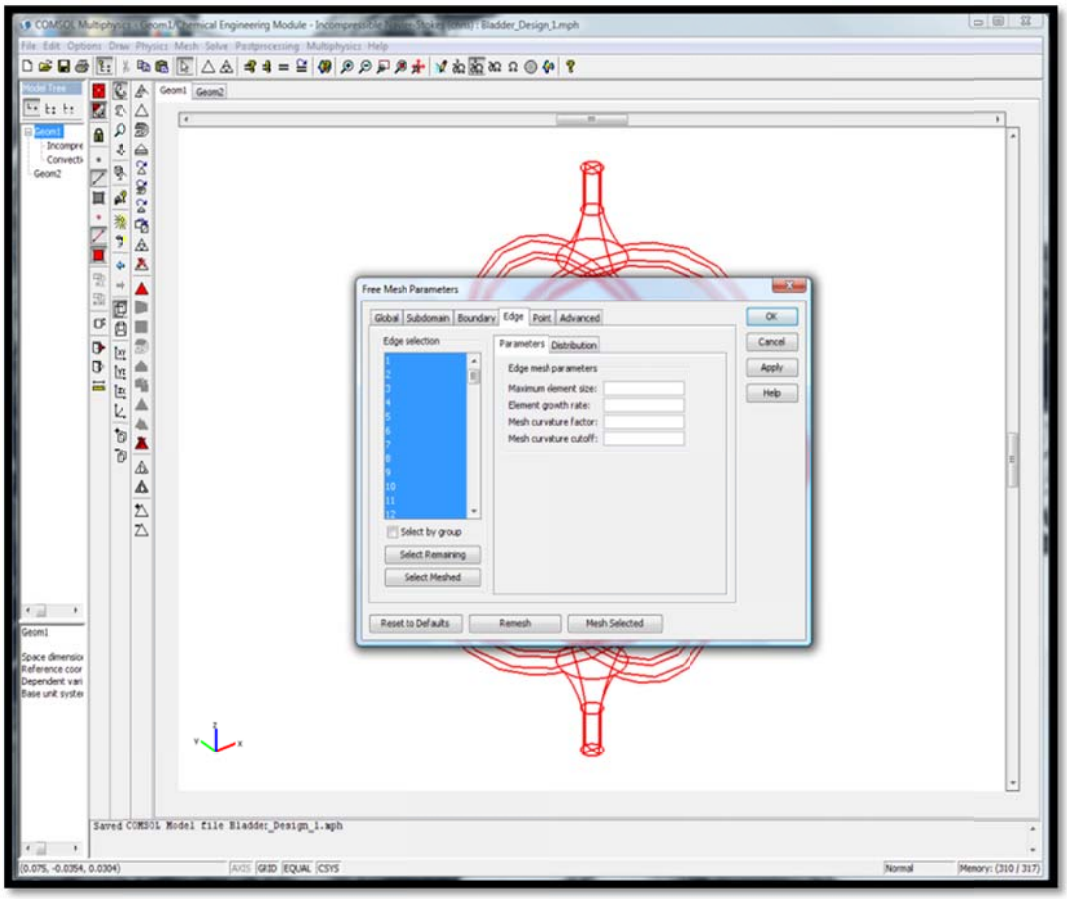

A.3. Building Constants.

1. In the **Menu bar** go to **Options > Constants >** Build constants library > **OK**.

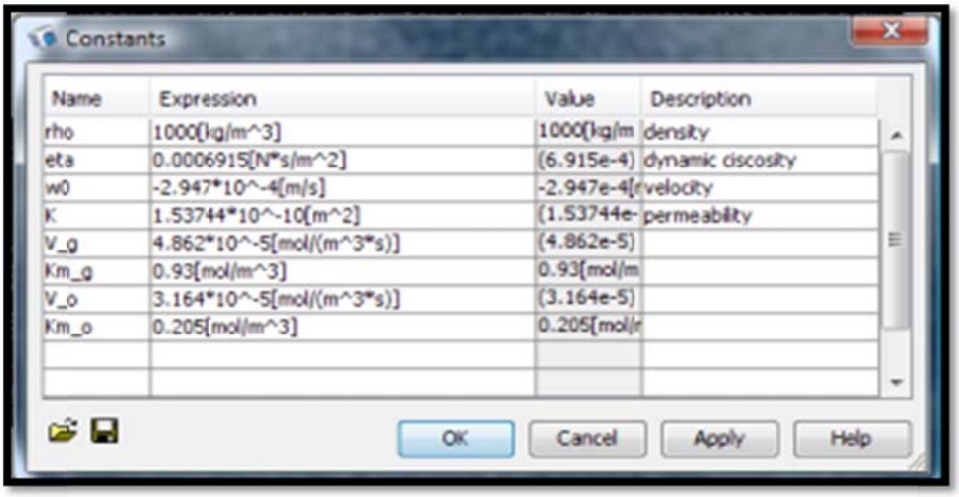

2. There are four columns; **Name**, **Expression**, **Value**, and **Description**. In the name column, type the name of parameters.

Description	Name	Unit
Density	rho	kg/m^3
Dynamic viscosity	eta	$N*s/m^2$
Velocity	w_0	m/s
Permeability	K	m^2
Reaction rate	V	mol/m^3*s
Michaelis constant	Km	mol/m^3

A.4. Building Subdomain and Boundary Conditions.

1. Select **Incompressible Navier-Stokes** > in the **Menu bar** go to **Physics > Subdomain Setting**.

2. Express density, dynamic viscosity, and permeability for both **porous** and **nonporous** > Set **Porosity** as **0.85** (85%) > Click **OK**.

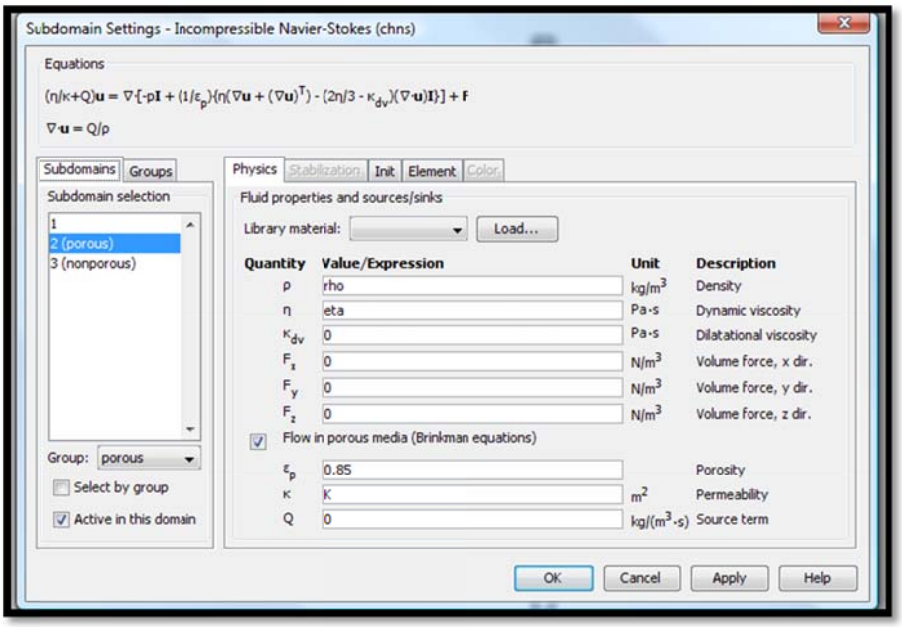

3. Select **Incompressible Navier-Stokes** > in the **Menu bar** go to **Physics > Boundary Setting**.

4. Select inlet area in the geometry > Set **Boundary type** as **Inlet** > Set x- and y-velocity as zero > Set z-velocity as **w0**.

5. Select outlet area in the geometry > Set **Boundary type** as **Outlet >** Select **Pressure** and set **P0** to zero > OK.

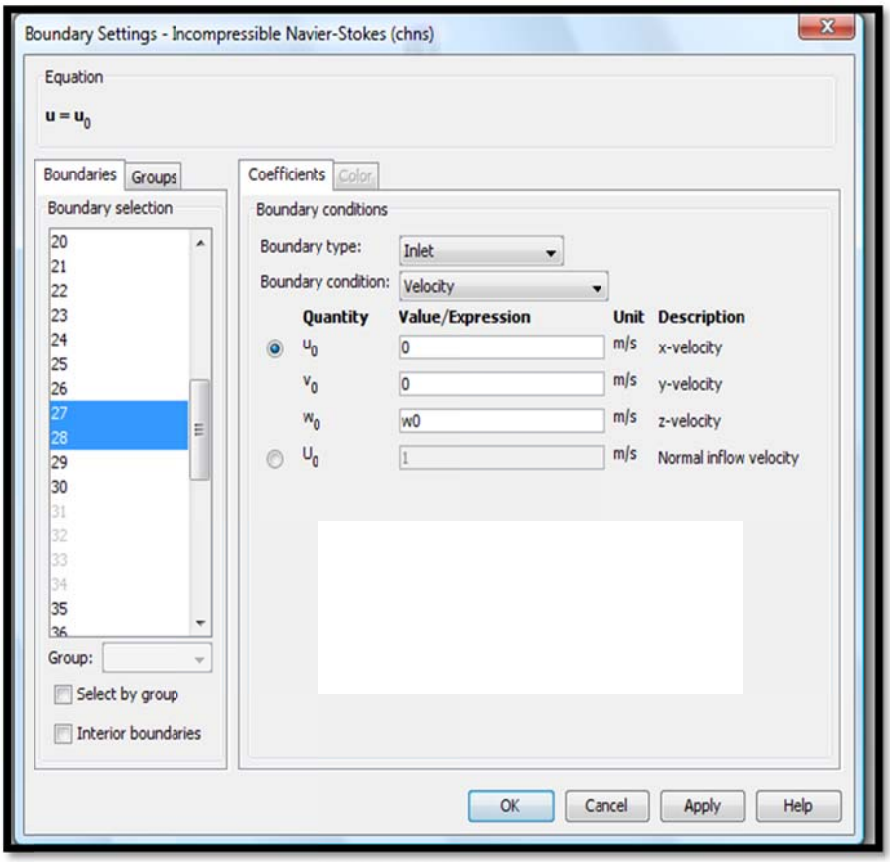

6. Select **Convection and Diffusion** > in the **Menu bar** go to **Physics > Subdomain Setting**.

7. Set **Diffusion coefficient** for oxygen (**c1**) and glucose (**c2**)and **Michaelis-Menten** equation to calculate reaction rate in the porous region.

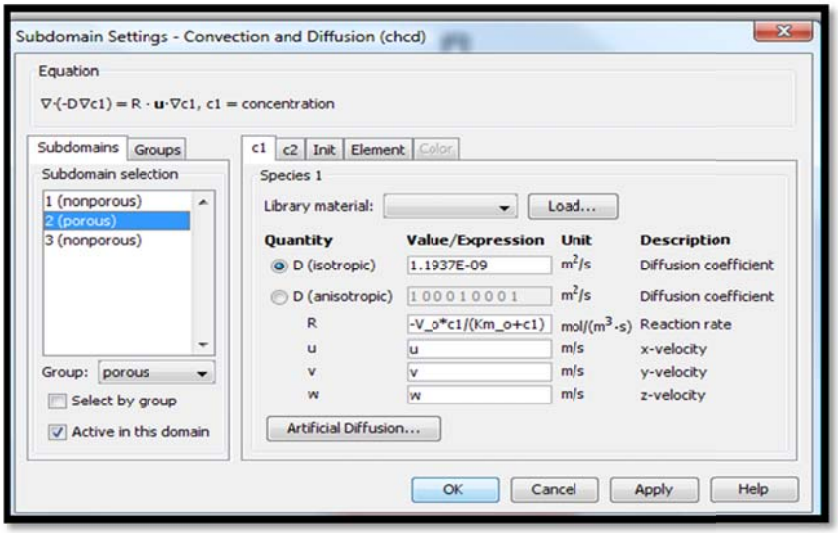

8. Select **Convection and Diffusion** > in the **Menu bar** go to **Physics > Boundary Setting**.

9. Set initial concentrations for oxygen (**c1**) and glucose (**c2**).

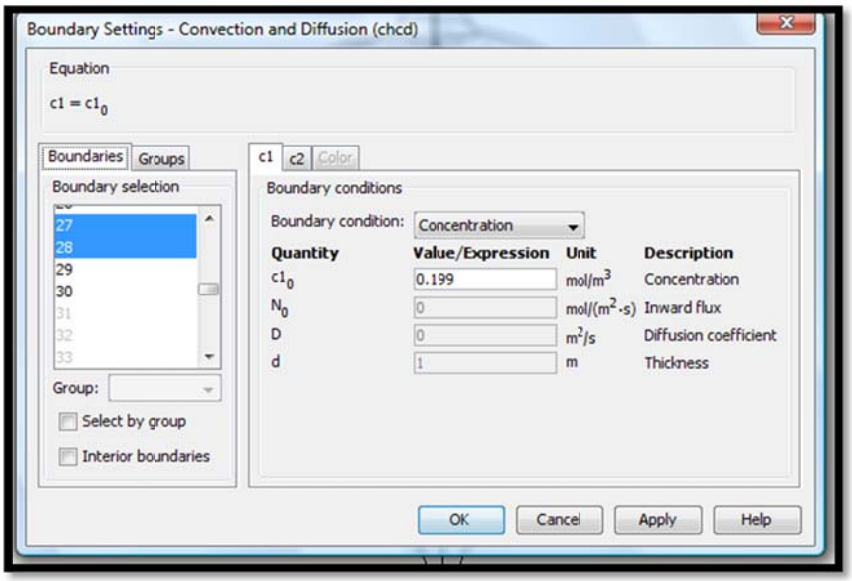

A.5. Solving Parameters.

1. In the **Menu bar** go to **Solve** > **Solve Parameter** > Set **Linear system solver** as **Direct (PARDISO)** > Click **OK**.

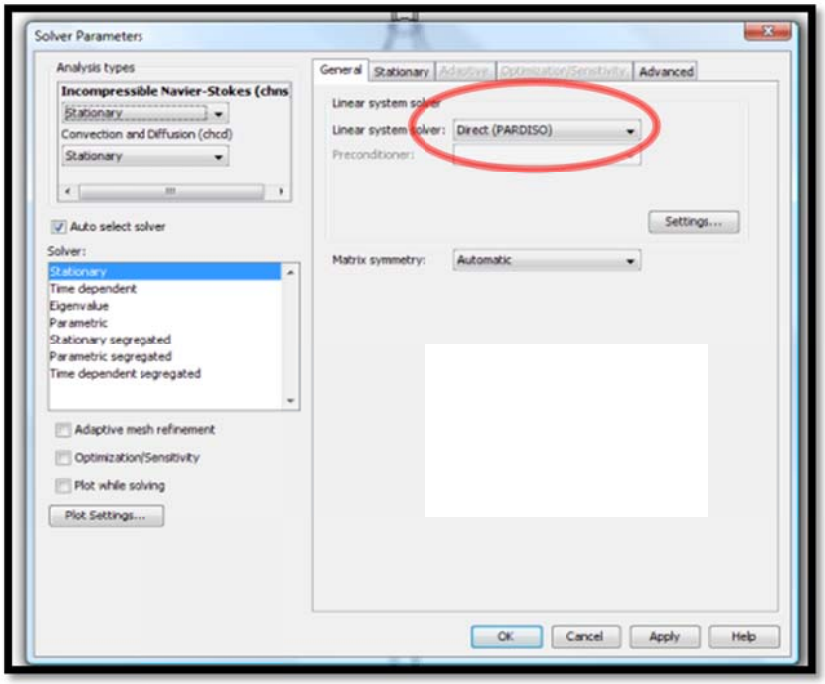

2. In the **Menu bar** go to **Solve** > **Solve Manager** > **Solve For** > Select **Incompressible Navier-Stokes** > Click **Solve**

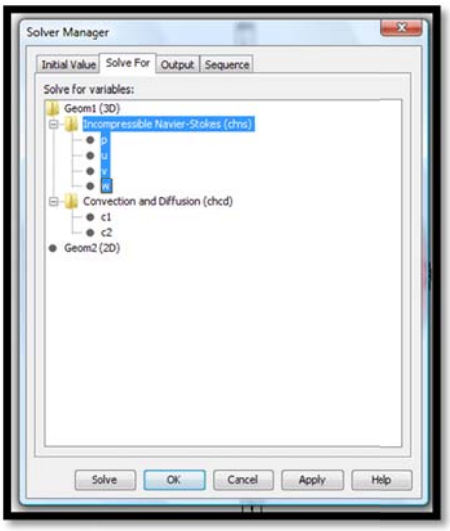

3. When solving is done, repeat step 19 for **Convection and Diffusion**

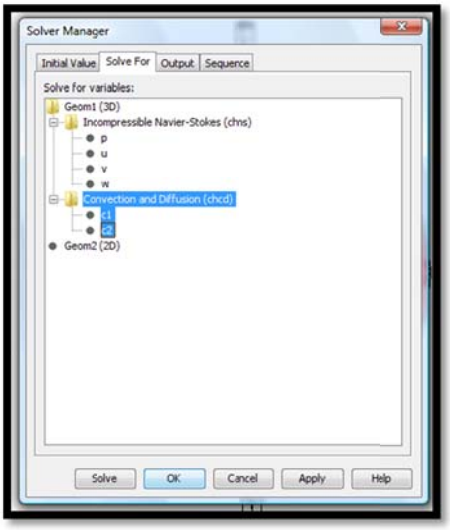

A.6. Analyzing Results.

1. To analyze results, in the Menu bar go to **Postprocessing** and choose one of the analysis methods.

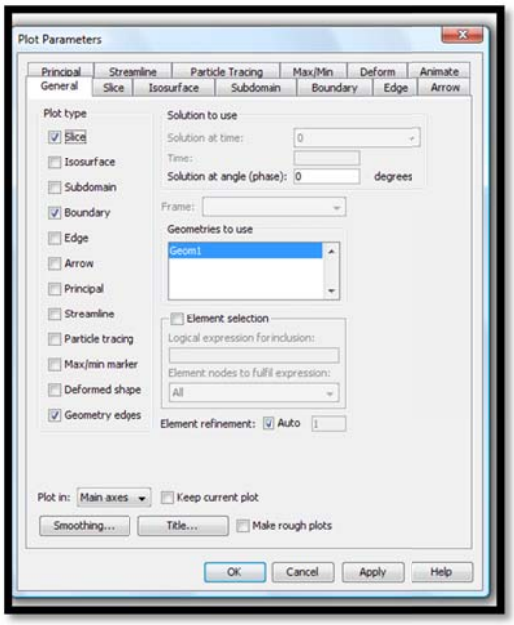

2. *Pressure Drop and Shear Stress Distribution*

- In the **Menu Bar** go to **Postprocessing** > **Plot Parameters** > A window will pop up.

  Select **Boundary** > Set **Predefined quantities** as **Pressure** > Set **Unit** accordingly > Click **OK**.

- In the **Menu Bar** go to **Postprocessing** > **Plot Parameters** > A window will pop up.

  Select **Boundary** > Set **Predefined quantities** as **Viscous force per area, z component** > Set **Unit** accordingly > Click **OK**.

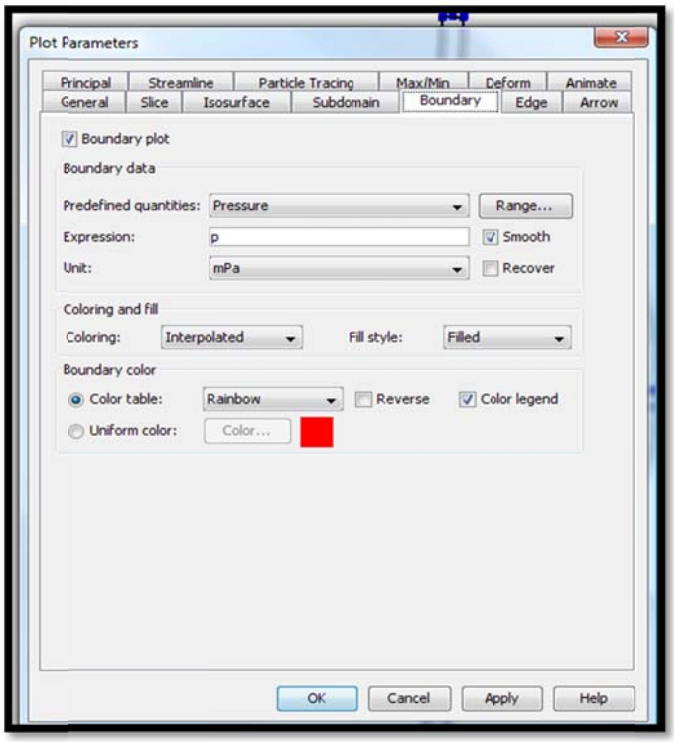

3. *Velocity Profile*

- In the **Menu Bar** go to **Postprocessing** > **Cross-Section Plot Parameters** > Click **Point** > Set **Predefined quantities** as **Velocity field** > Set **Unit** accordingly > Set **Coordinates** accordingly > Click **OK**.
- Result will be shown up, figure below,

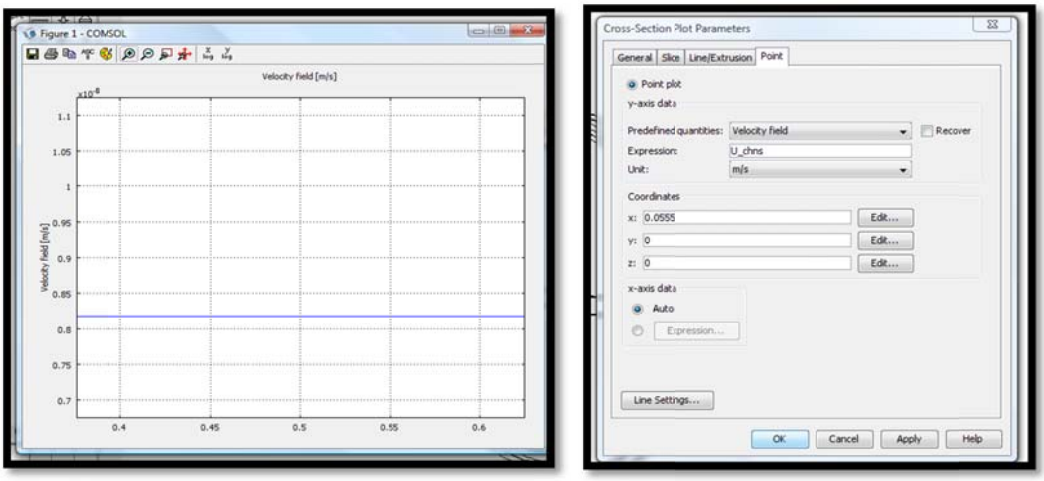

4. *Nutrient Concentration Profile*

- In the **Menu Bar** go to **Postprocessing** > **Plot Parameters** > Click **Slice** > Set **Predefined quantities** as **Concentration, c1** for oxygen OR **Concentration, c2** for glucose > Set **Unit** accordingly > Set **Number of levels** as 5 for x **levels** > Click **OK**.

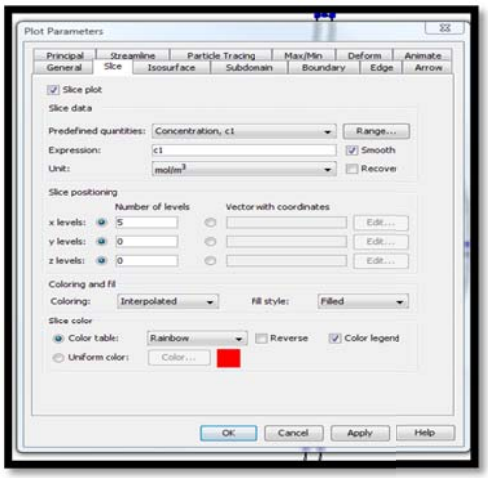

5. To export data and figure, in the **Menu Bar** go to **File** > **Export** > **Image** > Window will pop up, then click **Export** > Save with a desired name > **Export**.

VITA

Seokwon Pok

Candidate for the Degree of

Doctor of Philosophy/Education

Thesis: DESIGN OF SYNTHETIC SCAFFOLDS FOR TISSUE REGENERATION APPLICATIONS

Major Field: Chemical Engineering

Biographical:

Personal Data: Born on December 26, 1979 in Seoul, Korea.
Married on June 10, 2006

Education:

Completed the requirements for the Doctor of Philosophy in Chemical engineering at Oklahoma State University, Stillwater, Oklahoma in December, 2010.

Completed the requirements for the Master of Science in Chemical engineering at Oklahoma State University, Stillwater, Oklahoma in December, 2007.

Completed the requirements for the Bachelor of Science in Chemical engineering at Hoseo University, Asan, S. Korea in 2005.

Experience: Military service, Driver and mechanic of K-55 artillery, 27 Division, Kangwon-Do, S. Korea, January 2000 to March 2002
Lab assistant, Laboratory of Gas Application, Department of chemical engineering, Hoseo University, S. Korea, March 2002 to March 2005

Professional Memberships: American Institute of Chemical Engineers

Name: Seokwon Pok Date of Degree: December, 2010

Institution: Oklahoma State University Location: Stillwater, Oklahoma

Title of Study: DESIGN OF SYNTHETIC SCAFFOLDS FOR TISSUE REGENERATION APPLICATIONS

Pages in Study: 160 Candidate for the Degree of Doctor of Philosophy

Major Field: Chemical engineering

Scope and Method of Study: This study evaluated a novel process of PCL matrix formation, while independently regulating the mechanical, degradation, and biological properties. Its properties were compared with properties of scaffold formed by conventional method. Also, mimicking anatomically relevant structure of PCL scaffolds was also explored, and a bioreactor for 3-D scaffold was simulated to find optimized fluid dynamics. The results were obtained by experimental, analytical, and computational methods.

Findings and Conclusions: A novel method of forming PCL scaffolds in an aqueous environment was investigated to develop a biocompatibility and environment friendly process. Biodegradability of PCL was enhanced by blending low molecular weights of PCL, and gelatin-chitosan composite was hybridized to improve porous structure and to promote better cell adhesion. A bladder shape of scaffold was mimicked by self assembly and multi-layered scaffolds. Hence, this technique offers a significant opportunity to enhance the use of PCL in biomedical applications. In addition, fluid dynamics of the bioreactors contains large and 3-D scaffolds (mimicked bladder shape) were simulated and characterized using COMSOL 3.5a Multiphysics. These results can be used as a criterion while developing bioreactors for the human bladder tissue regeneration.

ADVISER'S APPROVAL: Dr. Sundararajan V. Madihally